Synthesis, Spectroscopy Studies and Applications of CdS Nanoparticles within MCM-41

By

Yanting Liao

A dissertation submitted to the Graduate Faculty in Chemistry in partial fulfillment of the requirements for the degree of Doctor of Philosophy, The City University of New York.

2005

INFORMATION TO USERS

The quality of this reproduction is dependent upon the quality of the copy submitted. Broken or indistinct print, colored or poor quality illustrations and photographs, print bleed-through, substandard margins, and improper alignment can adversely affect reproduction.

In the unlikely event that the author did not send a complete manuscript and there are missing pages, these will be noted. Also, if unauthorized copyright material had to be removed, a note will indicate the deletion.

ProQuest Information and Learning Company
300 North Zeeb Road
P.O. Box 1346
Ann Arbor, MI 48106-1346

This manuscript has been read and accepted for the Graduate Faculty in Chemistry in satisfaction of the dissertation requirement for the degree of Doctor of Philosophy.

April 26, 2005
Date

Daniel L. Akins
Chair of Examining Committee

April 26, 2005
Date

Gerard Koeppl (ada)
Executive Officer

Daniel L. Akins Daniel L. Akins

John Lombardi

James Batteas

Supervisory Committee

The CITY UNIVERSITY OF NEW YORK

ABSTRACT

Synthesis and Spectroscopy Studies of CdS Nanoparticles within MCM-41

By

Yanting Liao

Adviser: Daniel L. Akins

Cadmium sulfide nanoparticles have been successfully synthesized by the correspondent within both modified mesoporous aluminosilicate MCM-41 and siliceous SBA-15. The optical properties of the nanoparticles have been studied using XRD, UV-vis absorption, luminescence and Raman spectroscopies. Rigid chemically and thermally stable MCM-41 provides an ideal host for the nanoparticles synthesized therein, thus allowing the investigation of solvent effects on the optoelectronic properties of cadmium sulfide nanoparticles embedded in MCM-41 (referred to as CdS/MCM-41, hereinafter). The luminescence and photophysics of these nanoparticles were investigated by both steady-state and time-resolved emission spectroscopies. It was observed that the emission of cadmium sulfide nanoparticles in

polar solvent produces a red shift with increases in excitation wavelength, which is similar to the "red-edge-excitation-shift" effect (REES). The origin of REES effect is due to the dipolar interaction of fluorophore with the polar solvent or media in both ground and excited states. Such strong interaction results in a decrease of the transition energy, leading to a red shift in emission. Also, for both protic and aprotic solvents, the emission maximum of CdS shifted to longer wavelengths with increases in the polarity of the solvent. The other rare property discovered for CdS/MCM-41 is its emission polarization. This property may be exploited in potential applications for biological labeling and probing. In studies reported here, the time-resolved fluorescence measurement provided rich information on the surface and solvent effects on the luminescent of cadmium sulfides nanoparticles. The quenching behavior of cadmium sulfides by methyl viologen and copper ions was found to exhibit solvent and surface charge carries effects, as well as a strong influence associated with the hosting environment of mesoporous materials. A linear temperature dependence was observed for the emission of CdS/MCM-41 (over the wide range, 77 – 298 K) suggests the potential application for luminescence nano-thermometry. The spontaneous formation of reduced methyl viologen radicals ($MV^{+\bullet}$) within mesoporous materials was observed in the presence of sulphide and MV^{2+} ions. In this case, the mesoporous material, MCM-41, works both as a micro-reactor and a catalyst. The catalytic reaction leading to MV^{+}, a species whose location is determined by the optical absorption, provides a complementary means in combination with electron microscopy for probing the location of sulfide nanoparticles synthesized within the pores of mesoporous materials.

PREFACE

The synthesis and characterization of semiconductor nanoparticles have attracted intense research interest lately owing to the unique chemical and physical properties of the nanoparticles and the vast potential for practical applications of composite system incorporating the nanoparticles. Semiconductor nanoparticles have physical and chemical properties that may differ significantly from those of the bulk material. Such deviations are attributed to the small size of the particle and accompanying surface structure effects. And by controlling the size of the particle and surface structures, the electronic, optical, magnetic, mechanical, and chemical properties can be modified to suit a wide range of device application in optoelectronics, nonlinear optics, electronics, and chemical engineering.

The size distribution and dispersion of semiconductor nanoparticles are critical to their performance. Ordered mesoporous materials have been suggested as ideal hosts for forming ordered and well dispersed semiconductor nanocomposites due to their periodic and size-controllable pore channels (2-10 nm) and high surface areas. Also, mesoporous materials have been regarded as "natural micro-reactors" due to the strong localized electric fields within the channels. Properties of semiconductor nanoparticles are determined not only by the confinements of the host material but also by the properties of the host materials, which offer a means of manipulating the desirable performance of semiconductor nanoparticles.

The original and creative research described in this dissertation contributes to the body of knowledge concerning with cadmium sulfide (CdS) nanoparticles,

mesoporous materials (as hosts of the nanoparticles) and methyl viologen (a reversible redox indicator). CdS nanoparticles have been successfully fabricated within mesoporous materials, such as MCM-41 and SBA-15, and their optical characterizations have been achieved by XRD, UV-vis absorption, fluorescence at both room and cryogenic temperatures (300K and 77K), and Raman spectroscopy. MCM-41 served as a good host for the investigation of solvent effects on luminescence and photophysics of CdS nanoparticles embedded therein. Such investigations were carried out with both steady state and time-resolved spectroscopy, for which emission quenching and anisotropy measurements provided a wealth of information concerning the photoinduced processes and surface effects on the kinetics.

As reviewed in the literature, there have been a number of methodologies used to assemble semiconductor nanoparticles inside the channels of mesoporous materials. But, little in the way of spectroscopic analyses, especially Raman measurement, has been applied to characterize semiconductor nanocomposites. In Chapter I, I report successful synthesis of CdS nanoparticles within both modified mesoporous aluminosilicate MCM-41 and siliceous SBA-15. XRD, UV-vis absorption, fluorescence measurement at low temperature and Raman measurement were used to characterize the photophysical and chemical properties. The effects of temperature, excitation laser intensity and particle size on the acquired spectrum were also studied. Both MCM-41 and SBA-15 were functionalized by a silylation reagent, (3-mercaptopropyl) trimethoxysilane, for rigidifying the inner wall of mesoporous materials and facilitating proper guest-host interaction. Apparent blue shifts of the

absorption band edge of CdS were observed as a result of the quantum confinement effect. For Raman spectra, the relative intensity of the fundamental band and the overtone band of the nanoparticles were found to differ from that of the bulk material. This difference is discussed in terms of electronic anharmonicity. The blue shifts in Raman spectra between the CdS/MCM-41 and bulk CdS sample were observed and explained in terms of CdS lattice compression and/or sulfide vacancies. Further, it was suggested that the stoichiometry for the nanoparticle is more appropriately expressed in the form of CdS_{1-x}.

Although the investigation of the solvent effects on the optical property of semiconductor nanoparticles is essential to understanding the photogenerated carriers dynamics within the particle and to pursuing many potential applications such as biological sensing, review of literature reveals that little research of such solvent effects has been reported. The main challenge for studying the solvent effects is the suspension of nanoparticles in different solvents, especially those with a polarity (dielectric constant, ε) that differs drastically from that of the original solvent in which the nanoparticles were synthesized. Rigid, chemically and thermally stable MCM-41 affords an ideal host for nanoparticles. The rigid frame of MCM-41 makes nanoparticles approachable by solvents without re-precipitation. Chapter II presents the steady state spectroscopy investigation of CdS nanoparticles within MCM-41. The surface of CdS nanoparticles were modified with either ion doping or adsorption. Such a combined nanoparticle system is quite re-suspendable in both protic and aprotic solvents. Solvent polarity and surface modification affect the luminescence of CdS nanoparticles. The mechanism of the solvent dependence of luminescence is

discussed with regard to environment polarity. The interesting and rare property found for CdS nanoparticles within MCM-41 is the emission polarization. The origin of optical polarization of CdS nanoparticles within mesoporous materials is explained with regard to solvent relaxation. Constant positive anisotropy would allow for the possibility of using such nanoparticles for biological labeling.

To understand the fundamental processes and dynamics of the photogenerated charge carriers within the particle, the investigation of the solvent effects on the emission quenching of CdS nanoparticles was carried out. This is reported in detail in Chapter III. The time-resolved fluorescence measurement provided rich information on the surface structure and solvent effects on luminescence quenching of CdS nanoparticles. Such information helps us understand the relation between the surface structure of nanoparticles and their optoelectronic properties. It also provides important guideline to fabricate nanoparticles with optimized surface properties for application in certain types of optoelectronic devices, such as sensors. The quenching behavior of CdS was investigated mainly in systems using methyl viologen or copper ions as the quencher. The quenching kinetics was explained in terms of solvent effects, surface charge carriers and host influence of mesoporous materials.

The development of fluorescence nanothermometry has specific significance in industrial or biomedical diagnostic and treatment processes, in which it is imperative to detect real-time, spatial-resolved and precise temperature. There are several advantages to using fluorescence nanothermometry as opposed to the traditional ones, including high sensitivity, accuracy, and spatial resolution. In Chapter IV, a potential fluorescence nanothermometric material, cadmium sulphide

nanoparticles embedded in MCM-41 is introduced. It is found that the emission intensity of CdS/MCM-41 changed linearly with temperature in a wide temperature range from 77 K to 298 K. The excellent linearity of emission intensity on temperature promise nanocomposite to be used in fluorescence thermometry in industrial and biological fields or for thermal imaging.

Mesoporous materials have been regarded as "natural reactors" due to the strong electric fields existing in the channels and the electronic confinement of the guest molecules. In many cases, the preactivation of the reactant molecules under such strong electric fields results in efficient catalytic reactions. In Chapter V, an unusual reduction reaction of methyl viologen is reported. It is astonishing to observe the spontaneous formation of methyl viologen radicals within MCM-41. MCM-41 functions as a unique micro-reactor with a catalytic function and the sulphide ions function as the reductant. The mechanism of reaction was investigated by spectroscopic analysis of the methyl viologen radical, exploiting UV-vis and Raman measurements. The reaction is reasonably attributed to the space confinement effect and the enhanced localized electric field within the channels of MCM-41. The source of the sulfide ions can be either an added sulfide salt or coordinatively unsaturated surface sulfide ions of an occluded sulfide nanoparticle. The reduction reaction of methyl viologen within MCM-41 is not only a complementary means in combination with electron microscope to determine the presence and location of sulfide nanoparticles synthesized within such mesoporous materials, but also provides an opportunity to explore the dynamic mechanism of methyl viologen radicals.

Acknowledgements

To My Parents

And All the Other Wonderful People in My Life

Writing a dissertation is both a solitary and a collaborative endeavor. I spent many a late night alone in the lab conducting research and experiments, yet without the helping hands of many along the way, it would be hard for me to imagine my research and experiments ever bearing fruits. I wish to thank all my mentors, teachers, colleagues and friends, and acknowledge their significant contributions to my education and work.

In particular, I would like to express my heart-felt gratitude to Dr. Daniel L. Akins. As my mentor and advisor, he introduced me to the fascinating world of nanotechnology. A distinguished scientist widely respected in his fields, Dr. Akins has many commitments and a busy schedule, yet he has always been there for me throughout my Ph.D. program, giving me invaluable guidance, prodding me to explore new ideas and always encouraging me to grow as a young scientist. I am deeply indebted to him, and I thank him for his wisdom and friendship.

It has been a great honor for me to work with Dr. Ling Zang during the past two year, a crucial period in my Ph.D. program. Without his immense help, I would

not have been as focused and clear-headed about my research, and I would not have finished my dissertation timely. I wish to thank Dr. Zang for his always strong support and wonderful advices.

I also wish to thank Dr. Wei Xu, whom I met upon my arrival in the United States as a young graduate student. He helped me settle down in the new environment and become familiar with MCM-41 and CdS. His great help has enabled me to achieve what I have achieved today.

I would also like to express my appreciation to the members of my dissertation committee, Dr. John Lombardi, Dr. James. Batteas and Dr. David Adams, for taking the time for my committee meetings and defense. I have learned a great deal from each of them throughout my Ph.D. program, for which I am very grateful.

Most of all, I wish to express my love and gratitude to my family in Shanghai and to my husband for their tremendous and unwavering support, patience and love.

TABLE OF CONTENTS

Bibliography

LIST OF TABLES

LIST OF DIAGRAMS AND FIGURES

General Introduction

The driving force in the field of nanotechnology is to fabricate various kinds of nanodevices to build class of technologies that can revolutionize the world, such as was the case following the development of computers. The focus of this work is to understand completely the unique physical and chemical properties of cadmium sulfide (CdS) nanoparticles. This requires the fabrication of CdS nanoparticles in narrow size distribution and well dispersed in different solvents. One approach is to synthesize the nanoparticles within ordered mesoporous materials like MCM-41. MCM-41 not only functions as host but also prevents the semiconductor nanoparticles within from aggregating when re-dispersed into different solvents. In the dry state, the nanocomposites of CdS/MCM-41 show unique temperature dependence of the emission; the emission intensity changes linearly with temperature, leading to a promising application in luminescence thermometry. This observation should bring to the nanoscience community new insights into the optoelectronic properties of semiconductor nanoparticles, and help to pave the way to development of new devices of comprised nanoparticles.

This general introduction explains the significance and background of the research and clarifies some of the scientific terms which are correlated with the research topics.

I. Semiconductor Nanoparticles

Semiconductor nanoparticles, referred as quantum dots, with dimensions on the order of nanometers have been the subject of intense research in past decades, due to their unique optical, electronic and chemical properties.[1-14] There are potential applications for nanoparticles to be developed as optoelectronic nanodevices and biological nanosensors. The development of such applications requires extensive research of the fundamental properties of semiconductor nanoparticles.

Compared to corresponding bulk semiconductor materials, semiconductor nanoparticles have two distinguishing characteristics, both related to the size of individual nanoparticle. First, nanoparticles have a large ratio of surface atoms to those located in the crystal lattice, which makes the physical and chemical properties of semiconductor nanoparticles particularly sensitive to the surface structure. Second, nanoparticles have size dependent optical properties, so called "*quantum size effect*". As the dimension of the particle decreases, the bandgap energy of the nanoparticle increases. [15-18]

"Quantum size effect". The bandgap energy of semiconductor nanoparticle increases as their size decreases. The most notable size effect is the significant blue shift of electronic absorption and emission spectrum with decrease in size. Brus has developed a popular effective mass model that relates particle size (neglecting spatial correlation effects) to the bandgap energy of semiconductor nanoparticles[15-18]. As illustrated in Figure G-1, the quantum size effect causes the continuous band of the crystal to split into discrete, quantized levels and the bandgap of semiconductor nanoparticles to increase. As the nanoparticle decreases in size, the bandgap increases, approaching the energy difference between LUMO and HOMO for the

General Introduction

The driving force in the field of nanotechnology is to fabricate various kinds of nanodevices to build class of technologies that can revolutionize the world, such as was the case following the development of computers. The focus of this work is to understand completely the unique physical and chemical properties of cadmium sulfide (CdS) nanoparticles. This requires the fabrication of CdS nanoparticles in narrow size distribution and well dispersed in different solvents. One approach is to synthesize the nanoparticles within ordered mesoporous materials like MCM-41. MCM-41 not only functions as host but also prevents the semiconductor nanoparticles within from aggregating when re-dispersed into different solvents. In the dry state, the nanocomposites of CdS/MCM-41 show unique temperature dependence of the emission; the emission intensity changes linearly with temperature, leading to a promising application in luminescence thermometry. This observation should bring to the nanoscience community new insights into the optoelectronic properties of semiconductor nanoparticles, and help to pave the way to development of new devices of comprised nanoparticles.

This general introduction explains the significance and background of the research and clarifies some of the scientific terms which are correlated with the research topics.

I. Semiconductor Nanoparticles

states. Such strong interaction results in a decrease of the transition energy, leading to a red shift in emission.[19] Because long-wavelength excitation results in the photoselection of those fluorophores which interact most strongly with the polar solvent molecules, red shifts occur. The prerequisite for REES is that the dipolar relaxation (reorientation) for the solvent shell be comparable or slower than the emission of decay of fluorophore molecules (10^{-9} s). If the fluorophores are placed in a viscous or restricted space, the reorientation process occurs slowly. In this study, it was observed that the emission of cadmium sulfide nanoparticles in polar solvent produces a red shift with increases in excitation wavelength, which is similar to the REES effect observed for organic fluorophores. Such unique property of CdS nanoparticles can be utilized for hydrodynamic probing to investigate the dynamic properties of reference solvents, model membranes and proteins.

"Fluorescence Anisotropy". Samples exhibiting nonzero anisotropies are said to display polarized emission.[19] The origin of anisotropy is based on the existence of transition moments for absorption and emission which lie along specific directions within the fluorophore structure. The extent of polarization of the emission is described in terms of the anisotropy (r). The anisotropy measurement reveals the average angular displacement of the fluorophore that occurs between absorption and subsequent emission of a photon, thus providing information on the size, shape and rigidity of various molecular environments (e.g. proteins). Generally, the anisotropy is independent of the emission wavelength. If emission occurs from more than one excited state, and if these states produce different emission spectra, then the anisotropy becomes dependent on the emission wavelength. Anisotropy is often

observed in fluorophores with solvent relaxation, and it can be described by the Perrin equation, as shown in Eq. 3.

$$r = \frac{r_o}{1+(\tau/\theta)} \qquad \text{Eq. 3}$$

where r_0 is the anisotropy which would be measured in the absence of rotational diffusion, θ is the rotational correlation time for the diffusion process, and τ is the emission lifetime.

For spherical nanoparticles, the emission is not expected to display significant polarization due to the negligible dipole moment of the nanoparticles. Interestingly, CdS nanoparticles synthesized within MCM-41 display nonzero anisotropy, which is attributed to the asymmetric local electric field around the opening of the cavities of MCM-41. This property, along with the great stability in physiological environments makes CdS/MCM-41 nanocomposites promising candidates to be used as biophysical hydrodynamic probes.

II. Why CdS?

Colloidal CdS has long served as a model system for the study of charge carrier dynamics in nanoparticles.[6,9,12,20,21] There are various synthetic techniques for CdS nanoparticles with different particle sizes and narrow size distribution.[22-24] The static absorption and emission properties of CdS have been well characterized.[15,17,25-27] In addition, nanosecond and picosecond time-resolved photolysis, [28-30] as well as picosecond resonance Raman spectroscopies[22] have been performed on those particles. As a typical II-VI semiconductors, CdS has a wide bandgap (E_g = 2.53 eV) and thus emits in the green (λ = 490 nm). Changing the size and surface structure of

CdS nanoparticles can tune the emission wavelength across the whole visible spectrum. This makes CdS a unique material for fabrication as optoelectronic devices such as light emitting diodes (LED). Quantum yield of fluorescence is another important property for semiconductor nanoparticles that are fabricated as optoelectronic devices. Quantum yield of ~ 0.2 has been reported for CdS colloids with appropriate surface modification.[31] Recently, CdS nanoparticles wrapped with DNA have been successfully synthesized. The spectral properties of those particles strongly depend on DNA binding.[32-34] However, the solvent dependence of optical properties of CdS nanoparticles remains poorly understood, mainly due to the technical difficulty in re-dispersing the nanoparticles in different solvents. CdS nanoparticles synthesized within MCM-41 have proven a stable system capable for being re-dispersed in various solvents without aggregation or precipitation. This provides vast opportunities to investigate the solvent effect on optical properties and explore the potential application of the particles in hydrodynamic probing.

References

(1) Brus, L. E.; Efros, A.; Itoh, T. *J. Lumin.* **1996**, *76*, 1.

(2) Alivisatos, A. P. *Science* **1996**, *271*, 933.

(3) Colvin, V. L.; Schlamp, M. C.; Alivisatos, A. P. *Nature* **1994**, *370*, 354.

(4) Klein, V. L.; Lim, A. K. L.; Alivisatos, A. P.; McEuen, P. L. *Nature* **1997**, *389*, 699.

(5) Ridley, B. A.; Nivi, B.; Jacobson, J. *Science* **1999**, *286*, 746.

(6) Henglein, A. *Chem. Rev.* **1989**, *89*, 1861.

(7) Kamat, P. V. *Chem. Rev.* **1993**, *93*, 267.

(8) Bruchez Jr, M.; Moronne, M.; Gin, P.; Weiss, S.; Alivisatos, A. P. *Science* **1998**, *281*, 2013.

(9) Empedocles, S.; Bawendi, M. *Acc. Chem. Res.* **1999**, *32*, 389.

(10) Huynh, W. U.; Dittmer, J. J.; Alivisatos, A. P. *Science* **2002**, *295*, 2425.

(11) Nirmal, M.; Dabbousi, B. O.; Bawendi, M. G.; Macklin, J. J.; Trautman, J. K.; Harris, T. D.; Brus, L. E. *Nature* **1996**, *383*, 802.

(12) Nirmal, M.; Brus, L. E. *Acc. Chem. Res.* **1998**, *32*, 407.

(13) Redl, F. X.; Cho, K. S.; Murray, C. B.; O'Brien, S. *Nature* **2003**, *423*, 968.

(14) Shim, M.; Guyot-Sionnest, P. *Nature* **2000**, *407*, 981.

(15) Chestnoy, N.; Harris, T. D.; Hull, R.; Brus, L. E. *J. Phys. Chem.* **1986**, *90*, 3393.

(16) Brus, L. *J. Phys. Chem.* **1986**, *90*, 2555.

(17) Brus, L. E. *J. Phys. Chem.* **1983**, *79*, 5566.

(18) Steigerwald, M. L.; Brus, L. E. *Acc. Chem. Res.* **1990**, *23*, 183.

(19) Lakowicz, J. R. *Principle of Fluorescence Spectroscop 2nd* Kluwer Academic/Plenum, *New York*, **1999.**

(20) Zhang, J. Z. *Acc. Chem. Res.* **1997**, *30*, 423.

(21) Zhang, J. Z. *J. Phys. Chem. B* **2000**, *104*, 7239.

(22) Rossetti, R.; Brus, L. E. *J.Phys.Chem.* **1986**, *90*, 558.

(23) Fischer, C.-H.; Henglein, A. *J. Phys. Chem.* **1989**, *93*, 5578.

(24) Colvin, V. L.; Goldstein, A. N.; Alivisatos, A. P. *J. Am. Chem. Soc.* **1992**, *114*, 5221.

(25) Henglein, A. *Ber. Bunsen-Ges. Phys. Chem.* **1982**, *86*, 301.

(26) Henglein, A.; Gutierrez, M. *Ber. Bunsen-Ges. Phys. Chem.* **1983**, *87*, 852.

(27) Wang, Y.; Herron, N. *Phys. Rev. B* **1990**, *42*, 7253.

(28) Alfassi, Z.; Bahnemann, D.; Henglein, A. *J. Phys. Chem.* **1982**, *86*, 4656.

(29) Kamat, P. V.; Dimitrijevic, N. M.; Fessenden, R. W. *J. Phys. Chem.* **1987**, *91*, 396.

(30) Kamat, P. V.; Dimitrijevic, N. M. *J. Phys. Chem.* **1989**, *93*, 4259.

(31) Sooklal, K.; Hanus, L., H.; Ploehn, H., J.; Murphy, C., J. *Adv. Mate.* **1998**, *10*, 1083.

(32) Mahtab, R.; Rogers, J. P.; Murphy, C. J. *J. Am. Chem. Soc.* **1995**, *117*, 9099.

(33) Mahtab, R.; Rogers, J. P.; Singleton, C. P.; Murphy, C. J. *J. Am. Chem. Soc.* **1996**, *118*, 7028.

(34) Lakowicz, J. R.; Gryczynski, I.; Gryczynski, Z.; Murphy, C. *J. Phys. Chem. B* **1999**, *103*, 7613.

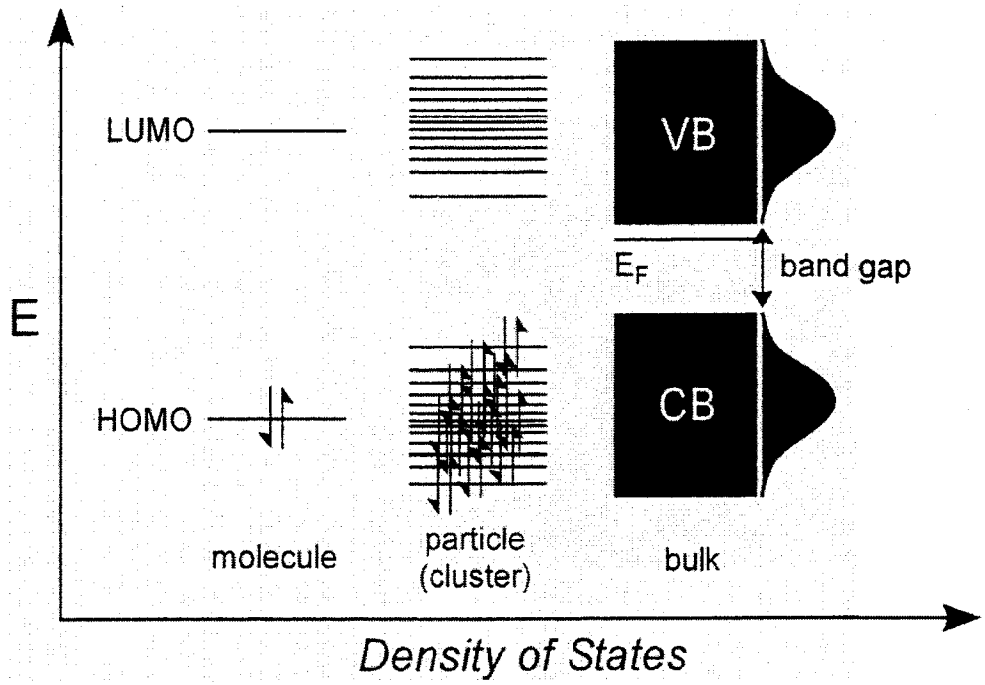

Scheme G-1: Schematic illustration of the energy levels as a function of density of states for different size systems of semiconductor.

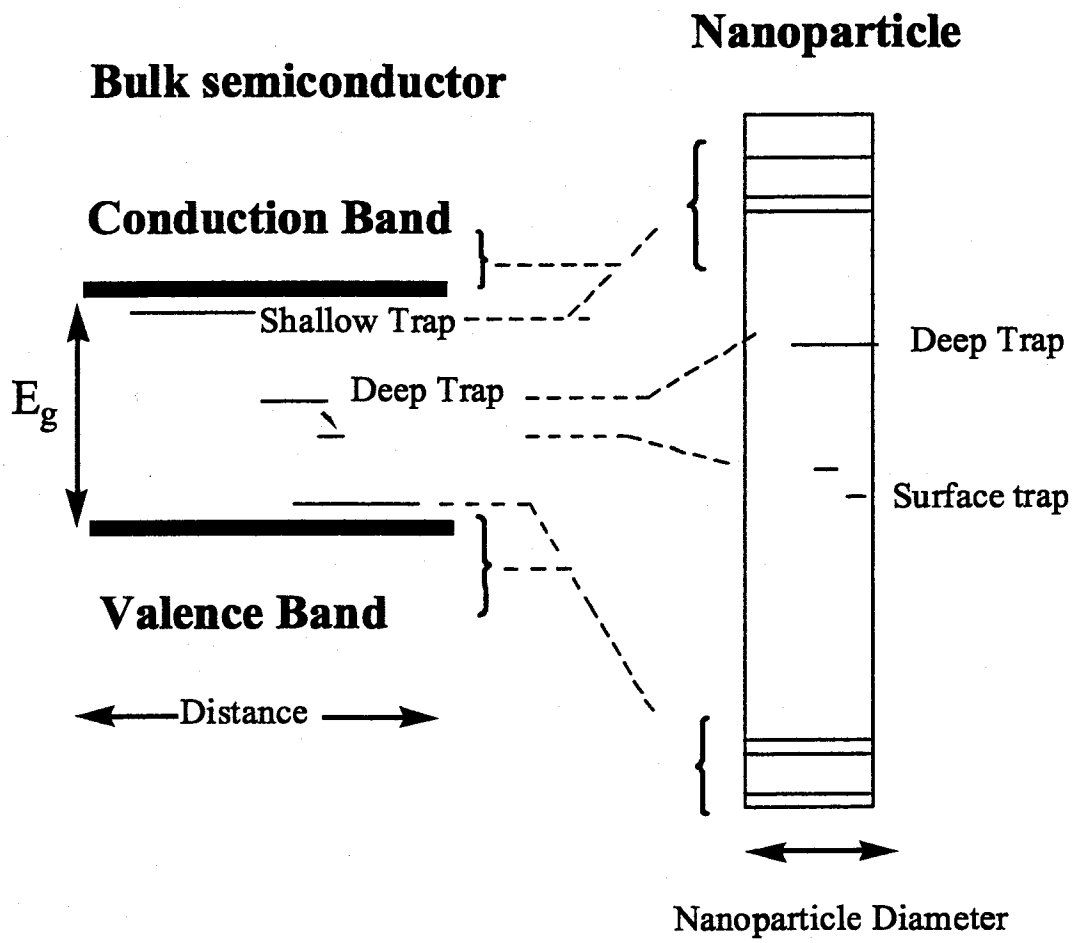

Scheme G-2. Schematic correlation diagram relating nanoparticle states to bulk crystal states.

Chapter I. Formation of Cadmium Sulfide Nanoparticles within Modified MCM-41 and SBA-15

Abstract

Cadmium sulfide nanoparticles were formed within both modified mesoporous aluminosilicate MCM-41 and siliceous SBA-15. Syntheses involved the formation of a monolayer of silylation reagent, (3-mercaptopropyl) trimethoxysilane, on the surfaces of both MCM-41 and SBA-15, which served to preposition the sulfide source within the mesoporous channels. A source of cadmium ions was then added, leading to reaction with the prepositioned sulfide and with added H_2S to result in occluded CdS nanoparticles. The average diameters of nanoparticles of CdS formed within the mesochannels of MCM-41 and SBA-15, as characterized by XRD and UV-vis diffuse reflectance, were ca. 2.1 nm and 3.4 nm, respectively. The thicker wall and larger pore size of SBA-15 compared to MCM-41, represents a more stable matrix for forming the occluded nanoparticle, as indicated by the stability of the XRD patterns for the nanocomposite utilizing SBA-15 versus that when MCM-41 was used. Also, from Raman spectra for the CdS/MCM-41 system, the relative intensities of the fundamental band and the overtone band were found to differ for the bulk and

nanoparticle samples. We discussed this observation in terms of electronic anharmonicity. Furthermore, blue shifts for both fundamental and overtone Raman bands were observed when compared to bulk CdS: 303 vs. 299 cm^{-1} and 605 vs. 599 cm^{-1}, respectively. We rationalized this observation in terms of CdS lattice compression and/or sulfide vacancies, particularly at the interface between the nanoparticle and the mesoporous cage matrix. We further suggest that the stoichiometry for the nanoparticle is more appropriately CdS_{1-x}. Lastly, photoluminescence shifts were rationalized based on nanoparticles size, incident excitation intensity, as well as temperature.

I. Introduction

Semiconductor nanoparticles, also referred to as quantum dots, have garnered enormous attention in recent years. And, in particular, compound II-VI semiconductor nanoparticles have been a focus because they are optoelectronic materials with functionalities in flat-panel displays, field-effect thin-film transistors, light-emitting diodes, and single-electron transistors [1-5]. Since the properties of semiconductor nanocrystals depend on both dimension and superlattice structure, it is important to control size and shape in their syntheses and to arrange them over useful dimensions.

Syntheses of nanoparticles within mesoporous silica, such as MCM-41 and SBA-15, which are one-dimensional, hexagonally arranged porous material of highly uniform dimensions, represent a constricted growth process that provides control of nanoparticle dimensions. Three methodologies have been developed to transport precursor molecules or ions for assembly of nanoparticles inside the channels of such materials: (a) direct impregnation [6, 7], (b) modification of the surface walls followed by loading of precursors through affinity interaction [8, 9], and (c) ion-exchange reaction [10]. Without doubt, the direct impregnation method alone, without the functionalizing of the surface walls, has generally proven unsuccessful in obtaining meaningful amounts of nanocrystals within the channels of silicates [6, 7]; in particular, in the case of synthesis of CdS within the channels, it has been found that under high loading and evaporation to remove solvent, although some of CdS nanoparticles are formed within the channels of MCM-41, the majority of CdS particles are located outside of the porous structure [8, 9]. Also, the ion-exchange reaction approach, as modified by passivating the external surface to facilitate ion-exchange incorporation

of a reagent ion, shows promise, but effectiveness of affinity loading the channels of the silicates is uncertain [10]. We deduced that the most promising approach is built around (b) above, and, in this chapter, apply the concept of functionalizing the interior wall of mesoporous MCM-41 and SBA-15 for the synthesis of encapsulated CdS by choosing a silylation reagent that incorporates one of the reactant ions.

Examination of the literature indicates that interest has been shown in the preparation of CdS nanoparticles within MCM-41. However, little in the way of spectroscopic analyses has been applied to the characterization of the nanocomposite system. In this chapter, we acquire UV-vis absorption, photoluminescence, and Raman spectra of nanocomposites involving CdS within both MCM-41 and SBA-15. We also study the effects of temperature, incident intensity, and particle size on the measured spectra, and deduce that sulfur vacancies are present within the mesoporous channel, which result in the stoichiometry of the occluded nanoparticles as being CdS_{1-x}, instead of the 1:1 stoichiometry (as occurs for bulk CdS) that has been reported in the literature.

II. Experimental Section

Synthesis of Functionalized MCM-41 and SBA-15: Polycrystalline powders of the mesostructural aluminosilicate MCM-41 were prepared by using cetyltrimethylammonium bromide (CTAB) as the template [11, 12]. Briefly, Na_2SiO_3 solution (Aldrich, ~27% SiO_2) and a calculated amount of $NaAlO_2$ (Alfa) solution (Si/Al = 10) were added to CTAB (Aldrich) solution according to the molar composition ratio $5SiO_2$:$0.25Al_2O_3$: CTAB: $610H_2O$. The pH was lowered to 11 with 2 M H_2SO_4 and the mixture was stirred for more than 3 h at about 318 K. the Temperature was then raised to 373 K, and the reaction allowed for 72 h in a Teflon-

lined autoclave. The resulting precipitate was filtered, washed thoroughly with distilled water, and calcined in air at 773 K to obtain the final product, MCM-41 (see discussions below of XRD patterns).

Polycrystalline powders of the mesostructural siliceous SBA-15 were synthesized by using a triblock copolymer as the template [13-15]. Specifically, in our case, 6.0 g of triblock poly (ethylene oxide)-poly (propylene oxide)-poly (ethylene oxide) ($EO_{20}PO_{70}EO_{20}$, also referred to as Pluronic 123, Aldrich) was dissolved in 170 ml of 2 M aqueous HCl with stirring. Next, at room temperature, 13.5 ml of tetraethyl orthosilicate (TEOS, Aldrich) was added drop wise to the resultant solution. The mixture was stirred for 24 h at ca. 313 K, then the temperature was raised to ca. 373 K, and the reaction allowed for 48 h in a Teflon-lined autoclave. The resulting precipitate, as in the case of the MCM-41 synthesis, was filtered, dried, and calcined in air at ca. 773 K to obtain the final product, SBA-15.

Both MCM-41 and SBA-15 were modified by subsequent treatment that involved the functionalizing and rigidizing of the inner surface walls of the silicates through reaction with the silylation reagent (3-mercaptopropyl)trimethoxysilane (MPTMS; $HS\text{-}(CH_2)_3\text{-}Si\text{-}(CH_3O)_3$). The method used is similar to that in our prior studies [16, 17], in which (aminopropyl) triethoxysilane (APTES; $NH_2\text{-}(CH_2)_3\text{-}Si\text{-}(C_2H_5O)_3$) was used as silylation reagent. The method involved, briefly, taking about 1.5 g of either calcined MCM-41 or SBA-15 and mixing it with a chloroform solution of MPTMS (100 ml, 0.4 M), which was stirred overnight at room temperature. The precipitate was filtered and washed with chloroform and dichloromethane.

Formation of CdS nanoparticles: A typical preparation of occluded cadmium sulfide nanoparticles within modified silicate involved stirring and

refluxing a mixture of 600 mg of modified MCM-41 or SBA-15 with 100 ml of cadmium(II) methanol solution (60 mg of $Cd(OAc)_2 \bullet 2H_2O$ dissolved in 100 ml of HPLC grade methanol) for 24 h. The solution was then centrifuged and the transparent aqueous solution decanted. The residue was washed with methanol to remove Cd^{2+} from the external surface and then dried at 333 K in vacuum. The final step involved the treatment with a flow of 5 vol. % H_2S in N_2 for 6 h at room temperature. The composites involving MCM-41 and SBA-15 are hereinafter also referred to as CdS/MCM-41 and CdS/SBA-15, respectively.

Instrumentation: Absorption spectra were recorded using a Perkin-Elmer Lambda 18, UV-vis-NIR spectrometer. The X-ray diffraction (XRD) instrument used was a Rigaku diffractometer using Cu $K_{\alpha 1}$ (0.154 nm) X-rays; typically run at a voltage of 40 kV and current of 30 mA. Photoluminescence was taken using a He-Cd laser, with the emission at 325 nm as the excitation wavelength. For temperature studies, the samples were mounted on the cold finger of a Janis cryogenic system (Model ST-300; which allowed cooling to 78 K using liquid nitrogen), and prior to cooling the system was pumped to ~10^{-4} Torr. For incident intensity studies, the excitation laser intensity was varied by using a set of neutral density filters whose transmissions varying from 50% to 3%. Luminescence was collected by optical lenses, focused on the slit of a Spex 1680-B spectrometer, and detected with a photomultiplier tube.

Raman spectra of bulk CdS (Aldrich, < 5 micron grains) and nanocomposite grains were excited with laser radiation of wavelengths 457.9, 488.0 and 514.5 nm, from a Coherent Innova 200 argon-ion laser. The excitation power was maintained at 120 mW, and the Raman scattering was collected and dispersed by a Spex 1877, 0.6-

meter spectrometer. A cooled (140 K) Spex Spectrum-1 CCD camera was coupled to the spectrometer and used as the detector.

III. Results and Discussion

A series of XRD patterns for pristine calcined MCM-41, modified MCM-41 and cadmium sulfide nanoparticles within MCM-41 are shown in Figure I-1. Similar measurements for the series involving SBA-15 are shown in Figure I-2.

The XRD patterns of the composites containing CdS (i.e., CdS/MCM-41 and CdS/SBA-15) show strong (100) peaks, suggesting that framework stability is exhibited when CdS is encapsulated within modified MCM-41 and SBA-15. Moreover, one can deduce that formation of CdS nanoparticles within the channels of modified MCM-41 and SBA-15 does not decrease the framework integrity of the two hosts (see parts B and C of Figure I-1 and Figure I-2). Furthermore, for the SBA-15 system (as shown in Figure I-2) one observes that all XRD patterns for the series also show strong (110) and (200) peaks, and that the relative intensities of these peaks are essentially constant, indicating a more integrated structure than that involving MCM-41. We attribute the more integrated character of the SBA-15 system to the thicker intercore spacing that it possesses (~ 40 Å) when compared to than that of MCM-41 (~10 Å) [15].

Returning to Figure I-1, we note the inset that shows the wide-angle XRD pattern for CdS/MCM-41 that contains cadmium nanoparticles. The mean particle size can be determined from the X-ray diffraction position and the peak width using the Scherrer formula, $d = 0.941\lambda / B\cos\theta_B$, where d is the mean diameter of the particle, λ is the wavelength of the Cu $K_{\alpha 1}$ line (0.154 nm), θ_B is the angle between the incident beam and the reflection lattice planes, and B is the width (in radians) of

the diffraction peak. From the width and position of the diffraction peak, the average size of nanoparticles is found to be ca. 21 Å, which is concordant with the pore size of modified MCM-41, which was determined in a prior study [16] in which (aminopropyl)triethoxysilane (APTES; NH_2-$(CH_2)_3$-Si-$(C_2H_5O)_3$) was the silylation reagent. Similarly, from the inset in Figure I-2, the average size of CdS nanoparticles within SBA-15 is calculated to be ca. 34 Å.

Diffuse reflectance (DR) UV-vis spectra of the series bulk-CdS, CdS/SBA-15, CdS/MCM-41 have been acquired (see Figure I-3, parts A, B and C, respectively). An obvious blue shift in the absorption band-edge (close to 550 nm) occurs as the CdS particle's size decreases. The direction of the blue shift is in line with expectation associated with particle size.

Representative resonance Raman spectra for bulk CdS, excited with 514 nm radiation, and CdS nanoparticles occluded within MCM-41 (i.e., CdS/MCM-41), excited with 457.9 nm radiation, are shown in Figure I-4, parts A and B, respectively. Both spectra contain a longitudinal optical (LO) phonon mode at ca. 300 cm^{-1} as well as the first overtone band at ca. 600 cm^{-1}. The bulk sample, however, exhibits higher overtones, likely indicating strong electronic anharmonicity. The relative intensities of the first overtone band and the fundamental band (e.g., I_{2LO}/I_{LO}, where I_{2LO} is the peak intensity of the first overtone and I_{LO} that of the fundamental) might be expected to provide insight on the structure of the CdS nanoparticle. Table I provides the Raman numerical results pertaining to a comparison of overtone- and fundamental-band measurements for bulk CdS and nanocomposite CdS/MCM-41, while Figure I-5 provides a plot of the relative intensities (I_{2LO}/I_{LO}) versus excitation wavelength. As shown in Figure I-5 and Table I, for bulk CdS, I_{2LO}/I_{LO} is always greater than the

same ratio for the composite for all excitation wavelengths. Moreover, the ratio is found to increase as the exciting frequency approaches the absorption band-edge, which is shown in Figure I-3, for both bulk and composite samples. We note, however, that the ratio of Raman intensities for the composite, when resonantly excited, giving I_{2LO}/I_{LO} = 0.30, is less than the ratio for the bulk (I_{2LO}/I_{LO} = 0.51), despite the fact that the exciting frequency is off-resonance for the latter. Hence, it appears, for the bulk sample, that the electronic anharmonicity plays a greater role in determining overtone intensity than does the Franck-Condon resonance contribution to the overtone intensity for the composite. Of course, I_{2LO}/I_{LO} is enhanced for both the bulk and composite samples as resonance is approached, as shown in Figure I-5. We will discuss the implications of this finding in a later publication.

Another aspect of the Raman measurements are blue shifts of both the fundamental and overtone bands for the nanoparticle-composite vis-à-vis the respective bands for bulk CdS (see Table I-1). An obvious explanation for the blue shifts is lattice compression resulting from the constricted dimension of the pore in which the nanoparticle is formed. A second explanation might be associated with site vacancies such as discussed by Spanier et al. [18] in their study involving CeO_2 nanoparticles. Spanier et al. [18], in which an approach developed by McBride et al. [19] was applied, suggested that the existence of oxygen vacancy site for CeO_2 can lead to a blue shift of Raman bands, and that the stoichiometric product is more appropriately represented by the formula CeO_{2-y}, where y corresponds to an "impurity" concentration. In our case, during the formation process of CdS nanoparticles with H_2S, some Cd (II) cations might be expected to incorporate and become stabilized within the nanocrystals by affinitive interaction with sulfur on the surface walls of the

functionalized MCM-41. As a result, interfacial sulfur vacancies are to be expected for the CdS nanoparticles and the stoichiometric description of the nanoparticle would be CdS_{1-x}, where x related to the vacancy concentration.

Both explanations for the blue shifts of the Raman bands suggest the existence of possible surface trap sites, which would likely evidence themselves in photoluminescence spectra—since electron-hole pair recombination from trap states results in Stokes shifted luminescence [20, 21]. In order to examine this point, we acquired low temperature photoluminescence spectra of bulk CdS and nanocomposite systems. As indicated in Figure I-6, the photoluminescences from the composites exhibit substantial Stokes shifts when compared to their respective absorption band edges; moreover, the shift increases with a decrease in the nanoparticle's diameter. Hence, the observed photoluminescence likely derives from recombination of holes and electrons at surface traps whose concentrations increase with decreasing particle size.

To complete our experimental measurements in the present study, we also examined temperature and excitation-intensity dependences of photoluminescence from the CdS/SBA-15 composite (see Figure I-7), in order to gauge whether our nanoparticles behave similar to others reported in the literature. In this regard we observed that at a fixed excitation power of 36 mW, but with temperature of either RT or 77 K, a difference in peak position occurs, 638 nm vs. 624 nm, respectively (compare parts A and D of Figure I-7). This finding is consistent with expectations since an increase in temperature is anticipated to cause thermal expansion of the lattice and a concomitant diminution of electron-phonon interactions, resulting in lowered bandgap energy [22]. Also, we note from Figure I-7 that with increasing

incident excitation intensity, at the temperature of 77 K, the photoluminescence peak shifts to higher energy, i.e., blue-shift (see parts B, C and D of Figure I-7). This finding is also consonant with expectations, since, based on exciton recombination lifetime measurements [23], increasing excitation intensity leads to the filling of lower energy exciton states, and the populating of higher exciton states, which, in turn, is reflected in a blue-shift of the photoluminescence.

IV. Conclusion

The combination of XRD, Raman scattering, UV-vis absorption, and photoluminescence measurements indicates that we have formed cadmium sulfide nanoparticles within the channels of modified MCM-41 and SBA-15, and that the nanoparticle formed within MCM-41 is smaller than that formed in SBA-15 (which have cage diameters of 2.1 and 3.4 nm, respectively). The functionalization of the interior wall of the mesostructure utilizing a sulfide containing alkoxysilane reagent facilitates incorporation of Cd (II) cations and the formation of cadmium sulfide. Comparison of fundamental and overtone band positions relative to those of bulk CdS for encapsulated CdS, suggest that both constricted vibrations of the CdS nanoparticles within the mesoporous materials as well as interfacial sulfur vacancies, leading to a stoichiometry for the nanoparticles as indicated in the chemical formula CdS_{1-x}, play roles in the direction of the shifts. Moreover, we deduce that that electronic anharmonicity plays a large role in determining the relative intensity of the fundamental and overtone bands. We have also observed the effect of nanoparticle size on photoluminescence peak wavelength, deducing that the smaller nanoparticle has more surface trap states, resulting in a greater red-shift in its exciton peak emission wavelength. Also, in our study of the effects of excitation power and

temperature on photoluminescence of CdS encapsulated within SBA-15, we have deduce that the expected lattice expansion effect with increased temperature and the population of higher exciton states with increased intensity explain our observations for CdS nanoparticles prepared by the unique procedure described herein.

V. Acknowledgment

This work was supported by the NSF and DoD-ARO, in part, through the following awards: (1) NSF-IGERT program under grant DGE-9972892, (2) NSF-MRSEC program under grant DMR-0213574, and (3) DoD-ARO under Cooperative Agreement DAAD19-01-1-0759. I am deeply indebted to Prof. D. L. Akins for his generous and kind support, Prof. Maria C. Tamargo for use of her XRD and photoluminescence instruments and Dr. W. Xu for his valuable discussion in preparation of this manuscript.

References

1. Brus, L. E.; Efros, Al.; Itoh, T. (Eds.), "Spectroscopy of Isolated and Assembled Semiconductor Nanocrystals", *J. Lumin.* **1996**, *76*, 1 (special issue).

2. Alivisatos, A. P. *Science* **1996**, *271*, 933.

3. Colvin, V. L.; Schlamp, M. C.; Alivisatos, A. P. *Nature* **1994**, *370*, 354.

4. Klein, D. L.; Roth, R.; Lim, A. K. L.; Alivisatos, A. P.; McEuen, P. L. *Nature* **1997**, *389*, 699.

5. Ridley, B. A.; Nivi, B.; Jacobson, J. M. *Science* **1999**, *286*, 746.

6. Chen, L.; Klar, P.; Heimbrodt, W.; Brieler, F.; Fröba, M. *Appl. Phys. Lett.* **2000**, *76*, 3531.

7. Chen, L.; Klar, P.; Heimbrodt, W.; Brieler, F.; Fröba, M.; Nidda, H.; Loidl, A. *Physica E* **2001**, *10*, 368.

8. Wellmann, H.; Rathoussky, J.; Wark, M.; Zukal, A.; Schulz-Ekloff, G. *Micro. Meso. Mater.* **2001**, *44-45*, 419.

9. Hirai, T.; Okubo, H.; Komasawa, I. *J Phys. Chem. B* **1999**, *103*, 4228.

10. Zhang, Z.; Dai, S.; Fan, X.; Blom, D., Pennycook, S. J.; Wei, Y. *J Phys. Chem. B* **2001**, *105*, 6755.

11. Kresge, C. T.; Leonowicz, M. E.; Roth, W. J.; Vartuli, J. C.; Beck, J. S. *Nature* **1992**, *359*, 710.

12. Beck, J. S.; Vartuli, J. C.; Roth, W. J.; Leonowicz, M. E.; Kresge, C. T.; Schmitt, K. D.; Chu, C. T.-W.; Olsen, D. H.; Sheppard, E. W.; McCullen, B.; Higgins, J. B.; Schlenker, J. L. *J. Am. Chem. Soc.* **1992**, *114*, 10834.

13. Zhao, D.; Feng, J.; Huo, Q.; Melosh, N.; Fredrickson, G. H.; Chmelka, B. F.; Stucky, G. D. *Science* **1998**, *279*, 548.

14. Zhao, D.; Huo, Q.; Feng, J.; Chmelka, B. F.; Stucky, G. D. *J. Am. Chem. Soc.* **1998**, *120*, 6024.

15. Xu, W.; Akins, D. L. *J. Phys. Chem. B.*, **2001,** in press.

16. Xu, W.; Guo, H.; Akins, D. L. *J. Phys. Chem. B.*, **2001,** *105*, 1543.

17. Xu, W.; Guo, H.; Akins, D. L. *J. Phys. Chem. B.*, **2001**, *105*, 7686.

18. Spanier, J. E.; Robinson, R. D.; Zhang, F.; Chan, S.-W.; Herman, I. P. *Phys. Review B* **2001**, *64* 245407.

19. McBride, I. R.; Hass, K. C.; Poindexter, B. D.; Weber, W. H. *J Appl. Phys.* **1994**, *76*, 2435

20. Murphy, C. J.; Coffer, J. L. *Appl. Spectr.* **2002**, *56(1)*, 21A.

21. Kamalov, V. F.; Little, R.; Logunov, S. L.; M. A. El-Sayed. *J Phys. Chem.* **1996**, *100*, 6381.

22. Perna, G.; Capozzi, V.; Pagliara, S.; Ambrico, M. *Appl. Surf. Sci.* **2000**, *154*, 238.

23. Matsuura, D.; Kanemitsu, Y.; Kushida, T.; White, C.W.; Budai, J. D.; Meldrum, A. *Jpn. J. Appl. Phys.* **2000**, *40*, 2092.

Figure Captions

Figure I-1: XRD patterns of (A) calcined MCM-41, (B) modified MCM-41, and (C) CdS/MCM-41. Inset shows diffraction in region corresponding to CdS.

Figure I-2: XRD patterns of (A) calcined SBA-15, (B) modified SBA-15, and (C) CdS/SBA-15. Inset shows diffraction in region corresponding to CdS.

Figure I-3: Diffuse reflectance UV-vis spectra of CdS in various environments: (A) bulk CdS, (B) CdS/MCM-41, and (C) CdS/SBA-15.

Figure I-4: Room temperature resonant Raman spectra of (A) bulk CdS, excitation wavelength = 514.5 nm; (B) nanocomposite CdS/MCM-41, excitation wavelength = 457.9 nm.

Figure I-5: Dependence of relative intensities (I_{2LO}/I_{LO}) on excitation wavelength: (A) bulk CdS, (B) CdS/MCM-41.

Figure I-6: Low temperature (77 K) photoluminescence spectra of (A) bulk CdS, (B) CdS/SBA-15, and (C) CdS/MCM-41. Excitation wavelength and radiation power of 325 nm and 36 mW, respectively.

Figure I-7: Temperature and excitation power dependence of photoluminescence for nanocomposite CdS/SBA-15. (A) Room temperature with excitation power of 36 mW; (B) 77 K with excitation power of 3.6 mW; (C) 77 K with excitation power of 18 mW; and (D) 77 K with excitation power of 36 mW.

Table I-1: Fundamental and overtone Raman bands positions as a function of excitation frequency for bulk CdS and CdS occluded in MCM-41.

Samples	LO	2LO	I_{2LO}/I_{LO}	LO	2LO	I_{2LO}/I_{LO}	LO	2L+	I_{2LO}/I_{LO}
	λ_{ex} = 457.9 nm			λ_{ex} = 488.0 nm			λ_{ex} = 514.5 nm		
Bulk CdS	300	601	0.51	299	604	0.56	299	599	0.69
CdS/MCM-41	302	605	0.30	302	607	0.29	303	605	0.16

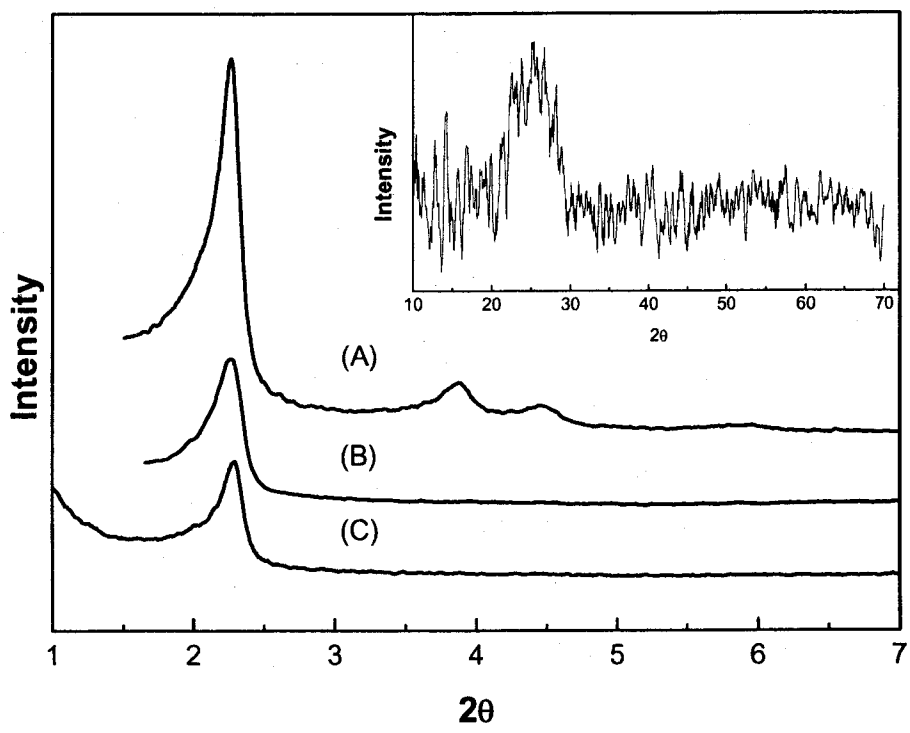

Figure I-1: XRD patterns of (A) calcined MCM-41, (B) modified MCM-41, and (C) CdS/MCM-41. Inset shows diffraction in region corresponding to CdS.

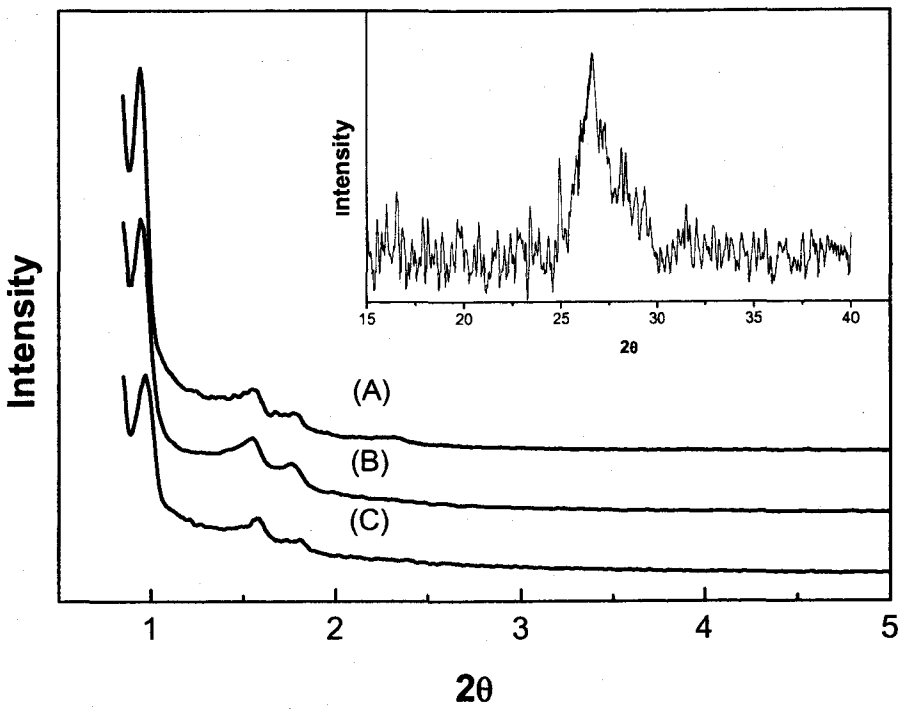

Figure I-2: XRD patterns of (A) calcined SBA-15, (B) modified SBA-15, and (C) CdS/SBA-15. Inset shows diffraction in region corresponding to CdS.

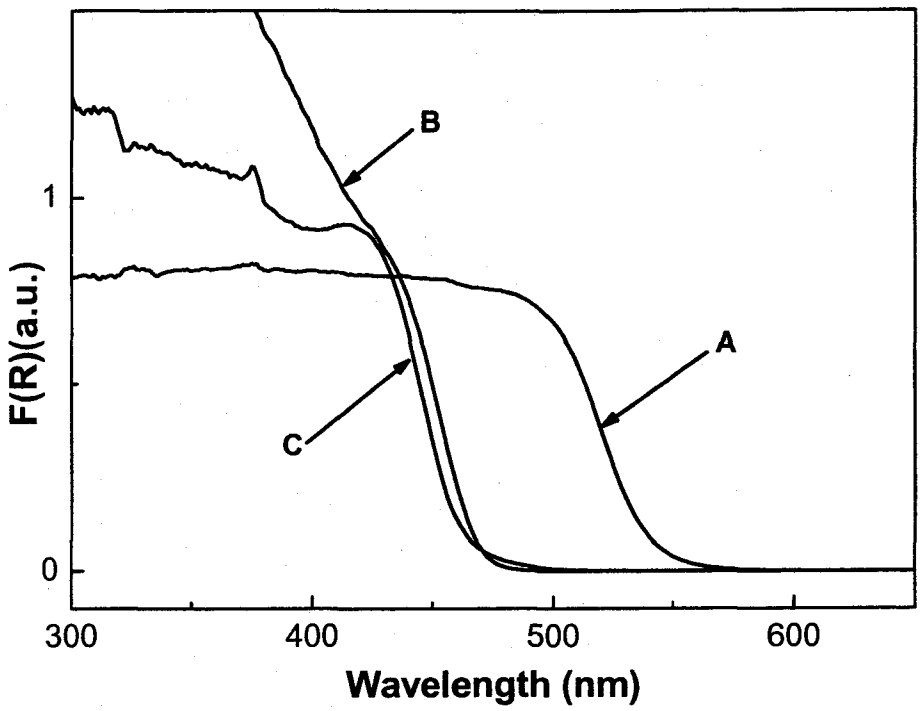

Figure I-3: Diffuse reflectance UV-vis spectra of CdS in various environments: (A) bulk CdS, (B) CdS/MCM-41, and (C) CdS/SBA-15.

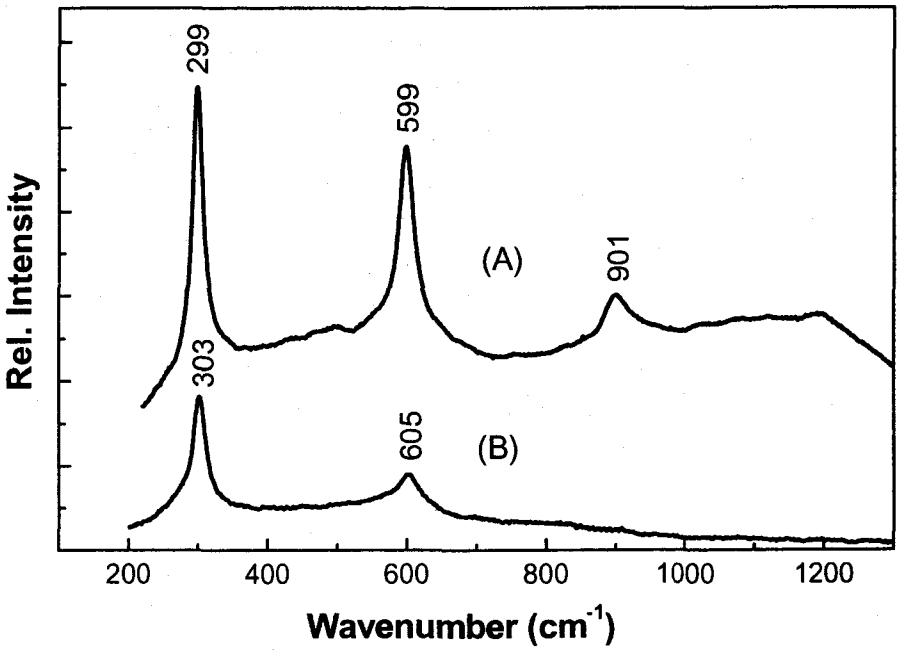

Figure I-4: Room temperature resonant Raman spectra of (A) bulk CdS, excitation wavelength = 514.5 nm; (B) nanocomposite CdS/MCM-41, excitation wavelength = 457.9 nm.

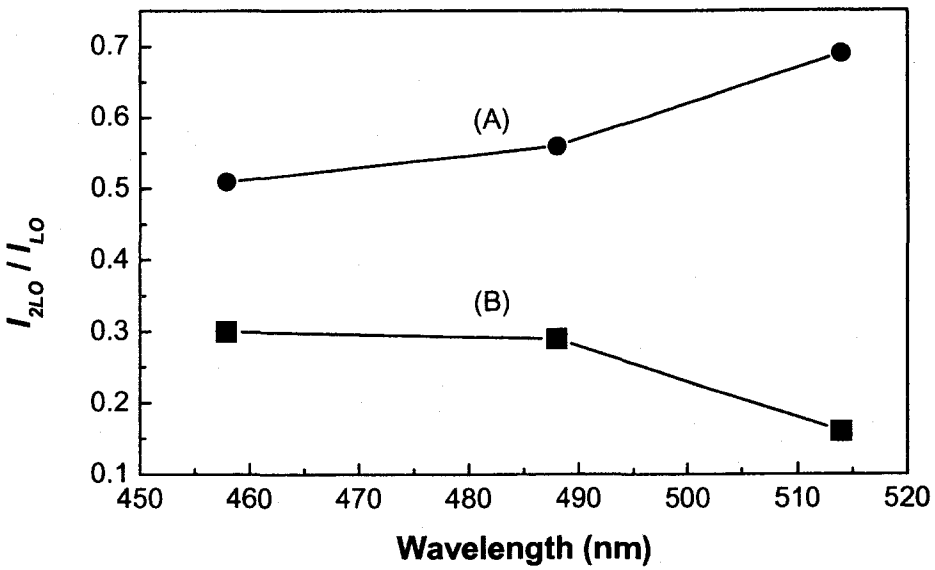

Figure I-5: Dependence of relative intensities (I_{2LO}/I_{LO}) on excitation wavelength: (A) bulk CdS, (B) CdS/MCM-41.

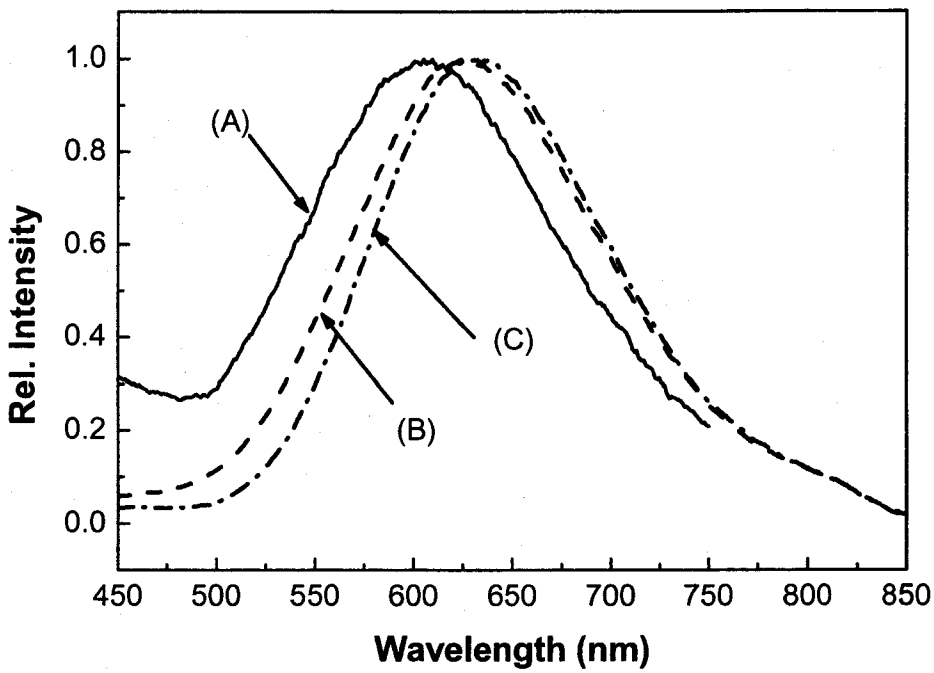

Figure I-6: Low temperature (77 K) photoluminescence spectra of (A) bulk CdS, (B) CdS/SBA-15, and (C) CdS/MCM-41. Excitation wavelength and radiation power of 325 nm and 36 mW, respectively.

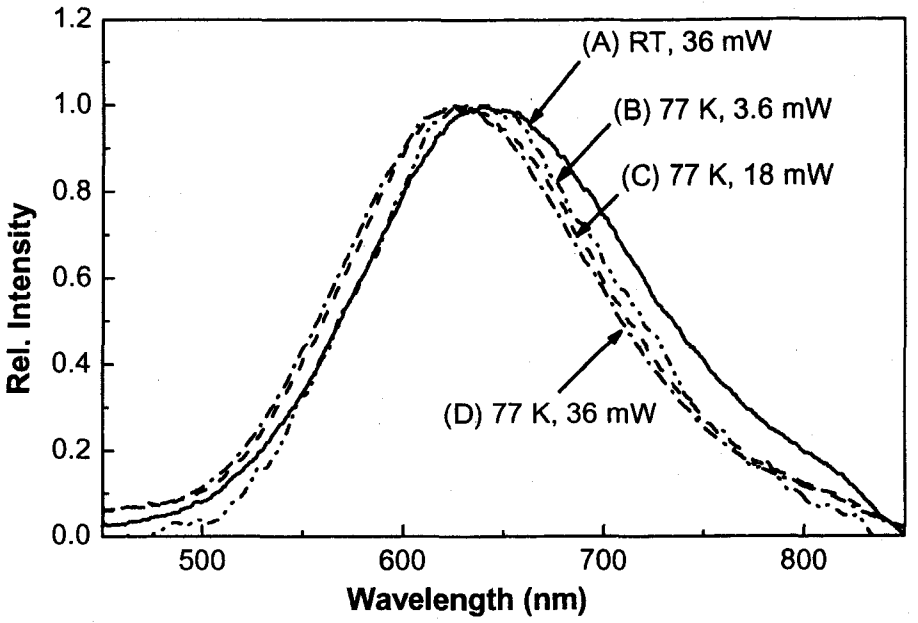

Figure I-7: Temperature and excitation power dependence of photoluminescence for nanocomposite CdS/SBA-15. (A) Room temperature with excitation power of 36 mW; (B) 77 K with excitation power of 3.6 mW; (C) 77 K with excitation power of 18 mW; and (D) 77 K with excitation power of 36 mW.

Chapter II: Solvent Effects on Luminescence and Photophysics of Cadmium Sulfide Nanoparticles Embedded in MCM-41: I. Steady State Spectroscopy Investigation

Abstract

Investigation of solvent effects on the optical properties of semiconductor nanoparticles is crucial for understanding the fundamental processes and dynamics of the photogenerated charge carriers within the particle. Nanoparticles synthesized by conventional methods are difficult to re-suspend in different solvents due to particle aggregation or precipitation. In this chapter, CdS nanoparticles with a size of ca. 2.1 nm have been synthesized within a surface modified MCM-41 through a gas-solid reaction developed in our lab. The protection provided by the rigid frame of MCM-41 prevents particles from aggregating when suspended in solvents. This offers an ideal system for investigating the solvent dependence of the optical properties of nanoparticles. . A variety of spectroscopy methods have been used to characterize the optical and electronic properties of CdS/MCM-41, as well as their dependence on solvent properties. It was found that the emission of CdS shifted to the red with

increases in the excitation wavelength. This is reminiscent of the "red-edge-excitation-shift" effect, which is typically observed for organic fluorophores when they have strong dipolar interaction with the solvent medium. For both protic and aprotic solvents, the emission maxima of CdS shifted to the longer wavelength with increases in the polarity of the solvent. Another interesting property found for CdS/MCM-41 is the emission polarization. The measured anisotropy depends on the polarity rather than viscosity of solvents, implying that the anisotropy is mainly determined by the rate of emission decay, not the rotation of the particle (Perrin equation). Surface modification of CdS with Cd^{2+} and S^{2-} was found to be effective to modulate the emission intensity and maximum, and the modulation did not show a strong dependence on the solvent. These results suggested that the surface sulfur vacancy dominates the emission of CdS/MCM-41.

I. Introduction

Semiconductor nanoparticles represent one of the most attractive nanostructures due to their tunable dimensional size, which falls into the transitional regime between individual molecules and their bulk counterparts. Nanoparticles retain the same crystalline structure as bulk crystals, but show unique size dependent physical and chemical properties; this phenomenon is known as the quantum *size effect*. This provides vast opportunities to control the optical and electronic properties of nanoparticles for applications in optoelectronics, magnetics, and biological labeling.[1-11] Compared with bulk semiconductor devices, the physical and optical properties of nanoparticles are sensitive to surface defects since the surface-to-volume ratio of particles increase dramatically with decreases in particle size below 5 nm. For a 2 nm CdS nanoparticle, more than 30% of the atoms are located at surface. In most cases, a broad emission band, rather than a sharp excitonic peak, is observed for nanoparticles, due to the surface trapping of the photogenerated charge carriers. Therefore, observation of the quantum size effect on luminescence requires that the particle surface be highly stabilized and controlled with appropriate capping groups.

On the other hand, the luminescence and photophysical properties of nanoparticles can be controlled by the surface conditions through doping, adsorption and coating.[1,2,9,12] However, such surface effects have mostly been investigated with the particles that were synthesized with capping ligands or stabilizers. These species surrounding the particle make the surface modification and the study of surface effects quite complicated. Furthermore, the as-synthesized particle systems are normally only stable in the original solvent. It is quite challenging to transfer the particle system from one solvent to the other without changing the particle size and

surface properties. The transfer process may cause breaking or distortion of the capping layers. This prevents the investigation of the solvent effects on the electronic and optical properties of the nanoparticles.

In this study, CdS nanoparticles were synthesized within the highly organized mesoporous material, MCM-41. The embedded particles were found to be stable and suspendable in a variety of solvents from dioxane (ε 2.2) to water (ε 80.2). Due to the protection of the rigid frame of MCM-41, no particle aggregation was found when nanoparticles were suspended in different solvents. This offers an ideal system for investigating the solvent dependence of the optical properties of nanoparticles. The small particle size (~ 2.0 nm, falling into the quantum size region), along with the one-dimensional channel structure of MCM-41, provides the potential possibility to develop such organized nanomaterials as optoelectronic nanodevices.[13-18]

The solvent effects referred to here can be considered as two facts. One is the direct modification of the particle surface by the solvent, i.e. the surface defect density and the electronic levels are different from solvent to solvent. The other can be referred to as the effect on the surface derivatization by other species, especially charged species. It has been suggested by previous studies and also implied in this work that the surface adsorption and the interfacial charge transfer of nanoparticles are dependent on the solvent properties.[2,19-21]

It has been found that properties such as the emission intensity, wavelength or lifetime of some of the semiconductor nanoparticles (e.g. CdS, Cd_3As_2) are sensitive to the properties of local environment, e.g. pH, solvent polarity, surface binding of amines, DNA, dendrimers and metal ions.[1,2,19,22-28] Such sensitivities lead to potential applications of these nanoparticles in biological labeling and probing. Nonetheless,

further study to pursue this goal requires a clear understanding of the surface effects on the photophysical properties and dynamics of charge carriers, which in turn requires a well defined or highly controlled surface condition. Excess of stabilizing species normally renders the surface too complicated to be investigated.

With certain surface modifications, such as dendrimer wrapping and Cd^{2+}-enrichment, CdS nanoparticles can show high emission anisotropy.[25-27] The origin of such a polarization property is open to question. To explore the surface dependence of the fluorescence anisotropy requires well-defined surface conditions and high re-suspendability in different solvents. The transition dipole of the particle might be dependent on the solvent polarity, and the rotational motion of the particle may depend on the solvent viscosity. It is very interesting to observe polarized emission (positive anisotropy) for CdS/MCM-41 nanoparticles in this study. Polarized emission is not common for nanoparticles, since normally the transition dipole of a round shape particle is close to zero. The emission anisotropy observed in this study is due to the one-dimensional electric field along the channel of MCM-41. In a few papers by Lackowicz,[25-27] the anisotropy was first observed for CdS particles with certain surface modifications. As suggested in these papers, constant positive anisotropy would provide the possibility of using such particles for biological labeling. Recently, Lin et al. developed an efficient drug delivery system with CdS/MCM-41 nanocomposite materials.[29] The high biological compatibility of MCM-41 materials opens an opportunity for developing the embedded CdS nanoparticles as biological sensors,[30,31] especially if the particle is detected with high emission anisotropy.[26,27]

II. Experimental Section

Materials and Methods. N-(2-aminoethyl)-3-(trimethoxysilyl) propylamine, hexadecyltrimethylammonium, sodium sulfide, cadmium acetate used for synthesis and surface modification of MCM-41 were obtained from Aldrich (Milwaukee, WI) and used as received. All the organic solvents were HPLC grade and used as received.

MCM-41 was prepared following the protocol previously developed in this laboratory, but without calcinations at the end.[13] The resulting mesoporous material was thus impregnated with the surfactant molecule, hexadecyltrimethylammonium, which was used as the synthesis template material. External surface passivation of MCM-41 was carried out by refluxing the as-synthesized sample in an ethanol solution of phenyltrimethoxysilane (ethanol : phenyltrimethoxysilane = 1:1 by volume) for 6 hours at room temperature, followed by removal of the encapsulated surfactant by washing the sample thoroughly with hot water and ethanol and then immersing it in a large volume of ethanol overnight and, lastly, rinsing it with ethanol five times.[15] The internal surface MCM-41 (now with external surface passivation) was functionalized by mixing ca. 1 g of the MCM-41 sample with 5 mL of N-(2-aminoethyl)-3-(trimethoxysilyl)propylamine in dry toluene for 12 hours at room temperature.[15] Synthesis of CdS nanoparticles in the externally passivated and internally functionalized MCM-41 was accomplished by the procedure described in one of our earlier papers.[13]

The surface cadmium-rich CdS nanoparticles were prepared by refluxing 0.5 g of the CdS/MCM-41 sample in 100 mL of ethanol containing 60 mg of cadmium

acetate for 10 h at 60 °C. The precipitate was filtered out and washed with 200 mL of ethanol to remove the excess unbound Cd^{2+} ions, followed by drying at 333 K in a vacuum oven. The surface sulfur-rich CdS nanoparticles were prepared by the same method, but with refluxing in an ethanol solution of sodium sulfide (1.2 g/100 mL).

Emission Measurement. Steady-state emission and excitation spectra were acquired using a SPEX Fluorolog-τ2 spectrofluorometer. For a typical emission measurement, 2 mg of CdS/MCM-41 was suspended in 10 mL of solvent, followed by 10 minutes of sonication. Emission anisotropy spectra were measured with a Jobin Yvon Fluorolog 3-22 spectrofluorometer with an internal Glan-Thompson polarizer.

III. Results and Discussion

Excitation and Emission Spectra in Different Media. The CdS nanoparticles embedded in the MCM-41 matrix (CdS/MCM-41) showed broad emission in both aqueous and organic solvents. Figure II-1A and II-1B showed the emission and excitation spectra of CdS/MCM-41 in methanol. The emission maxima were found to be dependent on the excitation wavelength (Figure II-1A). When longer excitation wavelengths were used, the emission shifted to the red, and at the same time the emission spectrum narrowed, i.e. the emission at shorter wavelengths was relatively decreased. This observation is consistent with previous reports for semiconductor nanoparticles,[27] but the explanation of this behavior has heretofore been unclear. Some studies attributed it to the heterogeneous distribution of particles of varying sizes, for which the longer wavelength selectively excites the larger particles that have smaller bandgap due to the quantum size effect. However, this does not seem to be the case depicted in Figure II-1A and B, if the particle size,

which can be estimated from both experimental measurements and theoretical calculations, is considered.[13,32] The most pronounced red shift was found at excitation wavelengths from 380 to 450 nm. This indicates a particle size range of~ 2.5 – 5.0 nm, which is larger than the pore size (~ 2.3 nm) of the substrate material, MCM-41.[13] In other words, the particles under investigation must be located outside the cavities of MCM-41. This is obviously not possible, because the particles were synthesized from the completely internally chelated Cd^{2+} ions through a gas-solid reaction. Indeed, the CdS particles synthesized in a previous study through a similar method were estimated using X-ray diffraction to be smaller than 2.1 nm in size.[13]

More likely, the emission shift shown in Figure II-1A was due to the well-known red edge excitation shift (REES), which has been observed for polar organic fluorophores in viscous solvents or frozen media.[33] The origin of the REES effect is attributed to the dipolar interaction of fluorophore with the polar solvent or media in both the ground and excited sates. Such strong interactions result in a decrease in the transition energy, a red shift in emission (Scheme 1). For a polar fluorophore, there exists a statistical distribution of the solvation states with decreased transition gap, depending on the extent of the dipolar interaction with solvents. The longer wavelength excitation selects for those fluorophores which have absorption transition at a lower energy. The prerequisite for REES is that the dipolar relaxation (reorientation) for the solvent shell be comparable or slower than the emission decay of the fluorophore molecule. This is normally achieved by using viscous solvents or frozen media in which the solvent molecules surrounding the fluorophore can hardly rotate and reorient. Under these conditions, a different population of the fluorophore states (solvent-relaxed states) is excited at a specific excitation wavelength, and the

difference in energy level (red-shifted emission wavelength) is maintained within the time scale of fluorescence lifetime. Some biologically related species, such as proteins, lipid membranes and micelles, provide highly viscous or rigid environments which often induce significant REES. Indeed, REES has been commonly used for probing the dynamic properties of these biological systems.[33]

In this study, CdS particles were embedded in the channel of MCM-41 powder. The rigid frame structure of MCM-41 offers little freedom for the dipole reorientation of the CdS particle. In such cases, the magnitude of REES depends mostly on the population of the fluorophores (here the CdS particles) which possess non-zero dipole moments and interact strongly with the media (i.e. the dipole gets stabilized upon interaction with polar media). The CdS particles with non-zero dipole moments are those close to the opening of the one-dimensional channels of MCM-41, where the surrounding dielectric field is not symmetric and thus causes the formation of a dipole moment along a fixed direction. Actually, such a fixed dipolar property is consistent with the observation of the polarized emission and excitation of CdS/MCM-41, which will be discussed later in this study.

Figure II-1B shows the excitation spectra of CdS/MCM-41 at different detection wavelengths. The REES effect can be seen clearly from this plot. The emission below 500 nm was mostly contributed by the central excitation of the CdS particle, while the emission at longer wavelengths was due more to the red edge excitation (Scheme 1). The excitation spectra at shorter wavelengths changes only slightly for different detection wavelengths, while the spectra at longer wavelengths shifts progressively with detection wavelength. The longer the emission wavelength detected, the more contribution from the red-edge excitation is seen.

It is expected that an increase in solvent viscosity or polarity would not enhance the REES effect of CdS/MCM-41, since the REES effect is mostly determined by the local environment of MCM-41 itself. This was confirmed by experiments in different solvents (both protic and aprotic) with different polarities. In methanol (Figure II-1), water (Figure II-S1, in supporting information), acetonitrile (Figure II-S2, in supporting information), and ethylene glycol (Figure II-2), the REES effect was found comparable. No significant difference was observed. Even in the frozen ethylene glycol (77 K), the REES effect was found to be very similar to that in fluid solvents (Figure II-2). These experiments imply that the REES effect found for CdS/MCM-41 is due to the local dielectric interaction between the CdS particle and the cavity surface of MCM-41. Indeed, the strong dielectric effect within the MCM-41 cavity was also implied from our previous study for the catalyzed reduction of MV^{2+} by S^{2-} ions, which are adsorbed inside the channels.[34]

It is noteworthy to mention that the emission of CdS/MCM-41 is dependent to some extent on temperature (Figure II-2). Compared emissions at 77 K, the emission at room temperature significantly shifted to the blue by 17 nm. Actually, the shift was mainly caused by the relative increase in emission at short wavelengths. This is likely due to the repopulation of the red-edge excited state up to the central excited state (Scheme 1). Such a repopulation process is favored at higher temperatures.[35,36] It seems that solvent molecules are crucial for the relaxation process to take place. The dynamic interaction (collision) between CdS particles and solvent molecules may provide additional energy for the phonon-exciton interaction within the particle. Indeed, the reverse relaxation of the excited state of semiconductor particles was found before in fluid media.[35-37] In contrast, for the dry CdS/MCM-41 sample

(powder spread on quartz surface), the emission showed no shift with temperature (see Chapter IV). From 77 K to room temperature, there was only a minimal shift in emission spectra.

Solvent effect on emission. The CdS particles stabilized in MCM-41 matrixes provide a unique system for studying the solvent effect of optical properties of semiconductor nanoparticles. The rigid and non-connected one-dimensional channel structure protects the particles against aggregation or precipitation into solution. The CdS/MCM-41 nanoparticles synthesized in this study have been successfully suspended in a wide variety of solvents, without breaking up the particles from the MCM-41 matrixes. Figure II-3 shows the emission spectra of CdS/MCM-41 suspended in water and different alcohols. The emission shifted gradually to the blue from water (ε = 80.2), with the highest dielectric constant, to butanol (ε = 17.8), with the lowest dielectric constant. Since both water and the alcohols are typical protic solvents, the emission shift observed here is likely due to the difference of solvent polarity (dielectric constant). This is reminiscent of the well-known solvent dependence of fluorescence of polar organic fluorophores.[33] Polar environments favor the relaxation of the excited state of CdS to the lower and more stable state, from which it decays to the ground state with longer wavelength emissions. The similar emission shift of CdS/MCM-41 was also found in aprotic solvents (see support information, Figure II-S3).

A notable solvent effect on emission is normally observed for the fluorophores with transition moments (typically for polar molecules). As discussed above, in the case of CdS/MCM-41, nanoparticles with significant dipole moments are those localized in an asymmetric electric field (most likely the ones close to the

MCM-41 channel opening). If the fact that the close-to-opening particles are more exposed to excitation light is considered, the detected emission of CdS/MCM-41 should be somehow dominated by these particles. To this end, emission at longer wavelengths should be mainly due to the decay of the dipolar excited state, which can be either relaxed from the higher equilibrium central excited state or directly generated by red-edge excitation (Scheme 1). Such a dipolar excited state must be sensitive to the solvent polarity, if the fact that CdS particles close to the channel opening interact closely with solvent molecules is considered. Indeed, as shown in Figure II-3, the solvent effect of CdS/MCM-41 was found mainly for the emission at longer wavelengths, while a relatively weak effect was observed for the emission at shorter wavelengths, where the emission was assumed to be due to the central (neutral) excited states. The solvent dependent emission of CdS/MCM-41 found in this study will provide an opportunity for developing a new class of fluorescence sensor for local environment properties.

Polarized emission in different media. It is very rare to observe polarized emission for semiconductor nanoparticles. This is mainly owing to their spheroidal shape, for which the transition dipole is negligible. However, Lakowicz and Murphy et al. have recently observed significant anisotropy for the emission of CdS nanoparticles capped with dendrimer or polyphosphate.[25-27] Although the origin of such polarized emission remains unclear, the positive anisotropy would create an opportunity to use those particles for hydrodynamic probing. While there have been some other reports on the polarized emission of semiconductor nanoparticles, the reported polarization was either negative or turned to be negative in a way implying a rapid process occurring inside the particle.[36,38] Significant positive anisotropies were

normally observed for prolate nanoparticles or nanorods,[39-41] where the transition dipole is generated along the elongated axis.

Surprisingly, significant polarization was found for the CdS/MCM-41 nanoparticles in this study (Figure II-4). The anisotropy was markedly dependent on the emission wavelength, which decreased gradually with wavelength across the whole emission spectrum. This is reminiscent of the case of organic fluorophores in viscous media. For organic molecules, the emission anisotropy normally does not show wavelength dependence in completely vitrified solvents, where solvent relaxation does not occur. Only in the presence of solvent relaxation (typically viscous environments) does the anisotropy become wavelength dependent, usually decreasing across the whole emission spectrum. This is because the average lifetime of emission is longer for the longer wavelengths, and the longer lifetime affords lower anisotropy as described by the Perrin equation,[33]

$$r = r_0 /(1 + \tau / \theta) \qquad (1)$$

where r is the measured anisotropy, r_0 the fundamental anisotropy, τ the average lifetime, and θ the rotational correlation time.

The excitation anisotropy spectrum of CdS (emission detected at 560 nm) is also shown in Figure II-4. At excitation wavelengths above 410 nm, the anisotropy increases rapidly with increasing excitation wavelength, while with the excitation below 410 nm, the anisotropy was found to depend little on the excitation wavelength. This manner is consistent with the dependence of the emission spectral shift on the excitation wavelength (Figure II-1A), where noticeable spectral shifts were only observed for excitation above 400 nm. The similar excitation wavelength dependence suggests that the emission polarization and spectral shifts are likely due

to the same property of CdS/MCM-41. As discussed above, the one-dimensionally directed electric field within the channel of MCM-41 may cause significant dipole moments within the embedded CdS nanoparticles, especially for those located close to the channel opening, where the electric field is highly asymmetric. The local electric field effect on the dipole of semiconductor nanoparticles was also suggested and implied by the previous work from the Bawendi lab.[40]

There may be other explanations for the origin of the emission polarization of CdS/MCM-41. For example, it may be due to the CdS particles formed in prolate spherical shapes, which may quite possibly be formed in the one-dimensional restricted matrix of MCM-41. However, this assumption is not consistent with the XRD measurements that were reported by us and others.[13,15] For the CdS nanocrystals made in MCM-41 matrixes, the diffraction peak was dominated by the (100) peak, whereas the contribution from (002) diffraction was minimal. Since the (002) peak normally indicates the preferential crystal elongation along the c-axis of wurtzite,[42-45] the weak (002) peak observed for CdS/MCM-41 implies that most of the particles formed inside MCM-41 are spherical, rather than prolate in shape.

Typically for organic fluorophores, the emission anisotropy can be enhanced in viscous solvents. This is because the anisotropy is proportional to the molecule rotational correlation time (Equation 4), which in turn is proportional to the solvent viscosity. To determine if the observed anisotropy of CdS/MCM-41 is also dependent on the solvent viscosity, we measured the emission anisotropy spectra in a series of protic solvents with different viscosities. The results are shown in Figure II-5. Interestingly, no obvious viscosity dependence was found for the emission anisotropy of CdS/MCM-41. The anisotropy in ethylene glycol is lower than that in methanol

and water, although the viscosity of the former is much higher than that of the latter. Within the frozen ethylene glycol (77 K), the anisotropy is diminished and almost undetectable, while for organic fluorophores the anisotropy generally reaches the highest when embedded in rigid media.[33] The independence of anisotropy on viscosity is not unexpected, if the restricted rotation of CdS within MCM-41 is considered. Since the restricted rotation is already much slower than the rate of emission decay, further increases in media viscosity would not lead to additional increases in the emission anisotropy.

The solvent dependence of anisotropy shown in Figure II-5 is likely due to the difference in polarity of the solvents, since the change of anisotropy is fairly consistent with the change of dielectric constant of the solvents, from water (80.2), to methanol (32.7) and ethylene glycol (37.7), and ethylene glycol at 77 K (< 4). The polarity effect on emission polarization is consistent with the Perrin equation (Equation 1), which describes the anisotropy as a function of emission lifetime. As will be reported in the next chapter,[46] the emission lifetime of CdS/MCM-41 is strongly dependent on the solvent polarity. At all wavelengths across the emission spectrum, the lifetime is generally shorter in solvents with higher dielectric constants. The shorter lifetime affords higher anisotropy as described by the Perrin equation (Equation 1).

Effects of surface modification. The solvent effect on the photochemical properties of CdS/MCM-41 could be different for different modifications of the particle surface. In this study, the CdS surface was modified with either Cd^{2+} or S^{2-} ions, which created a surface sulfur or cadmium vacancy. It is well accepted that the emission from the sulfur vacancy is located at longer wavelengths, while the decay

from the cadmium vacancy emits at shorter wavelengths.[1] This is consistent with the results shown in Figure II-6, where a significant blue-shift was observed for the sample modified with S^{2-} ions. Compared to the as-synthesized CdS/MCM-41, the emission of the sulfur-rich CdS particle shifted to the blue by about 17 nm. Upon addition of 5 mM S^{2-} ions to the sulfur-rich sample, the emission shifted even further to the shorter wavelengths, but mostly by decreases of the emission at longer wavelengths (Figure II-6). This is because the higher concentration of S^{2-} ions blocks more sulfur vacancies which might originally locate deeper on the surface.

It is interesting to observe that the cadmium-rich CdS did not show a significant emission shift compared to the as-synthesized sample. Addition of 5 mM Cd^{2+} ions to the cadmium-rich sample caused only a minor decrease in emission at the shorter wavelengths. This insensitivity of emissions upon Cd^{2+} modification suggests that the surface of the as-synthesized CdS particle is somehow in the cadmium-rich form. This is not surprising if considering the fact that the inner surface of the channel of MCM-41 is covered with free amine moieties, which are likely to be chelated with the surface cadmium ions. Such a surface chelation somehow prevents the saturation with sulfur ions, especially when the synthesis of CdS is through gas-solid reaction using H_2S (see experimental section). Indeed, the optical properties (e.g. emission anisotropy) observed for the as-synthesized CdS/MCM-41 is consistent with those observed for the cadmium-rich CdS nanoparticles synthesized in homogeneous aqueous solutions.[26]

The sulfur-rich CdS/MCM-41 was also measured in methanol and acetonitrile. As observed in water, the emission was blue shifted compared to that of the as-synthesized CdS/MCM-41 (see support information, Figure II-4 and II-5).

However, for the cadmium-rich sample, the emission spectrum in these two solvents showed little shift compared to that of the as-synthesized CdS/MCM-41, implying again that the surface of the as-synthesized particle was already in the cadmium-rich form.

IV. Conclusions

Semiconductor nanoparticles share many common optical and electronic properties with organic fluorophores, such as UV-vis absorption and emission, electron and energy transfer, and emission polarization. In this study, the solvent dependence of these properties was systematically investigated for CdS nanoparticles embedded in MCM-41 matrixes. Similar to their molecular counterparts, semiconductor nanoparticles show a strong solvent dependence for emission spectra and emission polarization. A significant red-edge-excitation-shift (REES) was found for CdS/MCM-41, likely due to the dipolar interaction between CdS particles and the local electric field within the channel of MCM-41. The observed solvent effect on emission was resulted mainly from the solvent relaxation of the red-edge excited state. This is reminiscent of the general solvent effect on the emission spectra of polar organic fluorophores. The CdS/MCM-41 particle was also found to have polarized emission, and the anisotropy is strongly dependent on the solvent polarity. The polarized emission observed provides an opportunity to use these nanocomposites for biological probing.

V. Acknowledgment.

This work was supported by the NSF and DoD-ARO, in part, through the following awards: (1) NSF-IGERT program under grant DGE-9972892, (2) NSF-MRSEC program under grant DMR-0213574, and (3) DoD-ARO under Cooperative

Agreement DAAD19-01-1-0759. I am deeply indebted to Prof. Akins for his generous and kind support, Prof. Turro and Dr. Jockusch for their kind help in the measurement, and Prof. Zang for his valuable discussion in preparation of this manuscript.

References

(1) Henglein, A. *Chem. Rev.* **1989**, *89*, 1861.

(2) Kamat, P. V. *Chem. Rev.* **1993**, *93*, 267.

(3) Zhang, J. Z. *J. Phys. Chem. B* **2000**, *104*, 7239.

(4) Zhang, J. Z. *Acc. Chem. Res.* **1997**, *30*, 423.

(5) Bruchez Jr, M.; Moronne, M.; Gin, P.; Weiss, S.; Alivisatos, A. P. *Science* **1998**, *281*, 2013.

(6) Empedocles, S.; Bawendi, M. *Acc. Chem. Res.* **1999**, *32*, 389.

(7) Huynh, W. U.; Dittmer, J. J.; Alivisatos, A. P. *Science* **2002**, *295*, 2425.

(8) Nirmal, M.; Dabbousi, B. O.; Bawendi, M. G.; Macklin, J. J.; Trautman, J. K.; Harris, T. D.; Brus, L. E. *Nature* **1996**, *383*, 802.

(9) Nirmal, M.; Brus, L. E. *Acc. Chem. Res.* **1998**, *32*, 407.

(10) Redl, F. X.; Cho, K. S.; Murray, C. B.; O'Brien, S. *Nature* **2003**, *423*, 968.

(11) Shim, M.; Guyot-Sionnest, P. *Nature* **2000**, *407*, 981.

(12) Chestnoy, N.; Harris, T. D.; Hull, R.; Brus, L. E. *J. Phys. Chem.* **1986**, *90*, 3393.

(13) Xu, W.; Liao, Y.; Akins, D. L. *J. Phys. Chem. B* **2002**, *106*, 11127.

(14) Chae, W.-S.; Ko, J.-H.; Hwang, I.-W.; Kim, Y.-R. *Chem. Phys. Lett.* **2002**, *365*, 49.

(15) Zhang, Z.; Dai, S.; Fan, X.; Blom, D. A.; Pennycook, S. J.; Wei, Y. *J. Phys. Chem. B* **2001**, *105*, 6755.

(16) Wellmann, H.; Rathousky, J.; Wark, M.; Zukal, A.; Schulz-Ekloff, G. *Micropo. Mesopor. Mater.* **2001**, *44-45*, 419.

(17) Martin-Palma, R. J.; Hernandez-Velez, M.; Diaz, I.; Villavicencio-Garcia, H.; Garcia-Poza, M. M.; Martinez-Duart, J. M.; Perez-Pariente, J. *Mater. Sci. & Eng., C: Biomimetic and Supramolecular Systems* **2001**, *C15*, 163.

(18) Hirai, T.; Okubo, H.; Komasawa, I. *J. Phys. Chem. B* **1999**, *103*, 4228.

(19) Pradhan, N.; Efrima, S. *J. Am. Chem. Soc.* **2003**, *125*, 2050.

(20) Fischer, C.-H.; Henglein, A. *J. Phys. Chem.* **1989**, *93*, 5578.

(21) Ramsden, J. J.; Webber, S. E.; Graetzel, M. *J. Phys. Chem.* **1985**, *89*, 2740.

(22) Dannhauser, T.; O扒eil, M.; Johansson, K.; Whitten, D.; McLendon, G. *J. Phys. Chem.* **1986**, *90*, 6074.

(23) Landes, C. F.; Braun, M.; El-Sayed, M. A. *J. Phys. Chem. B* **2001**, *105*, 10554.

(24) Kumar, A.; Mital, A. S. *J. Colloid Interface Sci.* **2001**, *240*, 459.

(25) Lakowicz, J. R.; Gryczynski, I.; Piszczek, G.; Murphy, C. J. *J. Phys. Chem. B* **2002**, *106*, 5365.

(26) Lakowicz, J. R.; Gryczynski, I.; Gryczynski, Z.; Nowaczyk, K.; Murphy, C. J. *Anal. Biochem.* **2000**, *280*, 128.

(27) Lakowicz, J. R.; Gryczynski, I.; Gryczynski, Z.; Murphy, C. J. *J. Phys. Chem. B* **1999**, *103*, 7613.

(28) Sooklal, K.; Hanus, L., H.; Ploehn, H., J.; Murphy, C., J. *Adv. Mater. (Weinheim, Germany)* **1998**, *10*, 1083.

(29) Lai, C.-Y.; Trewyn, B. G.; Jeftinija, D. M.; Jeftinija, K.; Xu, S.; Jeftinija, S.; Lin, V. S. Y. *J. Am. Chem. Soc.* **2003**, *125*, 4451.

(30) Mahtab, R.; Rogers, J. P.; Murphy, C. J. *J. Am. Chem. Soc.* **1995**, *117*, 9099.

(31) Mahtab, R.; Rogers, J. P.; Singleton, C. P.; Murphy, C. J. *J. Am. Chem. Soc.* **1996**, *118*, 7028.

(32) Brus, L. *J. Phys. Chem.* **1986**, *90*, 2555.

(33) Lakowicz, J. R. *Principles of Fluorescence Spectroscopy, 2nd.* Kluwer Academic/Plenum, *New York* **1999**.

(34) Liao, Y.-T.; Zang, L.; Akins, D. *Catal. Comm.* **2005**, *6*, 141.

(35) O'Neil, M.; Marohn, J.; McLendon, G. *J. Phys. Chem.* **1990**, *94*, 4356.

(36) Bawendi, M. G.; Carroll, P. J.; Wilson, W. L.; Brus, L. E. *Journal of Chem. Phys.* **1992**, *96*, 946.

(37) Eychmuller, A.; Hasserlbarth, A.; Katsikas, L.; Weller, H. *Ber. Bunsenges. Phys. Chem* **1991**, *95*, 79.

(38) Chamarro, M.; Gourdon, C.; Lavallard, P.; Lublinskaya, O.; Ekimov, A. I. *Physical Review B: Condensed Matter* **1996**, *53*, 1336.

(39) Empedocles, S. A.; Neuhauser, R.; Bawendi, M. G. *Nature* **1999**, *399*, 126.

(40) Empedocles, S. A.; Bawendi, M. G. *Science* **1997**, *278*, 2114.

(41) Hu, J.; Li, L.-S.; Yang, W.; Manna, L.; Wang, L.-W.; Alivisatos, P. *Science* **2001**, *292*, 2060.

(42) Yang, J.; Zeng, J.-H.; Yu, S.-H.; Yang, L.; Zhou, G.-E.; Qian, Y.-T. *Chem. Mater.* **2000**, *12*, 3259.

(43) Ye, C.; Meng, G.; Wang, Y.; Jiang, Z.; Zhang, L. *J. Phys. Chem. B* **2002**, *106*, 10338.

(44) Manna, L.; Scher, E. C.; Li, L.-S.; Alivisatos, P. A. *J. Am. Chem. Soc.* **2002**, *124*, 7136.

(45) Murray, C. B.; Noms, D. J.; Bawendi, M. G. *J. Am. Chem. Soc.* **1993**, *115*, 8706.

(46) Liao, Y.-T.; Zang, L.; Akins, D. *the second paper of this series, submitted simultaneously with this manuscript.*

Figure Captions

Figure II-1: (A) Excitation wavelength dependence of emission spectra of CdS/MCM-41 suspended in methanol: 330 nm (solid), 380 nm (dot), 400 nm (dash), 420 nm (dash-dot). (B) Excitation spectra at different detection wavelengths: 500 nm (solid), 540 nm (dot), 560 nm (dash), 580 nm (dash-dot).

Figure II-2: (Right) Emission spectra of CdS/MCM-41 suspended in ethylene glycol at 77 K excited at 360 nm (solid), 380 nm (dash), 420 nm (dash-dot); Emission spectrum at room temperature, excited at 380 nm (dot). (Left) Excitation spectrum at detection wavelength 500 nm.

Figure II-3: Emission spectra of CdS/MCM-41 in water and different alcohol solvents: (from left to right) water, methanol, ethanol, 1-propanol, 1-butanol. Excitation wavelength: 350 nm.

Figure II-4: Excitation spectrum (detected at 560 nm) and emission spectrum (excited at 380 nm) of CdS/MCM-41 in water. Also shown are the excitation and emission anisotropy spectra under the same conditions

Figure II-5: Emission anisotropy spectra of CdS/MCM-41 in different solvents and at different temperatures: water (■), methanol (●) and ethylene glycol (▲) at room temperature, and ethylene glycol at 77 K (▼). Excitation wavelength: 380 nm.

Figure II-6: Normalized emission spectra of CdS/MCM-41 with different surface modification in water: as-synthesized sample (solid), surface cadmium-rich (dot),

surface cadmium-rich plus 5 mM of Cd^{2+} (dash), surface sulfur-rich (middle), and surface sulfur-rich plus 5 mM of S^{2-} (left). Excitation wavelength: 350 nm.

Figure II-S1: (A) Excitation wavelength dependence of emission spectra of CdS/MCM-41 suspended in water: 340 nm (solid), 380 nm (dot), 400 nm (dash), 420 nm (dash-dot).

Figure II-S1: (B) Excitation spectra of emission spectra of CdS/MCM-41 suspended in water at different detection wavelengths: 540 nm (solid), 560 nm (dot), 580 nm (dash), 600 nm (dash-dot).

Figure II-S2: (A) Excitation wavelength dependence of emission spectra of CdS/MCM-41 suspended in acetonitrile: 320 nm (solid), 380 nm (dot), 400 nm (dash), 420 nm (dash-dot).

Figure II-S2: (B) Excitation spectra of emission spectra of CdS/MCM-41 suspended in acetonitrile at different detection wavelengths: 500 nm (solid), 540 nm (dot), 560 nm (dash), 580 nm (dash-dot).

Figure II-S3: Emission spectra of CdS/MCM-41 in different aprotic solvents: (from left to right) dioxane, THF, DMF, DMSO. Excitation wavelength: 350 nm.

Figure II-S4: Normalized emission spectra of CdS/MCM-41 with different surface modification in methanol: as-synthesized sample (solid), surface cadmium-rich (dash), surface sulfur-rich (dot). Excitation wavelength: 350 nm.

Figure II-S5: Normalized emission spectra of CdS/MCM-41 with different surface modification in actonitrile: as-synthesized sample (solid), surface cadmium-rich (dash), surface sulfur-rich (dot). Excitation wavelength: 350 nm.

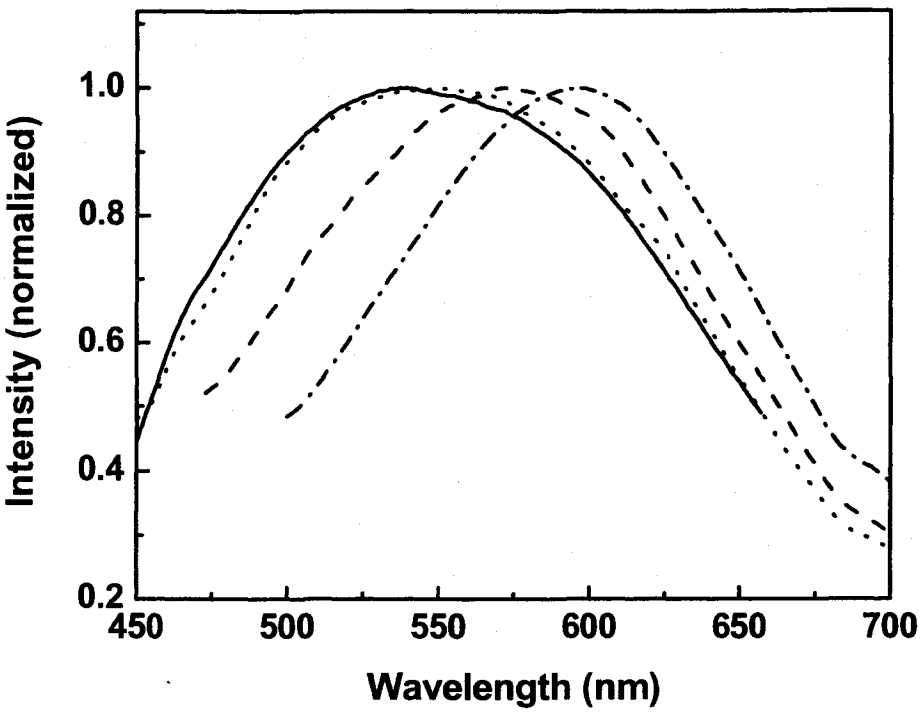

Figure II-1: (A)

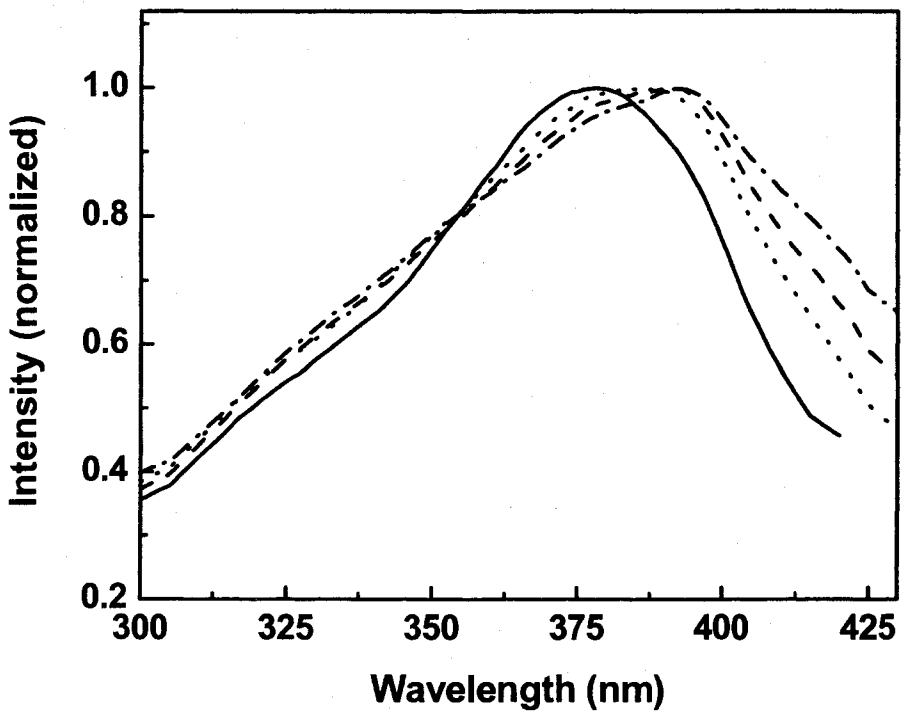

Figure II-1: (B)

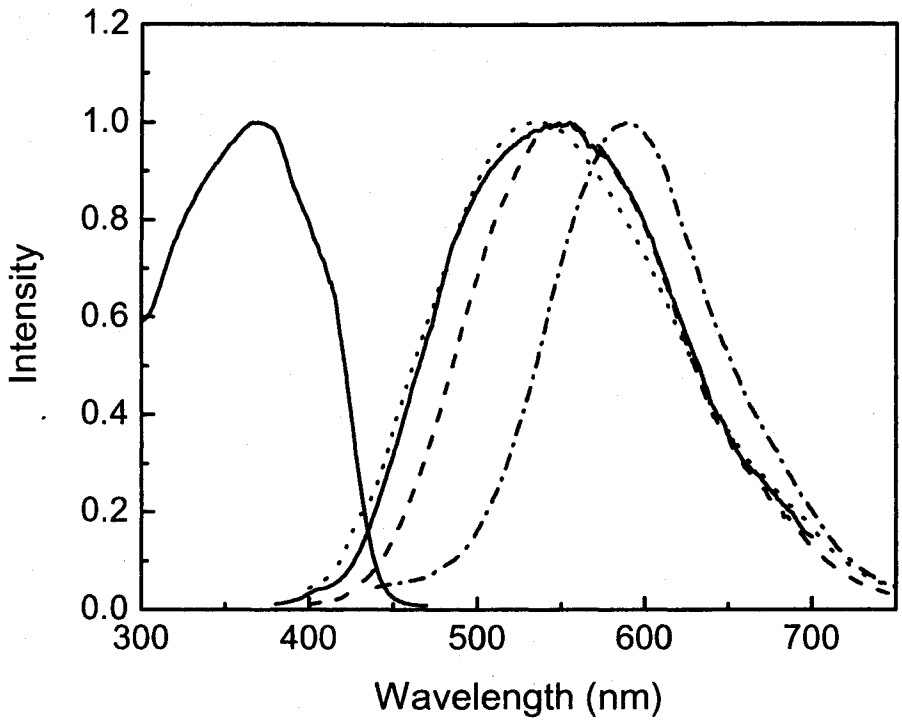

Figure II-2:

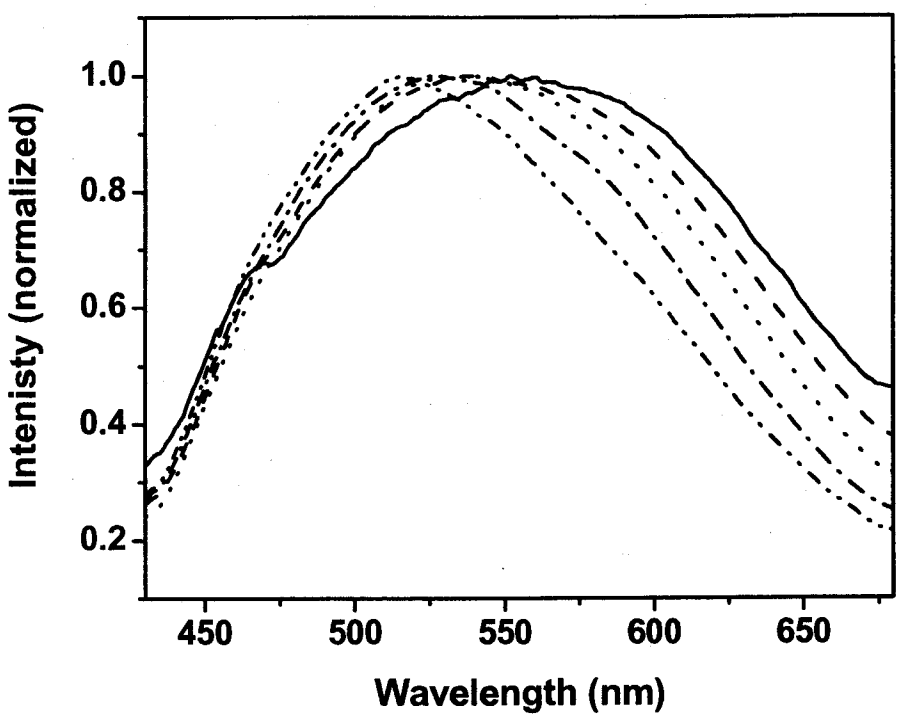

Figure II-3

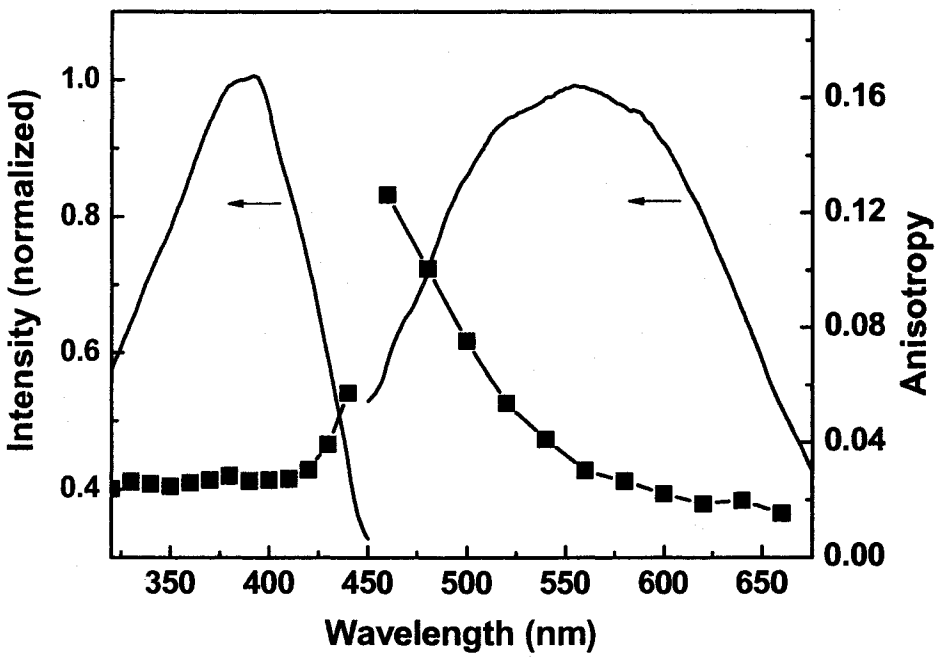

Figure II-4

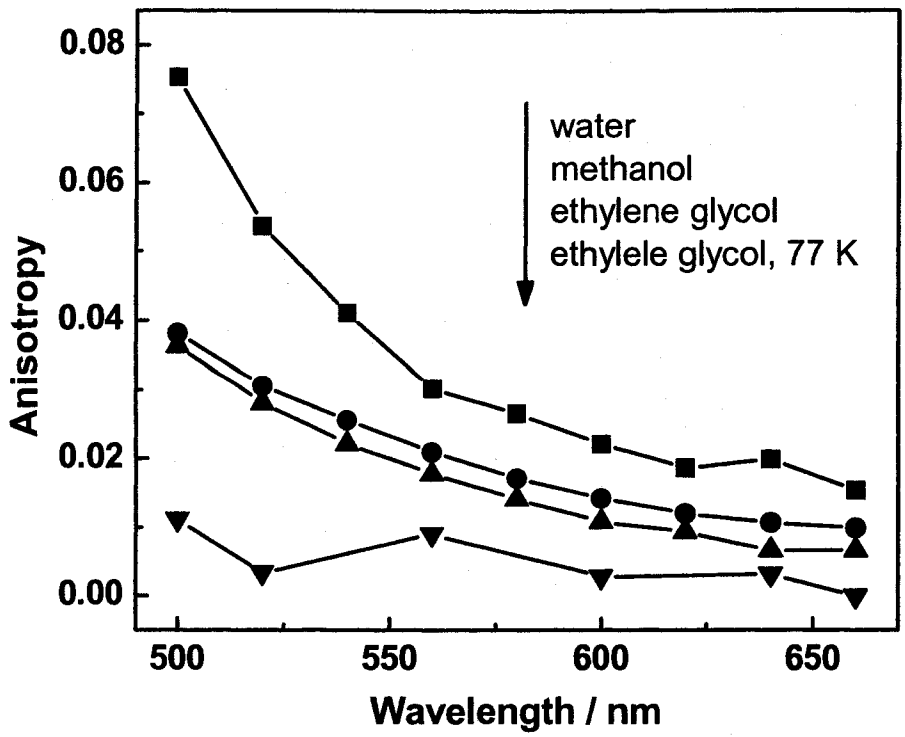

Figure II-5

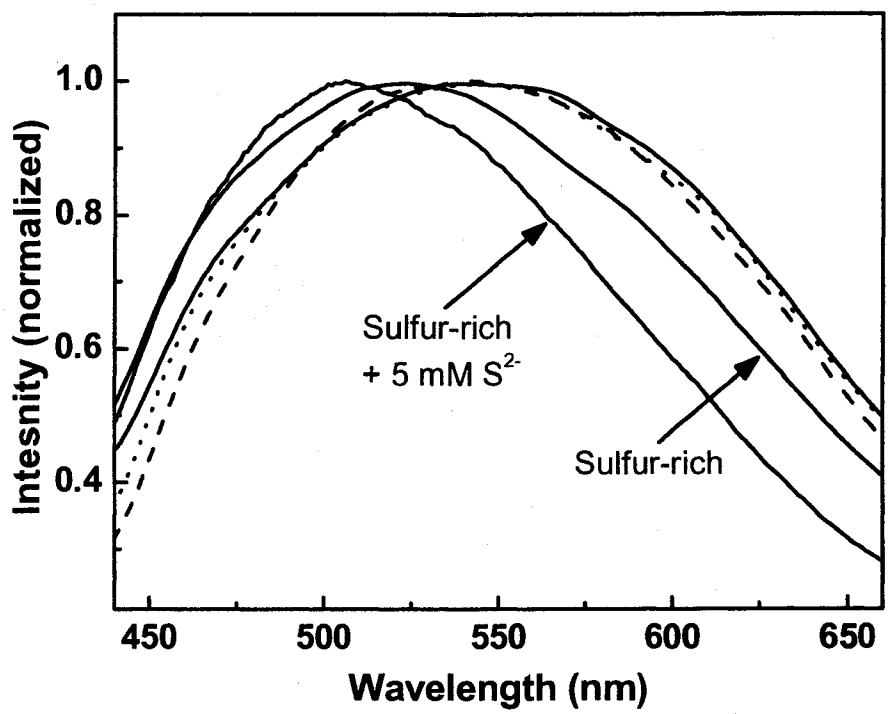

Figure II-6

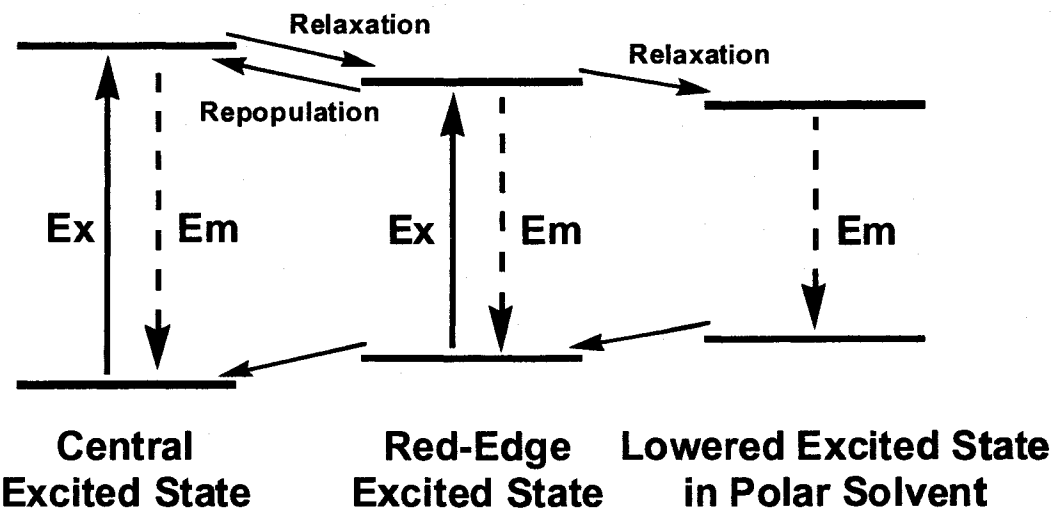

Scheme II-1

Supporting Information for

Chapter II. Solvent Effects on Luminescence and Photophysics of CdS Nanoparticles Embedded in MCM-41: I. Steady State Spectroscopy Investigation

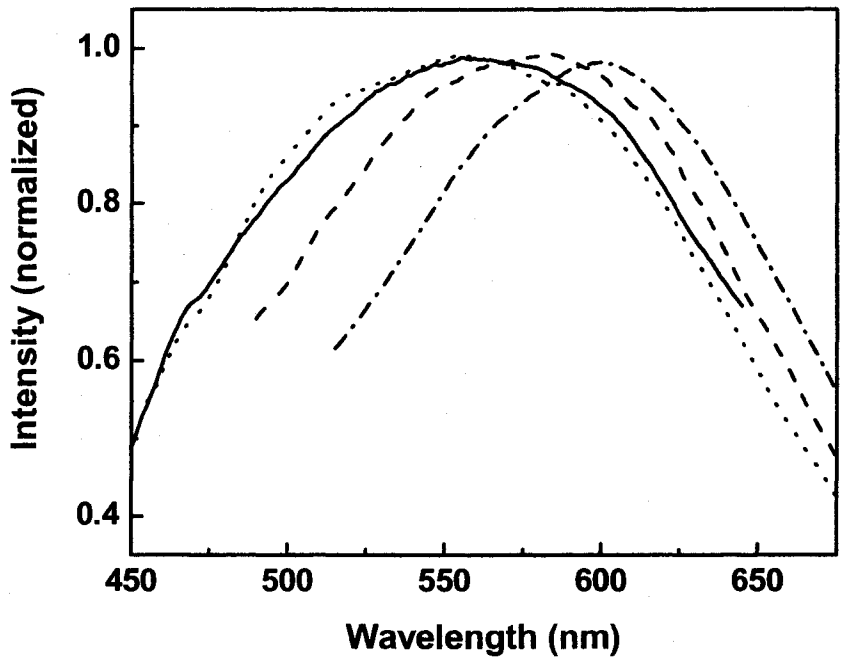

Figure II-S1: (A) Excitation wavelength dependence of emission spectra of CdS/MCM-41 suspended in water: 340 nm (solid), 380 nm (dot), 400 nm (dash), 420 nm (dash-dot).

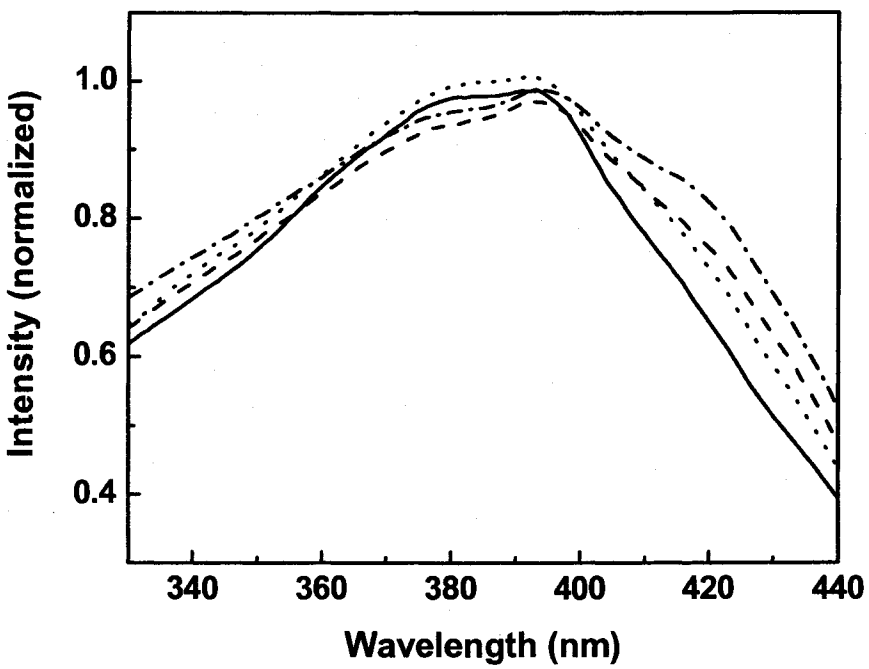

Figure II-S1: (B) Excitation spectra of emission spectra of CdS/MCM-41 suspended in water at different detection wavelengths: 540 nm (solid), 560 nm (dot), 580 nm (dash), 600 nm (dash-dot).

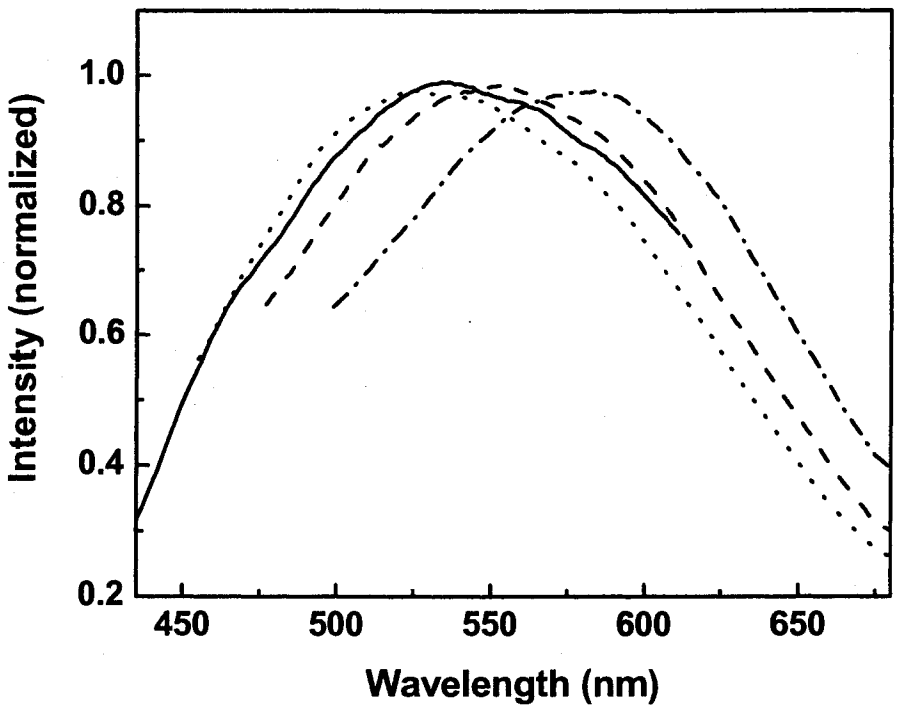

Figure II-S2: (A) Excitation wavelength dependence of emission spectra of CdS/MCM-41 suspended in acetonitrile: 320 nm (solid), 380 nm (dot), 400 nm (dash), 420 nm (dash-dot).

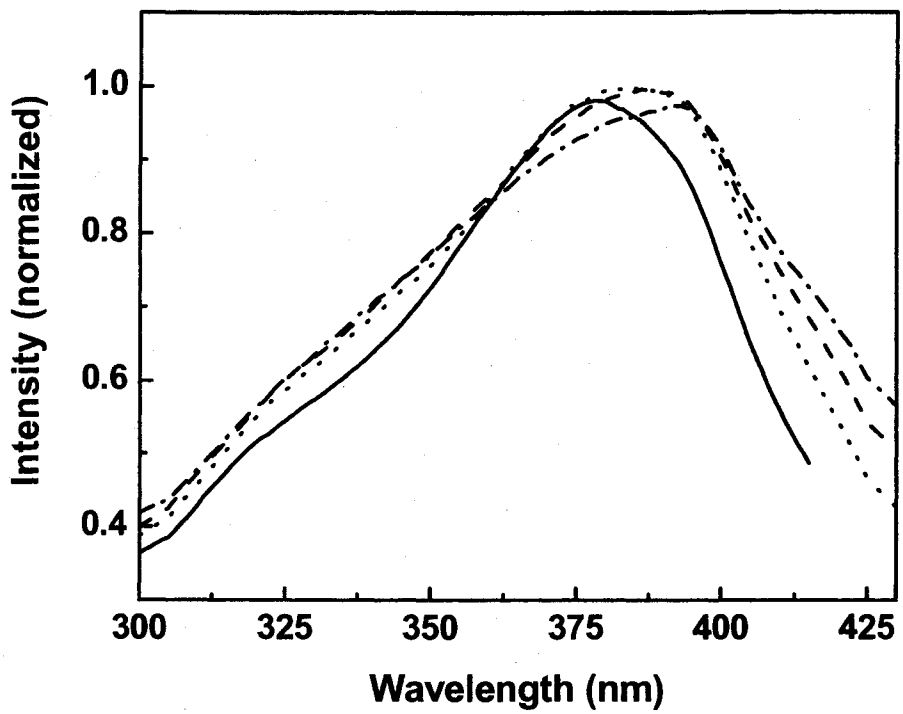

Figure II-S2: (B) Excitation spectra of emission spectra of CdS/MCM-41 suspended in acetonitrile at different detection wavelengths: 500 nm (solid), 540 nm (dot), 560 nm (dash), 580 nm (dash-dot).

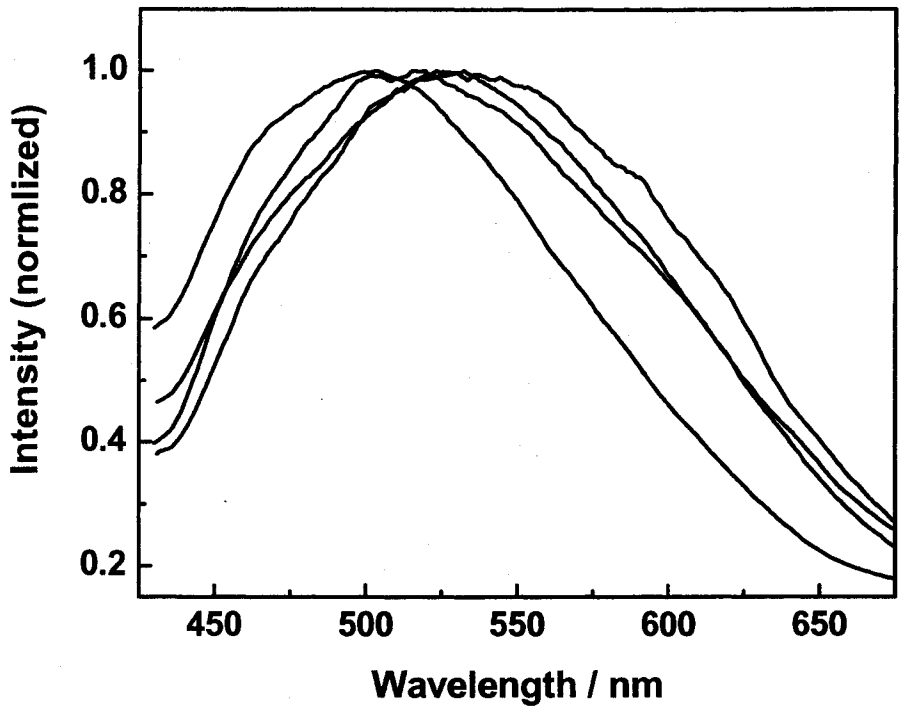

Figure II-S3: Emission spectra of CdS/MCM-41 in different aprotic solvents: (from left to right) dioxane, THF, DMF, DMSO. Excitation wavelength: 350 nm

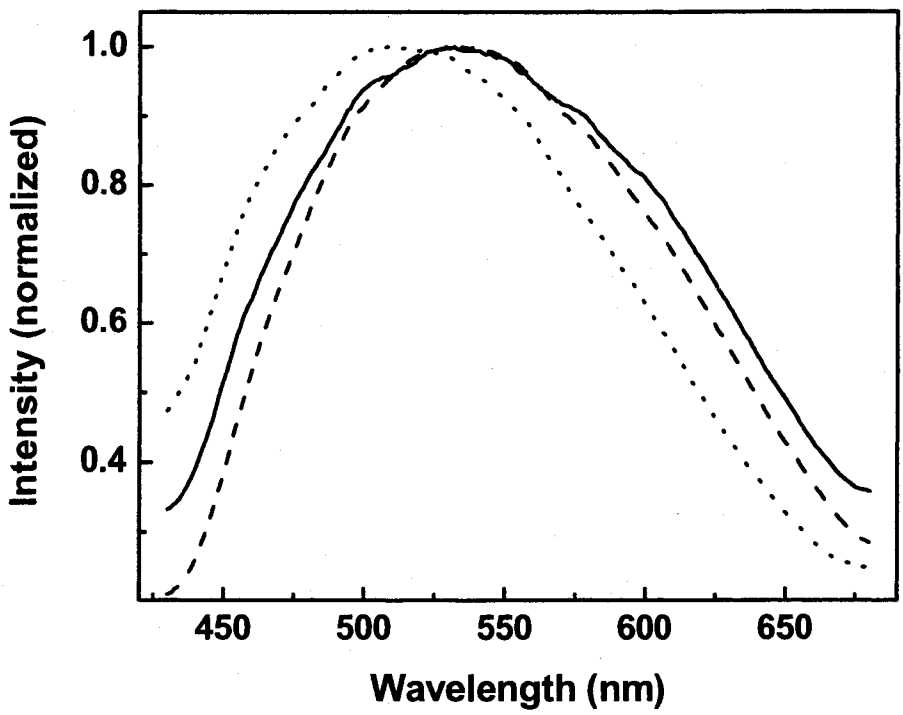

Figure II-S4: Normalized emission spectra of CdS/MCM-41 with different surface modification in methanol: as-synthesized sample (solid), surface cadmium-rich (dash), surface sulfur-rich (dot). Excitation wavelength: 350 nm.

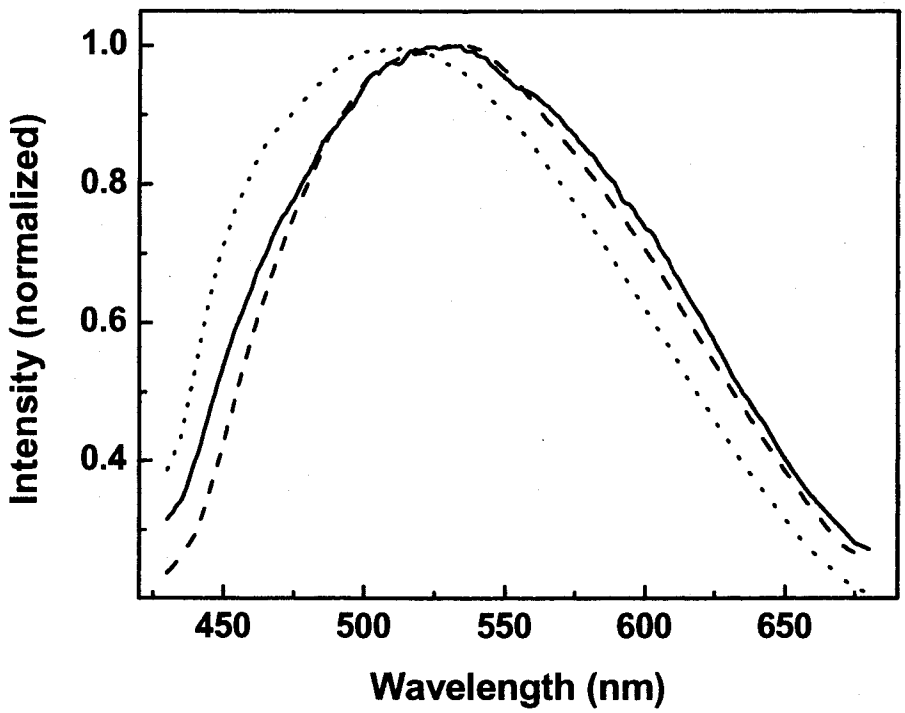

Figure II-S5: Normalized emission spectra of CdS/MCM-41 with different surface modification in actonitrile: as-synthesized sample (solid), surface cadmium-rich (dash), surface sulfur-rich (dot). Excitation wavelength: 350 nm.

Chapter III. Solvent Effects on Luminescence and Photophysics of CdS Nanoparticles Embedded in MCM-41: II. Emission Quenching and Time-Resolved Spectroscopies

Abstract

Investigation of solvent effects on the emission quenching of semiconductor nanoparticles is crucial for understanding the fundamental processes and dynamics of photogenerated charge carriers within the particle. The CdS nanoparticles synthesized within MCM-41 offer an ideal system for investigating the solvent dependence of the optical properties of nanoparticles. In this chapter, the time-resolved fluorescence spectroscopy was used to study the dynamics of the photophysics of a CdS/MCM-41 system. The time-resolved measurements revealed that the emission decay of CdS at all the wavelengths across the spectrum can be fitted into three components. The average lifetime (obtained through the James equation) increases approximately linearly with emission wavelength. This is reminiscent of the property of polar organic fluorophores. The wavelength dependence of the emission lifetime is mainly due to the fact that the emission at shorter wavelengths decays by both recombination

to the ground state and relaxation to the lower excited state (longer wavelength emission). The time-resolved emission spectra indeed showed the red-shifted emission at longer delay times. The interfacial charge transfer was studied through surface emission quenching by methyl viologen (MV^{2+}). In all the solvents investigated, the emission quenching showed linear Stern-Volmer plots, implying that only one type of quenching occurs, ether static quenching or dynamic quenching. The lifetime measurements indicated that the quenching was dominated by static quenching. The quenching efficiency of MV^{2+} was enhanced by the high solvent polarity as confirmed by the observation of quenching in water and alcohols (protic solvents). The effect of the surface modification of CdS/MCM-41 on the quenching efficiency was also investigated in aqueous solutions. It is found that for both the cadmium-rich (positive) and sulfur-rich (negative) CdS, the quenching by MV^{2+} got enhanced and was even more efficient than that by Cu^{2+} ions, which was believed to be strongly bound to the surface of CdS through complete lattice substitution of Cd^{2+}. Since a positive surface is normally detrimental to quenching by positively charged species, the enhanced quenching efficiency observed for the cadmium-rich CdS suggests that the effective association of MV^{2+} with CdS is mainly due to the effect of the local electric field within MCM-41.

I. Introduction

The emission quenching of semiconductor nanoparticles (*via* interfacial charge transfer) is strongly dependent on the surface charge and adsorption properties.[1-8] Studying the quenching process and dynamics helps understanding and improving the optoelectronic application of the nanoparticles. The kinetics of the charge transfer is determined by the interaction between the donor or acceptor molecules and the particle surface.[9-15] Such an interaction is in turn dependent on the solvent properties. Solvent effects on charge transfer have rarely been studied systematically, since no such nanoparticle system can be suspended in a wide range of solvents.[16-22] In general, the charge transfer kinetics of nanoparticles is difficult to explain due to the complicated surface environments, which are dominated by capping groups and counter ions. [4,8,23]

In the preceding chapter in this series,[24] we reported a universally suspendable nanoparticle system of CdS embedded in MCM-41, for which the solvent effects on spectral properties can be systematically investigated in a wide range of solvents. In this chapter, we will extend the investigation to the charge transfer quenching of emission of CdS by methyl viologen (MV^{2+}). MV^{2+} is a commonly used electron acceptor for charge transfer and separation systems. Both steady state and time-resolved emission spectral measurements have been carried out to investigate the solvent effects on the kinetics of the excited states and the interfacial charge transfer of CdS/MCM-41.

II. Experimental Section

The synthesis of CdS/MCM-41 was described in the preceding chapter.[24,25] The surface cadmium-rich CdS nanoparticles were prepared by refluxing 0.5 g of CdS/MCM-41 sample in 100 mL of ethanol containing 60 mg of cadmium acetate at

60 °C for 10 h. The precipitate was filtered out and washed with 200 mL ethanol to remove excess unbound Cd^{2+} and then dried at 333 K in a vacuum oven. The surface sulfur-rich CdS nanoparticles were prepared by the same method, but refluxing in an ethanol solution of sodium sulfide (1.2 g/100 mL).

The emission spectra of CdS/MCM-41 were recorded using a SPEX Fluorolog-τ2 spectrofluorometer, which was equipped with a stirring set to keep the nanoparticles homogeneously suspended during the measurement. For a typical emission measurement, 2 mg of CdS/MCM-41 was suspended into 10 mL of solvent, followed by 10 minutes of sonication. The emission quenching of CdS/MCM-41 in different solvents was carried out by adding an appreciated amount of MV^{2+} to the suspension of the nanoparticles. The quenching efficiency was calculated based on the integrated emission intensity. Methyl viologen chloride was obtained from Aldrich and used as received. All solvents were HPLC grade and used as received.

Time-resolved emission was measured with a Hamamatsu streak camera (Model C4334), which is optically coupled to a CCD array detector. This system allows for recording both the emission decay profile and the time-resolved emission spectrum. The femtosecond laser pulse is generated from a mode-locked Ti-Sapphire oscillator (Tsunami) pumped with a Millennia V laser (5 W at 527 nm). The pulse from Tsunami is amplified by a Spitfire chirp-pulse regenerative amplifier pumped with a frequency doubled Nd: YLF laser. The Spitfire produces a 100-fs laser pulse at 800 nm with a repetition rate less than 1k Hz. The output from Spitfire was further frequency doubled in a BBO crystal to generate a 400 nm light (1 mW/pulse, 150 fs), which is used to excite the sample in a quartz cuvette. Magnetic stirring was kept to make the suspension homogeneous. The instrument attached software (HPD-TA 6.1)

was used to process the data. The multiple component decay of emission was fitted to the best to make the $\chi^2 < 2$.

III. Results and Discussion

Emission quenching in different solvents. It is well-known that the surface adsorbed electron acceptors quench the excited state emission of semiconductor nanoparticles via interfacial electron transfer processes. One of the typically used electron acceptors is MV^{2+}, which has been widely used as a charge transfer relay in artificial photosynthetic and photovoltaic systems.[4,5] As observed previously for CdS nanoparticles prepared in homogeneous solutions, the emission of CdS/MCMC-41 was effectively quenched by MV^{2+} in various solvents. Figure III-1 shows the emission spectra of CdS/MCM-41 in water in the presence of different concentrations of MV^{2+}, where the emission intensity was gradually decreased with an increase in the concentration of MV^{2+}. The quenching efficiency appears to be constant across the entire emission spectrum. This implies that the surface electron transfer to MV^{2+} is dominated by the conduction band electron. Conduction band electrons are widely believed to be the precursor of the trapped electrons.[10] Therefore, the conduction band electron transfer quenches both band gap emission at short wavelengths and the emission of the trapped charge carriers at longer wavelengths.

The interfacial electron transfer from CdS to MV^{2+} is determined by the interaction between the two species. In the case of diffuse-controlled (dynamic) quenching, MV^{2+} ions are not in tight association with the particle surface, and thus most of the electron transfer to MV^{2+} comes from surface trapped electrons rather than conduction band electrons that are responsible for band-gap recombination. Therefore a diffusion-controlled dynamic process will predominately quench the

emission from trapped electrons at longer wavelengths, which have relatively long lifetimes (nanoseconds).

However, in the case of static quenching, where the MV^{2+} ions are strongly associated with the particle surface through electrostatic interaction, quenching of band-gap emissions of CdS at short wavelengths was observed (Figure III-1). The electron transfer to the surface adsorbed acceptor was believed to be very efficient, < 300 fs.[10] Such a fast process competes effectively with the surface trapping and band-gap recombination process. In other words, both the short wavelength emission (band-gap and near band-gap) and long wavelength emission (trapped) are quenched by the electron transfer to MV^{2+}. This results in no change in the shape of emission spectra due to the comparable quenching rates across the entire emission spectrum. This static quenching characteristic was also confirmed by the emission lifetime measurements of CdS/MCM-41 in the presence and absence of MV^{2+} (*vide infra*), which is presented in the later section of the chapter.

The surface of CdS synthesized in this study is believed to be neutral or slightly positive due to the surface hanging Cd^{2+} ions which are coordinated with the amine moieties at the inner surface of MCM-41.[24] No electrostatic interaction between MV^{2+} and CdS could thus be expected. The strong interaction implied by the emission quenching as discussed above is likely due to the compartmentation effect of the MCM-41 channel structure. Some strong interactions with the inner surface of MCM-41 bring MV^{2+} into the channel, where the viologen species are pushed to be in close proximity to the CdS surface due to the diminished space between CdS and the channel surface. The tight association of MV^{2+} with CdS is favorable for a large electronic coupling between the excitonic state of CdS and the charge transfer state

(CdS^{+}-$MV^{+\bullet}$). A strong electronic coupling is consistent with the fast electron transfer from CdS to MV^{2+} (< 300 fs).[10] Furthermore, the local electric field within the pore structure of MCM-41 may also affect the redox potential of MV^{2+}, making it a more favorable electron acceptor, i.e. the driving force (free energy change) of the electron transfer from CdS to MV^{2+} is increased. A large driving force is also consistent with the fast electron transfer from CdS to MV^{2+}. Indeed, the electric field effect of MCM-41 on the redox potential of ionic species was implied in our previous study of catalytic reduction of MV^{2+} within MCM-41.[25] Detailed experimental and theoretical investigations of the effect of external electric field on the electron transfer reaction have been reported by others.[26-29] The effects of the local electric field of porous silicate materials on reaction kinetics can be found in some recent reviews and periodic papers.[30-33]

The emission quenching of CdS/MCM-41 by MV^{2+} was investigated in a series of protic solvents (water and alcohols) to determine the solvent polarity dependence of quenching efficiency. Approximately linear Stern-Volmer plots were found for all solvents shown in Figure III-2. The linear plot suggests that the quenching mechanism is either purely static or purely dynamic. As will be proved later by the time-resolved measurements, the quenching is indeed a static process which involves a tight association between MV^{2+} and CdS. It is seen from Figure III-2 that the quenching efficiency varies significantly from solvent to solvent. From water to propanol, the Stern-Volmer constant (K_{SV}) decreased about 5 times. This is likely due to the decrease in polarity of the solvents. The higher the polarity (dielectric constant) of the solvent, the more favorable it is for increasing the electrostatic interaction between MV^{2+} ions and channel surface of MCM-41, thus enhancing the association

of MV^{2+} ions with the CdS surface. The major role played by MCM-41 in enhancing the static quenching by MV^{2+} will be inferred from the quenching observation of the surface modified CdS samples (*vide infra*).

Effects of surface modification. Surface modification of MCM-41 affects the interaction between MV^{2+} and CdS, which in turn determines the quenching efficiency of MV^{2+}. To investigate such a surface effect, the emission quenching experiments for the CdS/MCM-41 particles with different surface modifications (cadmium-rich vs. sulfur-rich) were carried out in aqueous solutions. The Cd^{2+} and S^{2-} modifications generate different surface charges, which in turn lead to different electrostatic interactions with MV^{2+}. For a cationic quencher, a negative surface is often favorable for increasing emission quenching, as found in the earlier investigations of homogeneous solutions of CdS particles.[11-13] This is consistent with the observations of the present study (Figure III-3). For the surface sulfur-rich CdS, the quenching efficiency was increased dramatically by about 2 orders of magnitude, compared to the as-synthesized sample (Table III-1). More interestingly, adding 5 mM excess of S^{2-} ions to the sulfur-rich sample did not produce an increase in the quenching efficiency. This implies that the surface of the sulfur-rich sample has already been saturated with sulfide species. Addition of more S^{2-} ions will not increase the negative charge on surface. This is not surprising, since the surface sulfur-rich sample was prepared in a much higher concentration of Na_2S (50 mM, see experimental section).

Generally, an increase in ionic strength is detrimental to the quenching efficiency of static quenching processes, since the electrostatic association between the quencher and fluorophore is weakened at higher ionic strengths. However, it is

not the case shown in Figure III-3, where addition of 10 mM NaCl to the sulfur rich sample did not cause notable change in quenching efficiency (Figure III-3). This leads to the assumption that static characteristics of the quenching process by MV^{2+} is mainly determined by the interaction between MCM-41 and MV^{2+}. It is widely accepted that MCM-41 and other porous silicates (e.g. zeolites) have strong adsorption for MV^{2+} due to the localized strong interaction between MV^{2+} and the cavity surface of MCM-41.[34-36] Such a strong interaction brings MV^{2+} into a close proximity with the surface of CdS which is embedded just inside the cavity. Although the interaction between MV^{2+} and MCM-41 is not clear, the strong hydrogen bonding between MV^{2+} and the surface hydroxyl group and/or the functioning amino moieties would play a significant role in determining the strong association of MV^{2+} inside MCM-41.[37,38]

The enhancement of MV^{2+} quenching by MCM-41 is also inferred from the quenching experiments of Cu^{2+} ions (Figure III-4). Since the solubility product of CuS is much lower than that of CdS, Cu^{2+} ions can be adsorbed onto the CdS surface by complete substitution of the surface Cd^{2+}.[39] However, in comparison to MV^{2+}, the more efficient adsorption of Cu^{2+} ions did not result in a relatively high quenching efficiency. The quenching efficiency of MV^{2+} for the sulfur-rich CdS (Figure III-3) is about 43 times higher than that of Cu^{2+} quenching (Table III-1). Even for the cadmium-rich CdS (Figure III-5), which is not favorable for MV^{2+} quenching, the quenching efficiency by MV^{2+} is about 40% higher than that by Cu^{2+} ions (Table 1). These results indicate that the strong quenching by MV^{2+} is not due to the direct electrostatic interaction between MV^{2+} and CdS surface, but rather to the strong association between MV^{2+} and the MCM-41 matrix as discussed above. The strong

local interaction (likely hydrogen bonding) between MV^{2+} and MCM-41 brings MV^{2+} into close proximity with CdS through the compartment effect, which enhances the association of MV^{2+} with CdS, and thus increases the quenching efficiency. The other possible cause for the increased quenching efficiency of MV^{2+} is the local electric field within MCM-41 cavities, which might decrease the reduction potential (making it more positive) of MV^{2+}, and thus increase the driving force for interfacial electron transfer from CdS to MV^{2+}.

The negative surface of CdS enhances, *but does not cause*, the contact with MV^{2+}. This is supported by the results shown in Figure III-5, where the positive surface of CdS still showed efficient quenching by MV^{2+}. Compared to the as-synthesized sample, the quenching efficiency for cadmium-rich CdS/MCM-41 was about 1.7 times higher. This would be unusual if not for the role played by MCM-41 in determining the association between MV^{2+} and the CdS surface. For most of the cases reported previously for CdS and other semiconductor nanoparticles, the positively charged surface prevents efficient quenching for a cationic quencher, since the latter can hardly become associated with the positive surface.[11-13] The results shown in Figure III-5 suggest again the important role of MCM-41 in associating MV^{2+} with CdS. The surface association of MV^{2+} with CdS can also be implied from the linear Stern-Volmer plot in Figure III-5, which suggests a static mechanism for the quenching process. A linear Stern-Volmer plot usually suggests a pure static or dynamic quenching process. But a dynamic process is less likely for the case of Cd/MCM-41, which provides little space for MV^{2+} diffusion. Furthermore, the static characteristic was inferred from the time-resolved emission quenching measurement (*vide infra*).

The origin of increased quenching for the cadmium-rich CdS is not clear at the current stage. The positive surface might favor the charge separation of the excitonic pair (photogenerated electron-hole) and thus enhance the interfacial electron transfer to the surface bound MV^{2+}. Another possibility may be that the positive surface strengthens the local electric field and consequently decreases the reduction potential (making it more positive) of MV^{2+}. The resulted higher driving force (higher rate) for the electron transfer to MV^{2+} leads to more efficient emission quenching. The increased emission quenching for cadmium-rich CdS was also found in other polar solvents like acetonitrile (results not shown).

In summary, the quenching efficiency of MV^{2+} is mainly determined by the interaction of MV^{2+} with the cavity surface of MCM-41. The strong local interaction between MV^{2+} and MCM-41 brings MV^{2+} into close proximity with CdS. This enhances the quench efficiency for both negatively and positively charged CdS surfaces. Our future study will move onto the investigation of other porous silicate materials (e.g. zeolites) which might afford different interactions with MV^{2+} and thus show different quenching efficiencies for CdS particles synthesized therein. Also, different surface modifications of MCM-41 will be carried out to adjust the interaction with MV^{2+}, and hopefully to get different quenching behavior of MV^{2+}.

Time-resolved emission spectra. Time-resolved emission spectra were measured with a streak camera system using a 400 nm pulsed laser (150 fs) as the excitation. Figure III-6 shows the emission spectra of CdS/MCM-41 in methanol at different time delays. It is clearly seen that the emission decay at shorter wavelengths is faster than that at longer wavelengths. As a result, the emission shifts to the red with the delay time. Figure III-7 depicts the decay profiles of the emission at three

different wavelengths, 512, 575 and 655 nm across the whole emission spectrum. For all wavelengths detected, the decay could be best fitted to three exponential decay kinetics, with lifetimes ranging from a few hundreds picoseconds to tens nanoseconds (Table 2). The similar decay behavior has also been observed for other CdS samples which were prepared in homogeneous solutions with surface stabilization.[40-44] The multiple exponential decay normally implies that the emission of CdS was not from a single excited state. Indeed, it is widely accepted that for a semiconductor like CdS different levels of trap sites exist inside the bandgap. The recombination of the charge carriers trapped at these sites generates emission at different wavelengths, i.e. a broad emission spectrum. For nanosized particles, the molar ratio of surface atoms is increased dramatically due to the small particle size. For example, more than 30% of atoms are at the surface for a 2 nm CdS nanaoparticles. The large population of surface atoms produces high density of surface defects, which often act as trap sites for charge carriers.

The faster decay at shorter wavelengths is likely due to the higher energy level of the shallow trap states, which decay by both emission and relaxation to the lower energy states (emitting at longer wavelengths). The similar phenomena have been observed previously for CdS and other semiconductor nanoparticles.[41,45,46] To test the wavelength dependence of emission lifetime, we carried out time-resolved measurement for the emission of CdS/MCM-41 in different solvents. Figure III-8 shows the results in water and methanol. For both the solvents, the average emission lifetime gradually (almost linearly) increased with an increase in wavelength. This is also observed in other polar solvents like acetonitrile. At any specific wavelength,

water gives the faster emission decay than methanol. This is reminiscent of the polar organic fluorophores, which normally show faster emission decay in polar solvents.[47]

It is striking to see that the presence of MV^{2+} did not decrease the average emission lifetime (Figure III-8). For each of the solvent, an appropriate amount of MV^{2+} was added to lead to 50% quenching of the emission intensity. However, the lifetime of the emission was kept almost unchanged upon addition of MV^{2+}. The similar phenomenon was also found in acetonitrile. This implies that the MV^{2+} quenching of the emission of CdS/MCM-41 is predominantly a static process, in which MV^{2+} ions are associated with CdS at a ground state. As discussed above, the strong association between MV^{2+} and CdS is mostly a result of local interaction between MV^{2+} ions and the channel surface of MCM-41. The static quenching mechanism was also consistent with the linear Stern-Volmer plots for the steady emission quenching measurements (Figure III-2, III-3, III-5).

IV. Conclusions

The CdS particle embedded in MCM-41 provides a unique system that can be universally suspended in different solvents. This offers the possibility to study the solvent effects of the photophysical properties and interfacial charge transfer of CdS nanoparticles. This study focused on the methyl viologen (MV^{2+}) quenching of the emission of CdS/MCM-41. Both steady and time-resolved emission measurements suggest a static charge transfer mechanism for the quenching process. The strong local interaction of MV^{2+} with MCM-41 is responsible for the static charge transfer process. The effective localization of MV^{2+} inside the MCM-41 channel pushes MV^{2+} to be associated with CdS due to the diminished space. Such a MCM-41 induced association results in an efficient quenching for MV^{2+} ions. For both the positive

(cadmium-rich) and negative (sulfur-rich) charged surface, the emission quenching by MV^{2+} is more efficient than that obtained for the as-synthesized CdS sample (neutral or slightly-positive charged surface). In general, the quenching efficiency of MV^{2+} seems dependent on the polarity of solvents. The higher polarity leads to more efficient quenching. This is reminiscent of the properties of polar organic fluorophores.

V. Acknowledgment.

This work was supported by the NSF and DoD-ARO, in part, through the following awards: (1) NSF-IGERT program under grant DGE-9972892, (2) NSF-MRSEC program under grant DMR-0213574, and (3) DoD-ARO under Cooperative Agreement DAAD19-01-1-0759. I am deeply indebted to Prof. Akins for his generous and kind support, Prof. Zang for his valuable discussion in preparation of this manuscript and H. Zhu for time-dependent fluorescence measurement.

References

(1) Empedocles, S.; Bawendi, M. *Acc. Chem. Res.* **1999**, *32*, 389.

(2) Zhang, J. Z. *Acc. Chem. Res.* **1997**, *30*, 423.

(3) Nirmal, M.; Brus, L. E. *Acc. Chem. Res.* **1998**, *32*, 407.

(4) Kamat, P. V. *Chem. Rev.* **1993**, *93*, 267.

(5) Henglein, A. *Chem. Rev.* **1989**, *89*, 1861.

(6) Weller, H. *Curr. Opin. Colloid & Interface Sci.* **1998**, *3*, 194.

(7) Rogach, A. L.; Talapin, D. V.; Weller, H. *Colloids and Colloid Assemblies* **2004**, 52.

(8) Zhang, J. Z. *J. Phys. Chem. B* **2000**, *104*, 7239.

(9) Chandler, R. R.; Coffer, J. L.; Atherton, S. J.; Snowden, P. T. *J. Phys. Chem.* **1992**, *96*, 2713.

(10) Logunov, S.; Green, T.; Marguet, S.; El-Sayed, M. A. *J. Phys. Chem. A* **1998**, *102*, 5652.

(11) Chandler, R. R.; Coffer, J. L. *J. Phys. Chem.* **1993**, *97*, 9767.

(12) Kuczynski, J.; Thomas, J. K. *J. Phys. Chem.* **1983**, *87*, 5498.

(13) Bavykin, D. V.; Savinov, E. N.; Parmon, V. N. *Langmuir* **1999**, *15*, 4722.

(14) Landes, C. F.; Braun, M.; El-Sayed, M. A. *J. Phys. Chem. B* **2001**, *105*, 10554.

(15) Haesselbarth, A.; Eychmueller, A.; Weller, H. *Chem. Phys. Lett.* **1993**, *203*, 271.

(16) Wilcoxon, J. P.; Parsapour, F.; Kelley, D. F. *Proc. Electrochem. Soc.* **1997**, *97*, 16.

(17) Ramsden, J. J.; Webber, S. E.; Graetzel, M. *J. Phys. Chem.* **1985**, *89*, 2740.

(18) Fischer, C.-H.; Henglein, A. *J. Phys. Chem.* **1989**, *93*, 5578.

(19) Biancardo, M.; Schwab, P. F. H.; Argazzi, R. B., C. A. *Inorg. Chem.* **2003**, *42*, 3966.

(20) Cowdery-Corvan, J. R.; Whitten, D. G.; McLendon, G. L. C. P., 176, 377. *Chem. Phys.* **1993**, *176*, 377.

(21) Hashimoto, K.; Hiramoto, M.; Sakata, T. M., H.; Takemura, H.; Fujihira, M. *J. Phys. Chem.* **1987**, *91*, 6198.

(22) Yuan, Y.; Fendler, J. H.; Cabasso, I. *Chem. Mater.* **1992**, *4*, 312.

(23) Zang, L.; Rodgers, M. A. J. *J. Phys. Chem.* **2000**, *104*, 468.

(24) Liao, Y.-T.; Zang, L.; Akins, D. *the first paper of this series, submitted simultaneously with this manuscript.*

(25) Liao, Y.-T.; Zang, L.; Akins, D. L. *Catal. Comm.* **2005**, *6*, 141.

(26) Franzen, S.; Lao, K.; Boxer, S. G. *Chem. Phys. Lett.* **1992**, *197*, 380.

(27) Seki, K.; Traytak, S. D.; Tachiya, M. *J. Chem. Phys.* **2003**, *118*, 669.

(28) Ohta, N.; Koizumi, M.; Umeuchi, S.; Nishimura, Y.; Yanazaki, I. *J. Phys. Chem.* **1996**, *100*, 16466.

(29) Hilczer, M.; Traytak, S.; Tachiya, M. *J. Chem. Phys.* **2001**, *115*, 11249.

(30) Garcia, H.; Roth Heinz, D. *Chem. Rev.*, *102*, 3947.

(31) Marquez, F.; Garcia, H.; Palomares, E.; Fernandez, L.; Corma, A. *J. Am. Chem. Soc.* **2000**, *122*, 6520.

(32) Zicovich-Wilson, C. M.; Corma, A.; Viruela, P. *J. Phys. Chem.* **1994**, *98*, 10863.

(33) Mirodatos, C.; Barthomeuf, D. *J. Catal.* **1985**, *93*, 246.

(34) Yoon, K. B. *Chem. Rev.* **1993**, *93*, 321.

(35) Yoon, K. B.; Hubig, S. M.; Kochi, J. K. *J. Phys. Chem.* **1994**, *98*, 3865.

(36) Yoon, K. B.; Kochi, J. K. *J. Am. Chem. Soc* **1988**, *110*, 6586.

(37) Simoncic, P.; Armbruster, T.; Pattison, P. *J. Phys. Chem. B* **2004**, *108*, 17352.

(38) Hennessy, B.; Megelski, S.; Marcolli, C.; Shklover, V.; Barlocher, C.; Calzaferri, G. *J. Phys. Chem. B.* **1999**, *103*, 3340.

(39) Stramel, R. D.; Nakamura, T.; Thomas, K. J. *J. Chem. Soc., Faraday Trans. 1: Phys. Chem. Condensed Phases* **1988**, *84*, 1287.

(40) Lakowicz, J. R.; Gryczynski, I.; Piszczek, G.; Murphy, C. J. *J. Phys. Chem. B* **2002**, *106*, 5365.

(41) Lakowicz, J. R.; Gryczynski, I.; Gryczynski, Z.; Nowaczyk, K.; Murphy, C. J. *Analy. Biochem.* **2000**, *280*, 128.

(42) Lakowicz, J. R.; Gryczynski, I.; Gryczynski, Z.; Murphy, C. J. *J. Phys. Chem. B* **1999**, *103*, 7613.

(43) Kumar, A.; Mital, A. S. *J. Colloid Interface Sci.* **2001**, *240*, 459.

(44) Matsumoto, H.; Uchida, H.; Matsunaga, T.; Tanaka, K.; Sakata, T.; Mori, H.; Yoneyama, H. *J. Phys. Chem.* **1994**, *98*, 11549.

(45) Chestnoy, N.; Harris, T. D.; Hull, R.; Brus, L. E. *J. Phys. Chem.* **1986**, *90*, 3393.

(46) O'Neil, M.; Marohn, J.; McLendon, G. *J. Phys. Chem.* **1990**, *94*, 4356.

(47) Lakowicz, J. R., *Principle of Fluorescence Spectroscopy*, 2nd. ed.; Kluwer Academic/Plenum, *New York*, **1999**.

Figure captions

Figure III-1: Emission spectra of CdS/MCM-41 in water at different concentrations of methyl viologen (MV^{2+}): from top to bottom, 0, 1.0×10^{-5}, 2.0×10^{-5}, 4.0×10^{-5}, 6.0×10^{-5}, 8.0×10^{-5}, 1.0×10^{-4}, 1.4×10^{-4} M.

Figure III-2: Stern-Volmer plots for emission quenching of CdS/MCM-41 by MV^{2+} in different solvents: water (■), methanol (●), ethanol (▲), 1-propanol (▼).

Figure III-3: Stern-Volmer plots for emission quenching of sulfur-rich CdS/MCM-41 by MV^{2+} in water: as-synthesized sulfur-rich sample (●), in the presence of 5 mM S^{2-} (■), in the presence of 10 mM NaCl (▲).

Figure III-4: Stern-Volmer plot for emission quenching of CdS/MCM-41 by Cu^{2+} ions in water.

Figure III-5: Effect of surface Cd^{2+} modification on MV^{2+} quenching of emission of different CdS/MCM-41 samples in water: as-synthesized CdS/MCM-41 (■), cadmium-rich CdS/MCM-41 (●), cadmium-rich CdS/MCM-41 in the presence of 5 mM of Cd^{2+} (▲).

Figure III-6: Time-resolved emission spectra of CdS/MCM-41 in methanol excited at 400 nm. Time delays (from top to bottom): 1.76-2.01 ns, 1.96-2.21 ns, 2.26-2.51 ns, 2.76-3.01 ns, 4.26-4.51 ns, 6.76-7.01 ns.

Figure III-7: Emission decay profiles of CdS/MCM-41 in methanol, observed at three emission wavelengths: 512 nm (▲), 575 nm (●), 665 nm (■). Excitation wavelength was 400 nm. The solid curves represent tri-exponential fitting of the data. The instrument response profile (dot) is shown for comparison. The fitting residues are shown at the bottom.

Figure III-8: Average emission lifetimes of CdS/MCM-41 as a function of wavelength in water (square) and methanol (circle) in the presence (solid) and absence (open) of MV^{2+}. Excitation wavelength was 400 nm. Concentrations of MV^{2+} ions were 10^{-4} M in water and 2×10^{-4} M in methanol.

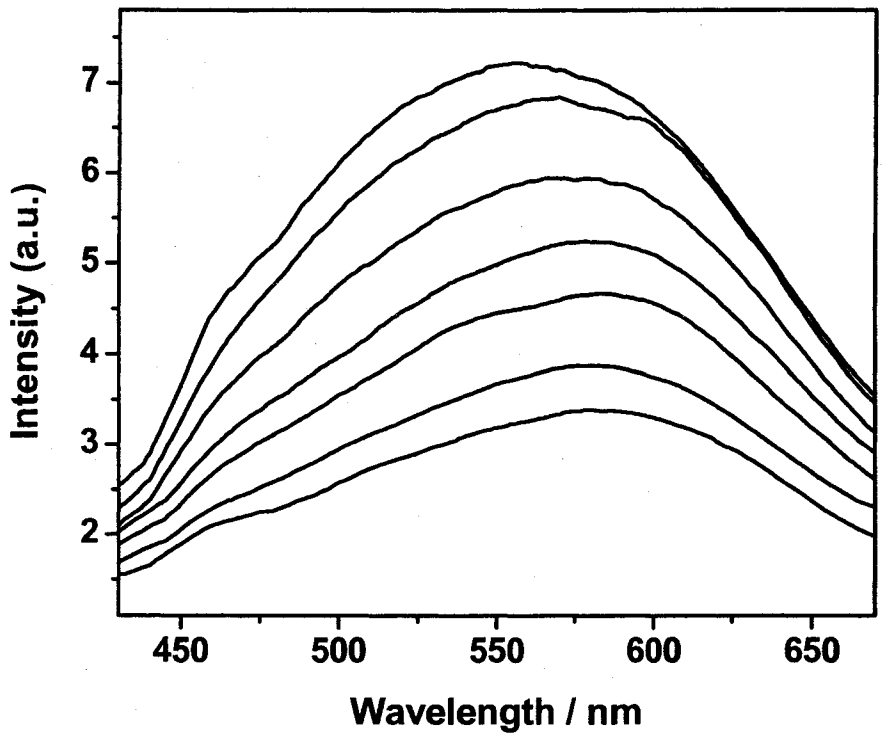

Figure III-1

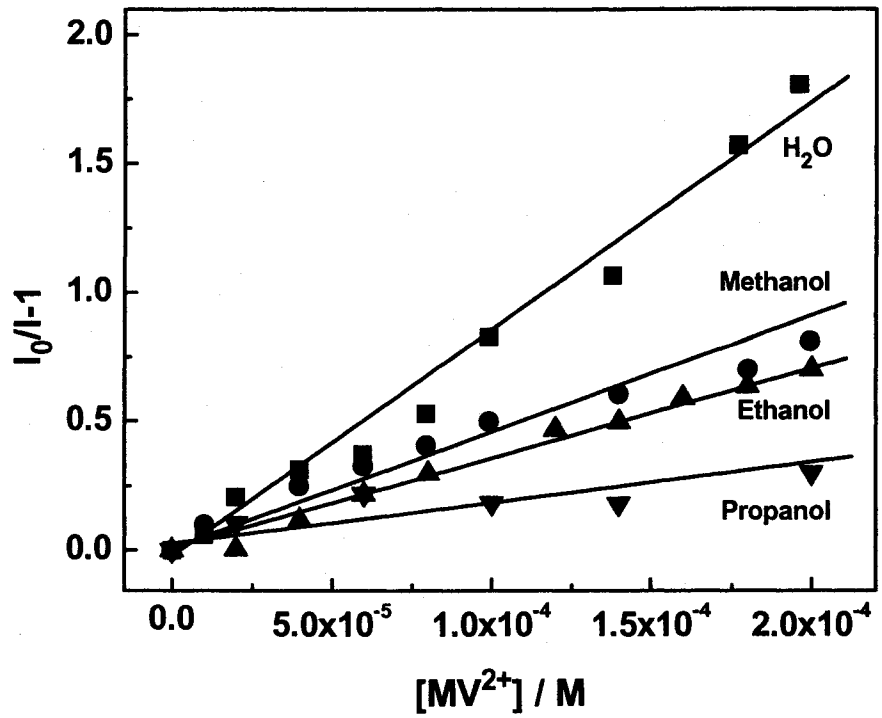

Figure III-2

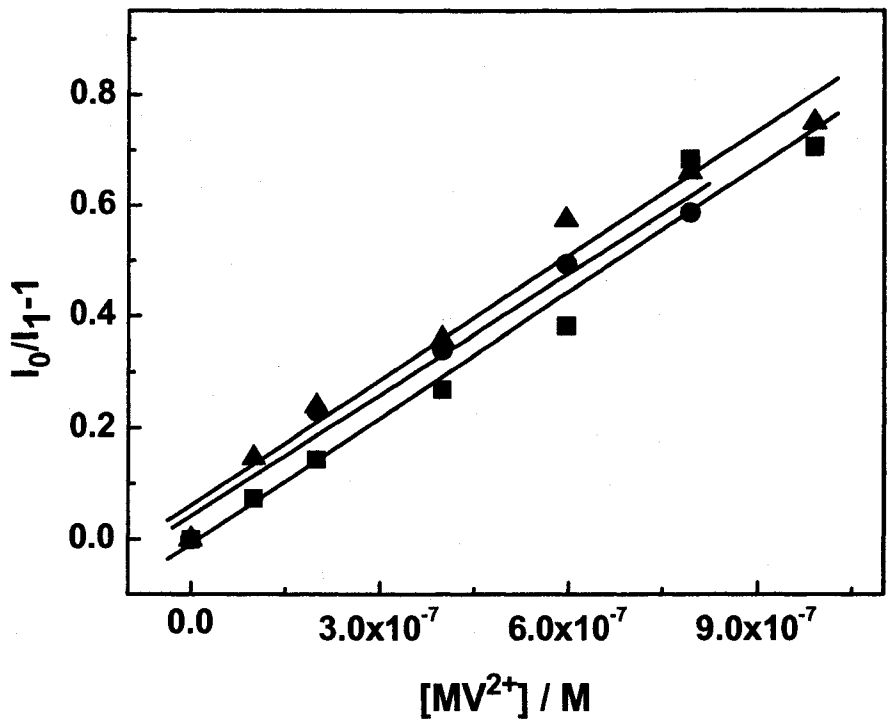

Figure III-3

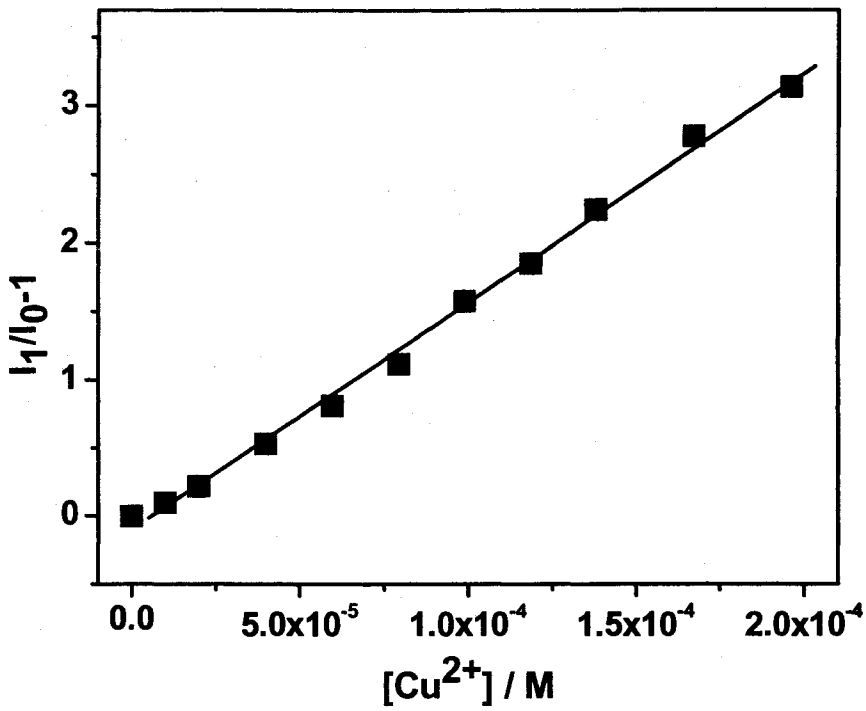

Figure III-4

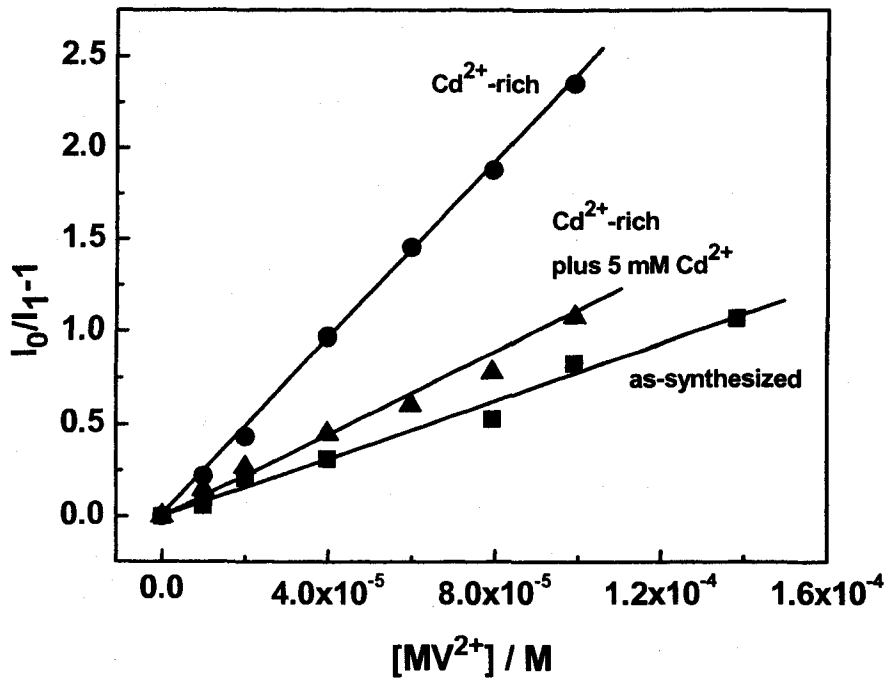

Figure III-5

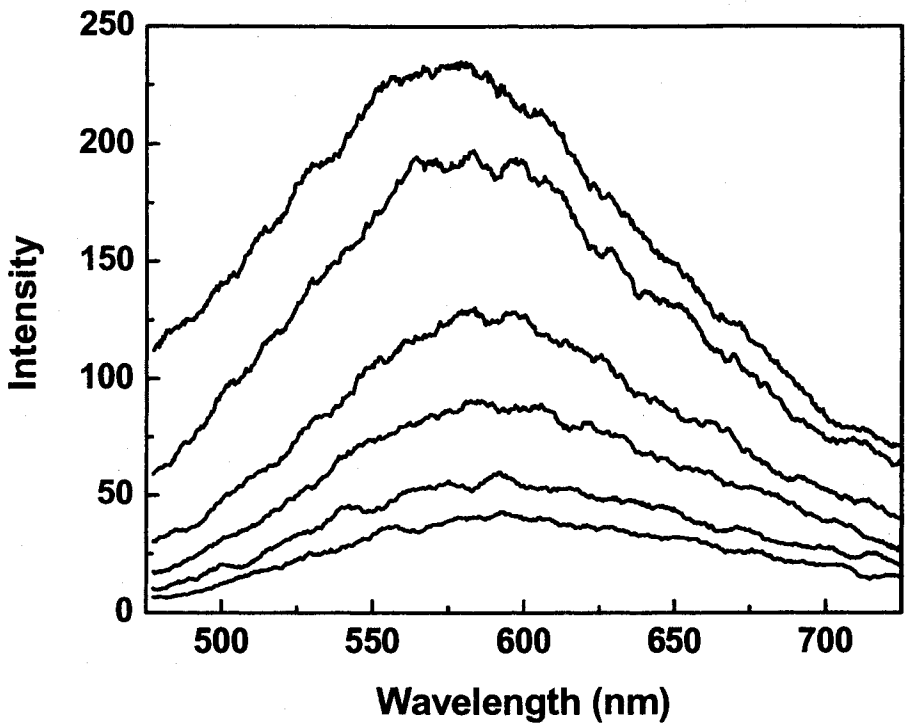

Figure III-6

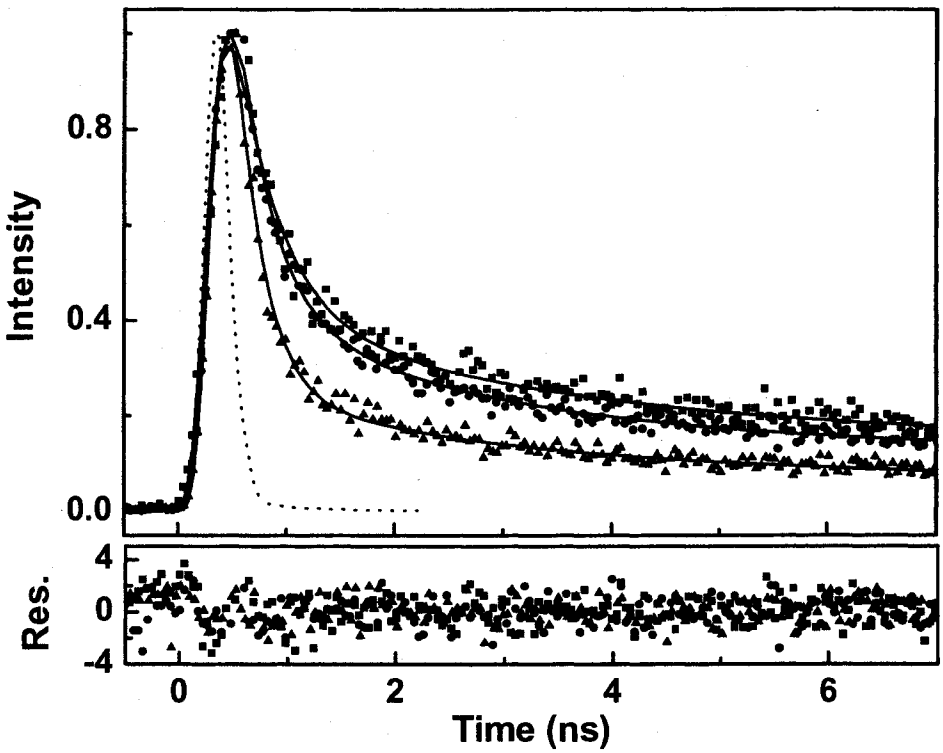

Figure III-7

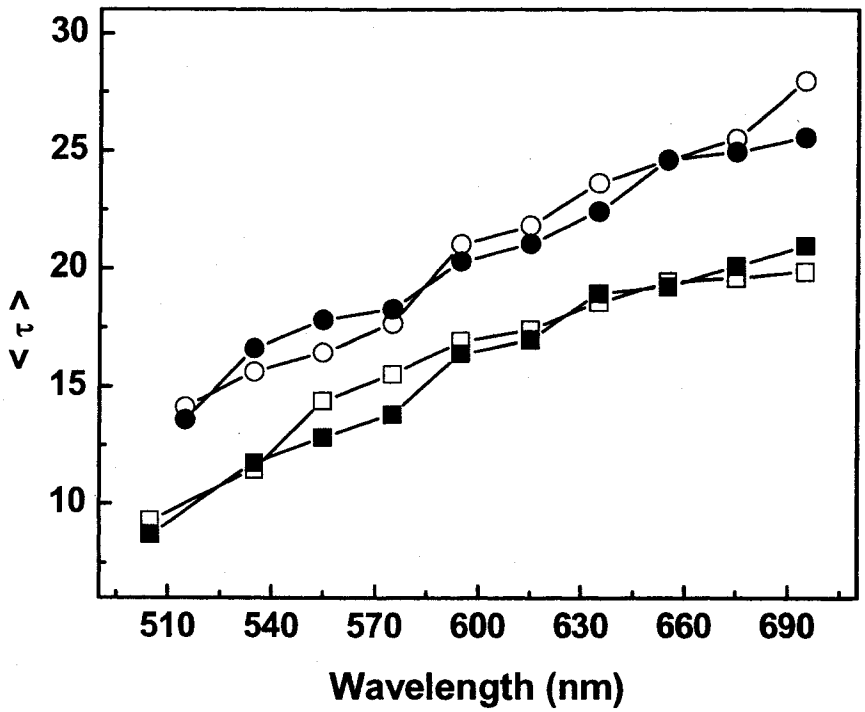

Figure III-8

Table III-1. Stern-Volmer constants (K_{SV}) for MV^{2+} quenching of CdS/MCM-41 with different surface modification. The value for static quenching of the as-synthesized sample by Cu^{2+} ion is shown for comparison.

Surface Modification	As-synthesized	Cadmium- rich	Sulfur-rich	As-synthesized (Cu^{2+} quench)
Stern-Volmer Constant	8965±427	23981±301	724391±65350	16671+-334

III-2. Multiple exponential decays of emission of CdS/MCM-41 at different wavelengths in methanol

Wavelength (nm)	τ_1 (ns)	A_1/α_1	τ_2 (ns)	A_2/α_2	τ_3 (ns)	A_3/α_3	$<\tau>$(ns)	Chi^2
515	0.22	1008.82	1.931	94.35	18.573	64.61	14.14	1.503
		0.160		0.114		0.868		
575	0.287	1115.75	1.667	278.91	21.24	169.5	17.63	1.214
		0.088		0.098		0.893		
655	0.367	607.89	2.235	151.64	28.5	117.9	24.63	1.256
		0.060		0.086		0.903		

Chapter IV: Linear temperature dependence of photoluminescence of CdS nanoparticles embedded in MCM-41

Abstract

Linear temperature dependence of photoluminescence intensity was observed for the cadmium sulphide (CdS) nanoparticles embedded in mesoporous materials, MCM-41, within a wide range of temperature, 77 - 298 K. This, together with the temperature independent emission wavelength of the nanocomposite, promises a potential application as optical indicators for luminescence thermometry.

I. Instruction

Luminescence thermometry is a non-contact technique for temperature measurement which exploits the temperature-dependent emission of luminescent probes.[1-3] While the emission intensity, wavelength, and lifetime may all depend on temperature, the emission intensity is often used to gauge temperature change due to its high sensitivity. Non-contact luminescence thermometry offers many advantages over traditional contact temperature measurements (e.g. thermocouples and thermistors), including its immunity to electromagnetic interference and high spatial resolution for mapping localized temperature profiles at either microscopic or nanoscopic scale.[2] One typical example is the mapping of heterogeneous distribution of surface temperature through the incorporation of luminescent probes in diagnostic coating material. A variety of luminescent materials including organic dyes,[1] inorganic phosphors,[2] and luminescent coordination complexes[4] have been investigated for temperature sensing.

Among all luminescent materials, luminescent nanoparticles offer unique advantages for temperature sensing when compared to traditional phosphers due to their quantum confinement. These advantages include a decrease in light scattering and an improvement of spatial resolution. The quantum confinement existing in nanoparticles often leads to higher quantum efficiency of photoluminescence and thus promises high-sensitivity for temperature sensing. The fast decay of photoluminescence of nanoparticles provides better temporal resolution for high-speed *in-vivo* temperature sensing in bio-medical applications.[5]

Due to the above-mentioned advantages, strong attention has been drawn recently to the study of temperature dependence of photoluminescence of

semiconductor nanoparticles (e.g. CdS, CdSe, CdTe, ZnS) and doped nanoparticles (e.g. ZnS:Mn^{2+}), for potential application in luminescence thermometry.[3,6-13] However, only in a few cases were semiconductor nanoparticles and doped nanoparticles found to have linear temperature dependent photoluminescence. Chen et al., [3] found a wide linear range (303 – 423 K) for the ZnS:Mn^{2+} nanoparticles without an organic stabilizer and tBaFBr:Eu^{2+} nanoparticles embedded in MCM-41. It seems that a clean surface of the nanoparticle and/or a strong interaction with the MCM-41 matrix is crucial for producing linearly temperature dependent emission.

In this chapter, we report that CdS nanoparticles embedded in MCM-41 show linear temperature dependence of emission in a much wider temperature range (77 – 298 K). To the best of our knowledge, this is the first observation of a wide-range linear temperature dependence of the emission of nanoparticles at cryogenic temperatures.

II. Experimental Section

CdS/MCM-41 was synthesized following the protocol developed previously in our lab.[14,15] The resultant mesoporous material was impregnated with the surfactant molecule hexadecyltrimethylammonium, which was used as the synthesis template material. When desired, the encapsulated surfactant could be removed by washing the sample thoroughly with hot water and ethanol and then immersing it in a large volume of ethanol overnight, followed by rinsing with ethanol five times[16]. Additionally, external surface passivation of MCM-41 was carried out by refluxing the as-synthesized sample with an ethanol solution of phenyltrimethoxysilane (ethanol/phenyltrimethoxysilane = 1:1 by volume) for 6 hours at room temperature.

The internal surface of the surfactant-removed and external surface passivated MCM-41 was functionalized by refluxing ca. 1 g of the sample with 5 mL of the chelating agent N-(2-aminoethyl)-3-(trimethoxysilyl) propylamine in dry toluene for 12 hours at room temperature[17]. Synthesis of the CdS nanoparticles in the externally passivated and internally functionalized MCM-41 was accomplished by the procedure detailed in an earlier published study.[14]

The particle size, measured by x-ray diffraction, was 2.1 nm. The rigid, chemically and thermally stable MCM-41 matrix provides an ideal host for nanoparticles synthesized therein. Due to the protection by the rigid frame of MCM-41, no particle aggregation occurred when suspended in solvents. In solutions, the CdS/MCM-41 nanocomposite showed several interesting optical properties such as emission polarization (positive anisotropy), red-edge excitation shift of emission, and solvent polarity dependence of emission.[18] All of these properties are reminiscence of polar organic fluorophores. This led us to the investigation of the effect of temperature on the emission properties of CdS/MCM-41.

The temperature dependence of the emission of CdS/MCM-41 was first observed for a sample suspended in ethylene glycol. When temperature decreased to 77 K, the emission intensity increased about 1.5 times compared to that at 298 K. To further investigate the temperature effect, the emission measurement was carried out for the solid sample to root up the temperature induced solvent effect. For temperature dependent luminescence, the samples were mounted on the coldfinger of a Janis cryogenic system (Model ST-300), which can be cooled to 78 K using liquid nitrogen. Prior to cooling, the system was pumped to ~ 10^{-4} Torr. The excitation laser used was a 325 nm He-Cd cw laser, with the laser intensity controlled by a set of

neutral density filters. During the measurement, the excitation laser intensity was kept constant, and the sample temperature between 77 K and room temperature was controlled by a temperature controller from Lake Shore Cryotronics, Inc (Westerville, OH). Luminescence spectra were collected by focusing the sample emission on the slit of a Spex 1680-B spectrometer using a (cylindrical) lens, and detected with a photomultiplier tube.

III. Results and Discussion

Figure IV-1 shows the emission spectra of the dry sample of CdS/MCM-41 at different temperatures. The spectra were measured on the front face in the cryostat chamber. From 77 to 298 K, the emission intensity progressively decreased, while the peak emission wavelength kept constant at 625 nm (inset of Figure IV-1). In contrast, the previous emission measurement of semiconductor nanoparticles showed that temperature-induced intensity changes were accompanied by a shift in emission wavelength.[6-8] Detailed mechanisms of the constant emission wavelength are unclear at the current stage. However, such a temperature insensitivity of the emission wavelength renders CdS/MCM-41 an attractive candidate for temperature sensing, since the temperature can be simply correlated to the emission intensity at a single wavelength.

More interestingly, the emission intensity of CdS/MCM-41 was found to be linearly dependent on temperature for a wide temperature range from 77 to 298 K (Figure IV-2). Such a wide linear dependence has not been observed before for semiconductor nanoparticles. While a few groups reported the similar linear change of emission intensity with temperature,[3,8] the linear temperature range obtained was not as wide as that observed in this study. The previous observation by Bawendi and

Nocera et al.[8] reported that the emission intensity of (CdSe)ZnS core-shelled particles decreased steadily with the increase in temperature from 100 to 315 K. However, the linear dependence was only observed in the narrower temperature range of 278-313 K.

While some theoretical models are available to explain the temperature dependence of semiconductor emission (particularly for the nanocrystals), the mechanism of linear temperature dependence remains unclear.[3,6] It is generally accepted that the linear decrease of intensity with temperature is due to the lower efficiency of the excited state transition of the charge carrier from the excitonic state to the surface non-rediative state (defect traps). Such less effective surface trapping may compensate for the exponential increase of non-radiative decay with temperature, leading to a weaker (and in some cases, linear) temperature dependence of the emission intensity. Obviously, more time-resolved quantitative measurements are needed to fully understand the mechanism of the linear temperature dependence of emission. Nevertheless, this does not prohibit the use of linear dependence to develop nanoparticle based temperature sensors or probes.[3,8] To this end, the much wider linear range found in this study would provide more application opportunities. From 298 to 77 K, the emission intensity of CdS/MCM-41 increased about 6.5 times (650%), corresponding to 2.9 ± 0.01% per °C. This value is even better than that obtained for the (CdSe)ZnS core-shell quantum dots, 2.4% per °C.[8] The higher sensitivity with temperature change indeed promises the feasibility of the development of CdS/MCM-41 as a temperature sensor.

It should be noted that the emission of CdS/MCM-41 is not sensitive to oxygen, as confirmed by emission measurements in aqueous suspensions. Bubbling

with nitrogen produced no difference in emission intensity compared to that saturated with air. In conclusion, temperature-dependent emission measurements were carried out on CdS nanoparticles embedded in MCM-41; the emission intensity was found to be a linear function of temperature from 77k to 298k, while the emission maximum remained unchanged. The excellent temperature linearity, constant emission wavelength, and the oxygen insensitivity make the CdS/MCM-41 system an excellent optical indicator for luminescence thermometry.

IV. Acknowledgements

This work was supported by the NSF and DoD-ARO, in part, through the following awards: (1) NSF-IGERT program under grant DGE-9972892, (2) NSF-MRSEC program under grant DMR-0213574, and (3) DoD-ARO under Cooperative Agreement DAAD19-01-1-0759. I am deeply indebted to Prof. Akins for his generous and kind support, Prof. M. Tamargo's group for helping with low temperature emission measurement, and Prof. Zang for his valuable discussion in preparation of this manuscript.

References

(1) Gallery, J.; Gouterman, M.; Callis, J.; Khalil, G.; McLachlan, B.; Bell, J. *Rev. Sci. Instrum.* **1994**, *65*, 712.

(2) Allison, S. W.; Gillies, G. T. *Rev. Sci. Instrum.* **1997**, *68*, 2615.

(3) Wang, S.; Westcott, S.; Chen, W. *J. Phys. Chem. B* **2002**, *106*, 11203.

(4) Maruszewski, K.; Andrzejewski, D.; Strek, W. *J. Lumin.* **1997**, *72-74*, 226.

(5) Kauppinen, J. P.; Loberg, K. T.; Manninen, A. J.; Pekola, J. P. *Rev. Sci. Instrum.* **1998**, *69*, 4166.

6) Wang, Y.; Herron, N. *J. Phys. Chem.* **1988**, *92*, 4988.

(7) Joly, A. G.; Chen, W.; Roark, J.; Zhang, J. Z. *J. Nnanosci. Nanotech.* **2001**, *1*, 295.

(8) Walker, G. W.; Sundar, V. C.; Rudzinski, C. M.; Wun, A. W.; Bawendi, M. G.; Nocera, D. G. *Appl. Phys. Lett* .**2003**, *83*, 3555.

(9) Sebald, K.; Michler, P.; Passow, T.; Hommel, D.; Bacher, G.; Forchel, A. *Appl. Phys. Lett* . **2002**, *81*, 2920.

(10) Soloviev, V. N.; Eichhoefer, A.; Fenske, D.; Banin, U. *J. Am. Chem. Soc.* **2001**, *123*, 2354.

(11) Zhao, J.; Dou, K.; Chen, Y.; Jin, C.; Sun, L.; Huang, S.; Yu, J.; Xiang, W.; Ding, Z. *J. Lumin.***1996**, *66&67*, 332.

(12) Bol, A. A.; Van Beek, R.; Ferwerda, J.; Meijerink, A. *J. Phys. Chem. Solids* **2003**, *64*, 247.

(13) Tanaka, M.; Masumoto, Y. *Chem. Phys. Lett.***2000**, *324*, 249.

(14) Xu, W.; Liao, Y.; Akins, D. L. *J. Phys. Chem. B* **2002**, *106*, 11127.

(15) Liao, Y.-T.; Zang, L.; Akins, D. *Catal. Commu.*, ***2005***, *6*, 141.

(16) Zhang, Z.; Dai, S.; Fan, X.; Blom, D. A.; Pennycook, S. J.; Wei, Y. *J. Phys. Chem. B* **2001**, *105*, 6755.

(17) Zhang, W.-H.; Shi, J.-L.; Chen, H.-R.; Hua, Z.-L.; Yan, D.-S. *Chem. Mater.* **2001**, *13*, 648.

(18) Liao, Y.-T.; Zang, L.; Akins, D. *to be published somewhere else.*

Figure Caption

Figure IV-1: Emission spectra of dry samples of CdS/MCM-41 excited at 325 nm at different temperatures, from top to bottom: 77, 120, 180, 240, 273, 298 K. Inset: normalized spectra are overlapped each other, showing no spectral shift with temperature.

Figure IV-2: Integrated emission intensity of CdS/MCM-41 as a function of temperature. Linear fitting (R: 0.999) of the data is also shown.

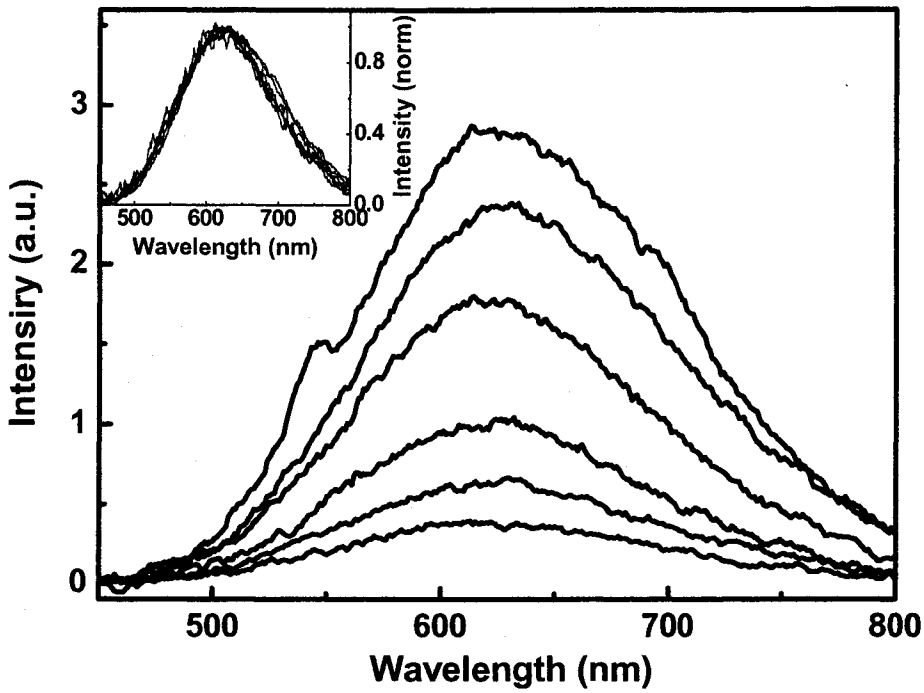

Figure IV-1 Emission spectra of dry samples of CdS/MCM-41 excited at 325 nm at different temperatures, from top to bottom: 77, 120, 180, 240, 273, 298 K. Inset: normalized spectra are overlapped each other, showing no spectral shift with temperature.

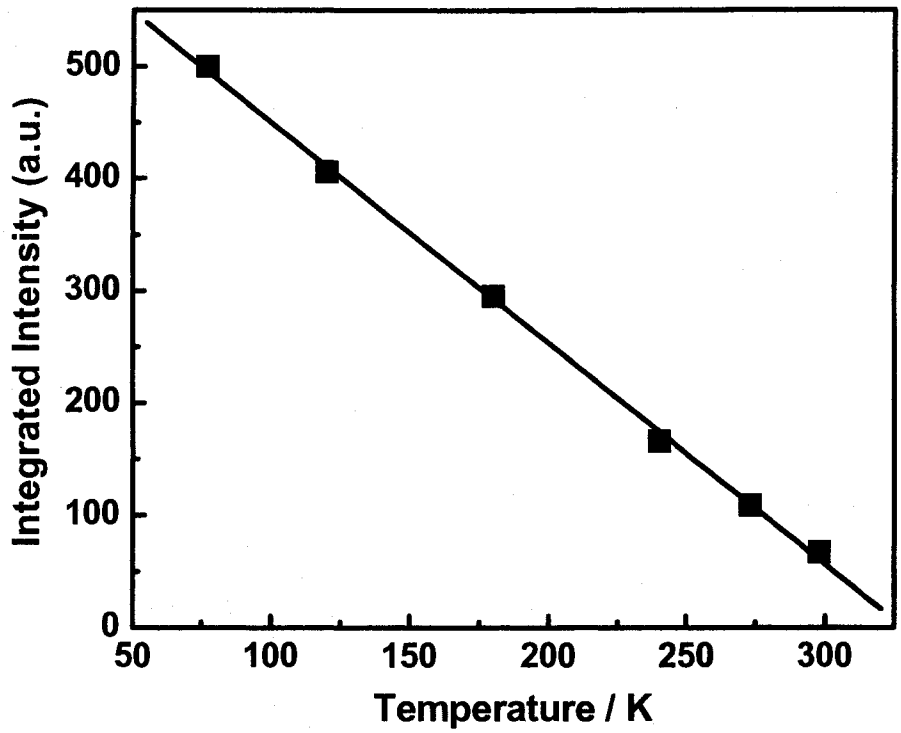

Figure IV-2 Integrated emission intensity of CdS/MCM-41 as a function of temperature. Linear fitting (R: 0.999) of the data is also shown.

Chapter V: Catalytic Reduction of Methyl Viologen by Sulfide Ion within MCM-41

ABSTRACT

Methyl viologen in the presence of mesoporous MCM-41 and sulfide ions is found to undergo a spontaneous catalytic reduction to methyl viologen radical ($MV^{+\cdot}$). Various control conditions, including passivation of the external surface and modification of the internal surface of MCM-41, suggest that the catalytic reduction occurs principally within the pores of MCM-41. The source of the sulfide ions can be either an added sulfide salt or coordinatively unsaturated surface sulfide ions of an occluded sulfide nanoparticle. The present system offers a means for the spontaneous formation of methyl viologen radicals, which might serve as a complementary measurement for electron microscopy probing of the location of sulfide nanoparticles synthesized within the pores of mesoporous materials.

I. Introduction

MCM-41 is an amorphous, mesoporous silicate material that is principally defined by domains of highly organized hexagonal arrays of one-dimensional, parallel cylindrical channels throughout its structure. The effective pore size of the channels of MCM-41 is tunable through the choice of the templating reactant used in its synthesis, with the effective size controllable from 1.5 to 10 nm. Moreover, the pore size distribution can often be made extremely narrow, leading to essentially monosized pores throughout the material. The narrowness of the size distribution has led to substantial interest in using this ordered mesoporous material as a catalyst or catalyst support.[1-3]

The vast majority of the catalysts developed so far that involve mesoporous silicates are surface-doped with transition metal ions or metal complexes, which act as catalytically active sites. Such doped active sites have proven to be indispensable for reactions with high activation barriers. Moreover, the restricted cavity environment and thus the strong local electric field within the as-synthesized mesoporous materials can be expected to catalyze, as a result of electrostatic activation, some bimolecular redox reactions with slightly unfavorable free energies that do not spontaneously occur in homogeneous solution.[4] Indeed, in the case of zeolites, both experimental and theoretical investigations indicate that a strong electric field accompanying electronic confinement within the channel of zeolites does induce significant preactivation of encapsulated molecules, thus enhancing reaction kinetics. [5-7] In many such cases, the preactivation can be related to an increase in reducing power (more negative oxidation potential) of the reactant molecule.

In this paper, we report a case where the reduction of methyl viologen, MV^{2+}, by S^{2-} is catalyzed (as shown in Eq. (1)) within the MCM-41 pores without the presence of metal ions, and where sulfide ions can be provided by way of sulfide salts or as coordinatively unsaturated surface sulfide ions of occluded sulfide nanoparticles.[8]

$$2\,MV^{2+} + S^{2-} \overset{MCM-41}{\leftrightarrow} 2\,MV^{+\bullet} + S, \qquad (1)$$

MV^{2+} is methyl viologen: 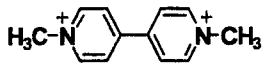

It is to be noted that the redox potentials of MV^{2+} ($E^{\circ}(MV^{2+}/MV^{+})$: -0.45 V vs. NHE) and S^{2-} ($E^{\circ}(S/S^{2-})$: -0.48 V vs. NHE) are nearly equal, [8] and thus the reduction of MV^{2-} in homogeneous aqueous solution is only weakly favored, since the driving force for electron transfer is quite small. For such a system it is possible that the redox reaction can be facilitated by either a slight increase in the reduction potential of the oxidant or a slight decrease in the oxidation potential of the reductant; such a redox pair might provide a good system for probing the effect of electric fields within mesoporous materials on the kinetics of charge transfer reactions. Additionally, the environment in which the reduced product is formed might act to stabilize it, as has been found to occur for the $MV^{+\bullet}$ radical stabilized in zeolites. [9,10] Thus, with the appropriate reductant, the methyl viologen redox system might provide the opportunity for an ordinary UV-vis absorption measurement to monitor the catalytic reaction through the observation of the conversion of MV^{2+} to $MV^{+\bullet}$ (a strongly absorbing chromophore).

Moreover, since the synthesis of semiconductor nanoparticles within mesoporous materials is widely utilized, the catalyzed reduction of MV^{2+} may help spatially probe the location of such nanoparticles in mesoporous structures, where they are difficult to detect, especially with electron microscopy techniques, including high resolution TEM. This detection difficulty is principally due to the weak contrast between the silicate framework and the nanoparticle, as is found for many nanoparticles, including CdS, [11] ZnS, [12] ZnO, [13] Fe_2O_3, [14] and GaN. [15] However, the catalyzed reduction of MV^{2+} with S^{2-}, reported herein, may allow the use of optical spectroscopy to ascertain whether sulfide containing nanoparticles are synthesized within the MCM-41 matrix, since the catalytic reaction (Eq.(1)) is found to occur only inside the pores of MCM-41.

Moreover, since TEM can precisely detect a nanocrystalline phase formed on the external surface of zeolites or MCM-41, a combined probing technique of TEM and the MV^{2+}/S^{2-} redox system may offer an effective way to quantitatively gauge to what extent nanoparticles are synthesized inside the channels of porous materials.

The elemental sulfur that would be formed according to Eq. (1) would not be expected to dramatically affect the catalytic reduction of methyl viologen since its neutral characteristic (zero charge) makes diffusion feasible, and if the catalytic reaction, as we infer, is to a large extend attributable to electrostatic field activation, the generation and presence of neutral species like sulfur would not be expected to poison the catalytic process.

II. Experimental Section

MCM-41 was prepared following the protocol previously developed in our laboratory, but without calcining the material. [11] As a result, the resultant

mesoporous material was impregnated with the surfactant molecule hexadecyltrimethylammonium, which was used as the synthesis template material. And, when desired, the encapsulated surfactant could be removed by washing the sample thoroughly with hot water and ethanol and then immersed in a large volume of ethanol overnight, followed by rinsing with ethanol five times. [16] Additionally, external surface passivation of MCM-41 was carried out by refluxing the as-synthesized sample with an ethanol solution of phenyltrimethoxysilane (ethanol/phenyltrimethoxysilane = 1:1 by volume) for 6 h at room temperature.

The internal surface of the surfactant removed and external surface passivated MCM-41 was functionalized by refluxing ca. 1 g of the sample with 5 mL of the chelating agent N-(2-aminoethyl)-3-(trimethoxysilyl) propylamine in dry toluene for 12 h at room temperature. [12] Synthesis of CdS nanoparticles in the externally passivated and internally functionalized MCM-41 was accomplished by the procedure detailed in an earlier published study. [11]

UV-vis absorption measurements were conducted using a 2 mm pathlength cuvette containing MCM-41 suspensions. The concentrations of the sample was maintained at sufficiently low values that scattering by the suspensions were insignificant, allowing absorption measurements to monitor the concentration of methyl viologen radical. Such an approach has been utilized in several investigations involving suspensions containing methyl viologen radicals, and it has been shown that at sufficient dilution of a suspension an optical transmission measurement can be used to measure a concentration. [17,18]

The absorption spectrum of the catalytically generated $MV^{+\bullet}$ radical was obtained from difference spectra for the reaction suspension and the suspension

containing MCM-41 powder alone. The absorption spectrum of $MV^{+\bullet}$ thus obtained was consistent in shape with that found for the homogeneous solution (i.e., the ratio of the two main peaks at 395 and 602 nm remained essentially constant). [19] In a typical study, a predefined amount of S^{2-} was added to an aqueous suspension of 2 mg/mL MCM-41 containing 2 mM of MV^{2+}, followed by 10 minutes of sonication for complete encapsulation of MV^{2+} into the channels. This was followed by transferring ca. 0.5 mL of the suspension to the 2 mm pathlength cuvette, which was then sealed with a tight septum and placed in the UV-vis spectrometer. Formation of $MV^{+\bullet}$ was monitored by absorption measurements, as shown in Figure V-1. As a further measure of the formation of methyl viologen radical, Raman spectra of MV^{2+} and $MV^{+\bullet}$in the MCM-41 suspension were excited with laser radiation at 457.9 nm (see Figure V-3 caption for details).

III. Results and Discussion

Figure V-1 shows the temporal formation of $MV^{+\bullet}$ for suspensions of MV^{2+} in surfactant impregnated MCM-41. No dimer or other aggregate bands for the radical are found, despite the fact that dimers of $MV^{+\bullet}$, in particular, have been observed in the smaller, cross-linked supercages of zeolite-Y. [10,20] The absence of aggregates makes it possible for reaction kinetics to be easily interpreted in terms of concentration. Moreover, we principally focused on the main absorption band at ca. 603 nm, where only insignificant light scattering occurs, allowing the absorption measurement to be closely related to the concentration.

The reaction was investigated by changing the S^{2-} concentration from 0.0 to 5.0 mM. As mentioned earlier, time evolution results are shown in the inset of Figure

V-1. Without S^{2-} ions, or with its concentration lower than 0.5 mM, no radicals were detected, despite the presence of MV^{2+}, indicating that MCM-41 alone does not provide appropriate sites for the reduction. We also found that the reaction in homogeneous solution does not occur even when high concentrations of S^{2-} and MV^{2+} ions are present, indicating that MCM-41 is required for the reduction (see Figure V-2). This latter finding is interpreted as suggesting that the pore structure and (possibly) the associated strong localized electric fields (i.e., electrostatic field activation) play important roles in the reduction of methyl viologen and S^{2-} ions.

As mentioned earlier, Raman spectra were also measured for the spontaneously formed radical and the MV^{2+} precursor. Figure V-3 shows the Raman spectrum for the species formed as a result of the catalytic reduction process that occurs for the MCM-41 system. Comparison with the literature confirms that the scattering species formed upon reduction is $MV^{+\bullet}$.[21-24] It is to be noted that the observed Raman spectrum of the radical does not contain bands that have been assigned to the dimmer,[20, 21] which is consistent with the absence of dimer (and higher aggregate) bands in the UV-vis absorption spectrum that we measured (see Figure V-1).

As a rough test of the effect of reaction volume, we investigated the effect of increased reaction volume on reaction kinetics. For this study, the catalytic reduction was investigated for an MCM-41 sample that had the surfactant in the pores of the as-synthesized material removed. We found that the reaction yield (defined as the limiting concentration (or absorbance) of the radical formed as the reaction time approaches infinity) decreased by about 30% compared to that for the surfactant-

impregnated MCM-41. The higher yield found for the surfactant-impregnated sample is attributable to the smaller reaction space that exists when the surfactant template is present. In this latter case, one can envision that the S^{2-} ions are localized around the positively charged surfactant head groups, and the restricted space between the surfactant and the surface lattice leads to enhanced electric field strength and gradient, whose impact on the reducing power of S^{2-} ions is implicated by the apparent increased reducing power of the anion.

Another experimental finding, from studying the catalysis of external surface passivated MCM-41 (as shown in Figure V-2), is that the external surface only weakly affects catalytic reaction dynamics, despite the fact that the presence of the hydrophobic passivation layer would be expected to decrease the adsorption of MV^{2+} and S^{2-} ions onto the outside surface of MCM-41, promoting a greater level of incorporation of the two ions within the pores. This finding suggests that the catalytic reduction of MV^{2+} takes place predominantly inside the cavity of MCM-41.

We also investigated the effect of blocking the Lewis acid sites (SiIV and AlIII) in MCM-41. Such a process would be expected to decrease the adsorption of S^{2-} and, hence, decrease the overall catalytic activity of MCM-41. This was confirmed by the result depicted in Figure V-4, which shows the effects of modifying the pore lining in MCM-41. Specifically, the inner surface of the external surface passivated MCM-41 was functionalized with N-(2-aminoethyl)-3-(trimethoxysilyl)propylamine, which also, as mentioned earlier, was used by us as a chelating ligand for incorporating Cd^{2+} ions in the synthesis (via gas phase reaction with H_2S) of CdS nanoparticles.[11] Functionalization of the inner surface blocks

Lewis acid sites and is found to significantly decrease the reactivity of MCM-41, resulting in a pronounced induction period and lower reaction yield. Again, internal surface modification leads to diminished reaction rate, suggesting that the catalysis predominantly occurs within the pores of MCM-41.

As regards whether the reaction is either a surface reaction or occurs in solution within the pores of the mesoporous material, our observations are not definitive, since the series of studies that we have performed (*vide supra*) can be interpreted, to some extent, as supporting either or both reaction venues. However, since electrostatic activation is a fundamental aspect of the mechanism that we believe applies in the catalytic reduction of methyl viologen, which does not necessitate the existence of surface binding sites, we would conclude that liquid phase reaction within the pores plays a substantial role in the catalytic process.

We also studied the effect of encapsulated CdS nanoparticles on the catalytic reduction of MV^{2+}. Upon using the same MCM-41 sample as indicated above, but with encapsulated CdS nanoparticles, a substantially faster dynamics was found even without the addition of free S^{2-} ions. The overall reaction efficiency, as measured by the limiting yield, was nearly twice that of the best found for the surfactant-impregnated MCM-41 (see supporting information). We deduce that the coordinatively unsaturated surface sulfide ions of the CdS nanoparticles are responsible for reduction of methyl viologen, and the greater reactivity is reasonably attributed to a space constriction effect, with resultant enhanced electric fields, associated with the close fit of the nanoparticle within the mesopores of MCM-41; indeed, the synthesized nanoparticle (~2.1 nm; as determined by XRD measurements, see Ref. 10) would severely diminish the space available to the reactants. Moreover,

the electrostatic field associated with the negatively charged surface of CdS nanoparticle could be expected to lead to higher field gradients ref. 4.

IV. Conclusion

The catalytic reaction as presented here might be used to spatially probe CdS or other sulfide nanoparticles synthesized inside the matrix of MCM-41. Moreover, since semiconductor nanoparticles synthesized in mesoporous materials like MCM-41 are usually difficult to be imaged by TEM techniques, mainly due to the poor contrast between the silica frameworks of MCM-41 and the nanoparticles.[11-15] Combining a TEM measurement and the methyl viologen catalytic reaction, we may be able to verify whether and to what extent nanoparticles are synthesized within the pore structure of a mesoporous material. Also, the present catalytic approach offers a technique for the spontaneous formation of methyl viologen radicals, allowing for spectroscopic study of this widely used charge transfer partner.

V. Acknowledgment

This work was supported by the NSF and DoD-ARO, in part, through the following awards: (1) NSF-IGERT program under grant DGE-9972892, (2) NSF-MRSEC program under grant DMR-0213574, and (3) DoD-ARO under Cooperative Agreement DAAD19-01-1-0759. I am deeply indebted to Prof. Akins for his generous and kind support and Prof. Zang for his valuable discussion in preparation of this manuscript.

References

(1) Beck, J. S.; Vartuli, J. C.; Roth, W. J.; Leonowicz, M. E.; Kresge, C. T.; Schmitt, K. D.; Chu, C. T. W.; Olson, D. H.; Sheppard, E. W.; McCullen, S. B.; Higgins, J. B.; Schlenker, J. L. *J. Am. Chem. Sot.* **1992**, *114*, 10834.

(2) Moller, K.; Bein, T. *Chem. Mater.* **1998**, *10*, 2950.

(3) Corma, A. *Chem. Rev. (Washington, D. C.)* **1997**, *97*, 2373.

(4) Garcia, H.; Roth, H. D. *Chem. Rev.* **2002**, *102*, 3947.

(5) Marquez, F.; Garcia, H.; Palomares, E.; Fernandez, L.; Corma, A. *J. Am. Chem. Soc.* **2000**, *122*, 6520.

(6) Zicovich-Wilson, C. M.; Corma, A.; Viruela, P. *J. Phys. Chem.* **1994**, *98*, 10863.

(7) Mirodatos, C.; Barthomeuf, D. *J. Catal.* **1985**, *93*, 246.

(8) Dean, J. A.; (Ed.) *Lange's Handbook of Chemistry, 13th ed.*; McGraw-Hill, 1985.

(9) Yoon, K. B.; Hubig, S. M.; Kochi, J. K. *J. Phys. Chem.* **1994**, *98*, 3865.

(10) Yoon, K. B.; Kochi, J. K. *J. Am. Chem. Soc* **1988**, *110*, 6586.

(11) Xu, W.; Liao, Y.; Akins, D. L. *J. Phys. Chem. B* **2002**, *106*, 11127.

(12) Zhang, W.-H.; Shi, J.-L.; Chen, H.-R.; Hua, Z.-L.; Yan, D.-S. *Chem. Mater.* **2001**, *13*, 648.

(13) Zhang, W.-H.; Shi, J.-L.; Wang, L.-Z.; Yan, D.-S. *Chem. Mater.* **2000**, *12*, 1408.

(14) Abe, T.; Tachibana, Y.; Uematsu, T.; Iwamoto, M. *J. Chem. SOC., Chem. Commun.* **1995**, 1617.

(15) Winkler, H.; Birkner, A.; Hagen, V.; Wolf, I.; Schmechel, R.; Von Seggern, H.; Fischer, R. A. *Adv. Mater. (Weinheim, Germany)* **1999**, *11*, 1444.

(16) Zhang, Z.; Dai, S.; Fan, X.; Blom, D. A.; Pennycook, S. J.; Wei, Y. *J. Phys. Chem. B* **2001**, *105*, 6755.

(17) Borja, M.; Dutta, P. K. *Nature (London, United Kingdom)* **1993**, *362*, 43.

(18) Castagnola, N. B.; Dutta, P. K. *J. Phys. Chem. B* **2001**, *105*, 1537.

(19) Watanabe, T.; Honda, K. *J. Phys. Chem.* **1982**, *86*, 2617.

(20) Melendres, C. A.; Lee, P. C.; Meisel, D. *J. Electrochem. Soc.* **1983**, *130*, 1523.

(21) Forster, M.; Girling, R. B.; Hester, R. E. *J. Raman Spectrosc.* **1982**, *12*, 36.

(22) Forster, M.; Hester, R. E. *Chem. Phys. Lett.* **1982**, *85*, 287.

(23) Hester, R. E.; Suzuki, S. *J.Phys. Chem.***1982**, *86*, 4626.

(24) Feilchenfeld, H.; Chumanov, G.; Cotton, T. M. *J. Phys. Chem.***1996**, *100*, 4937.

Figure Captions

Figure V-1: Absorption spectra of the reaction suspension of the surfactant impregnated MCM-41 (2 mg/mL) containing 2 mM of MV^{2+} and 5 mM of S^{2-} at different time intervals after being sealed from air. The time intervals from bottom to top are: 3, 8, 13, 23, 33, 68 and 93 min. The inset shows the growth of the absorption at 603 nm as a function of time for different concentrations of added S^{2-}: (A) 0.5 (■), (B) 1.5 (●), (C) 3.5 (▲), and (D) 5.0 mM (▼).

Figure V-2: Growth of the absorption at 603 nm as a function of time for the reaction suspensions of different MCM-41 samples: homogeneous aqueous solution without MCM-41 (●); as-synthesized MCM-41 with surfactant present (■); as-synthesized MCM-41 with surfactant removed (□); external surface passivated MCM-41 with surfactant removed (▲). Reaction condition: 2 mg/mL of MCM-41, 2 mM of MV^{2+} and 5 mM of S^{2-}.

Figure V-3: Raman spectra of (A) MV^{2+}/MCM-41 and (B)$MV^{+\cdot}$ /MCM-41 suspensions in water using argon-ion laser excitation of 457.9 nm (power at the laser head: 150 mW).

Figure V-4: Absorbance at 603 nm as a function of time for two reaction suspensions. (A) External surface passivated and internal surface functionalized MCM-41 (2 mg/mL) plus 2 mM of MV^{2+} and 5 mM of S^{2-} (●). (B) External surface passivated and internal surface functionalized MCM-41 with encapsulated CdS nanoparticle (2 mg/mL) plus 2 mM of MV^{2+} (■).

Figure V-S1. Growth of absorption at 603 nm as a function of time for the reaction suspension of the external surface passivated and internal surface functionalized MCM-41 (2 mg/mL) and 2 mM of MV^{2+} with different concentrations of added S^{2-} ions: 1.0 (■), 2.5 (●), 3.5 (▲), 5.0 mM (▼).

Figure V-S2. Absorption spectra of the reaction suspension of the external surface passivated and internal surface functionalized MCM-41 with CdS nanoparticle encapsulated (2 mg/mL) containing 2 mM of MV^{2+} at different time intervals; from bottom to top: 3, 10, 23, 43, 73, 93 min. The inset shows the growth of the absorption at 603 nm as a function of time.

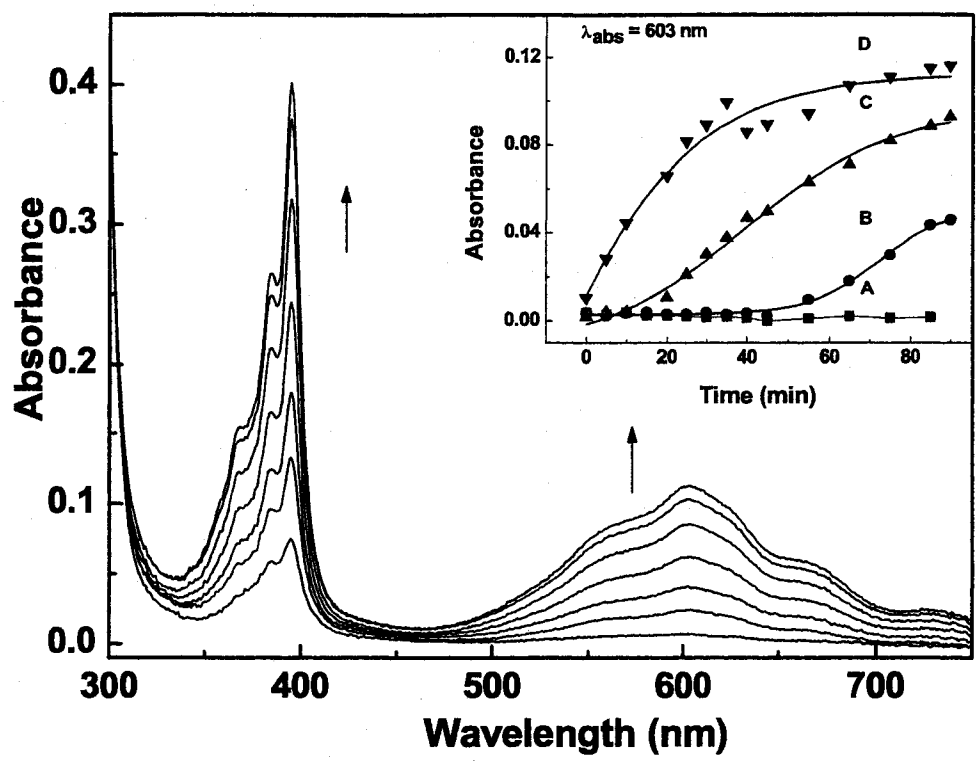

Figure V-1: Absorption spectra of the reaction suspension of the surfactant impregnated MCM-41 (2 mg/mL) containing 2 mM of MV^{2+} and 5 mM of S^{2-} at different time intervals after being sealed from air. The time intervals from bottom to top are: 3, 8, 13, 23, 33, 68 and 93 min. The inset shows the growth of the absorption at 603 nm as a function of time for different concentrations of added S^{2-}: (A) 0.5 (■), (B) 1.5 (●), (C) 3.5 (▲), and (D) 5.0 mM (▼).

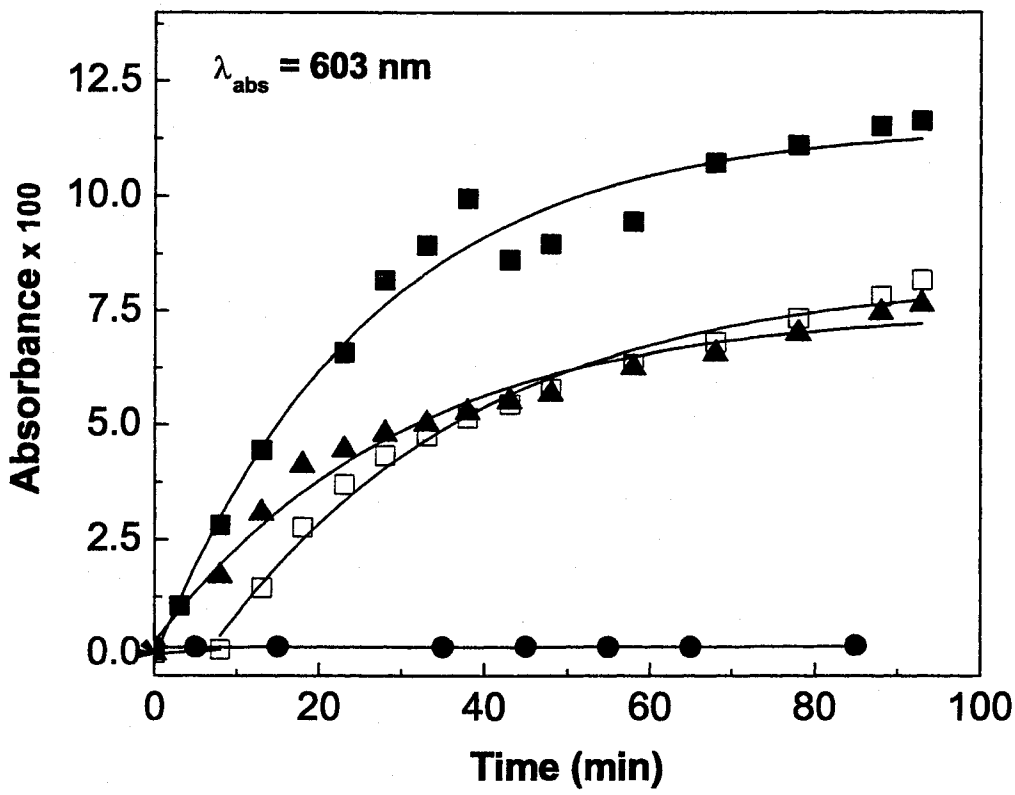

Figure V-2: Growth of the absorption at 603 nm as a function of time for the reaction suspensions of different MCM-41 samples: homogeneous aqueous solution without MCM-41 (●); as-synthesized MCM-41 with surfactant present (■); as-synthesized MCM-41 with surfactant removed (□); external surface passivated MCM-41 with surfactant removed (▲). Reaction condition: 2 mg/mL of MCM-41, 2 mM of MV^{2+} and 5 mM of S^{2-}.

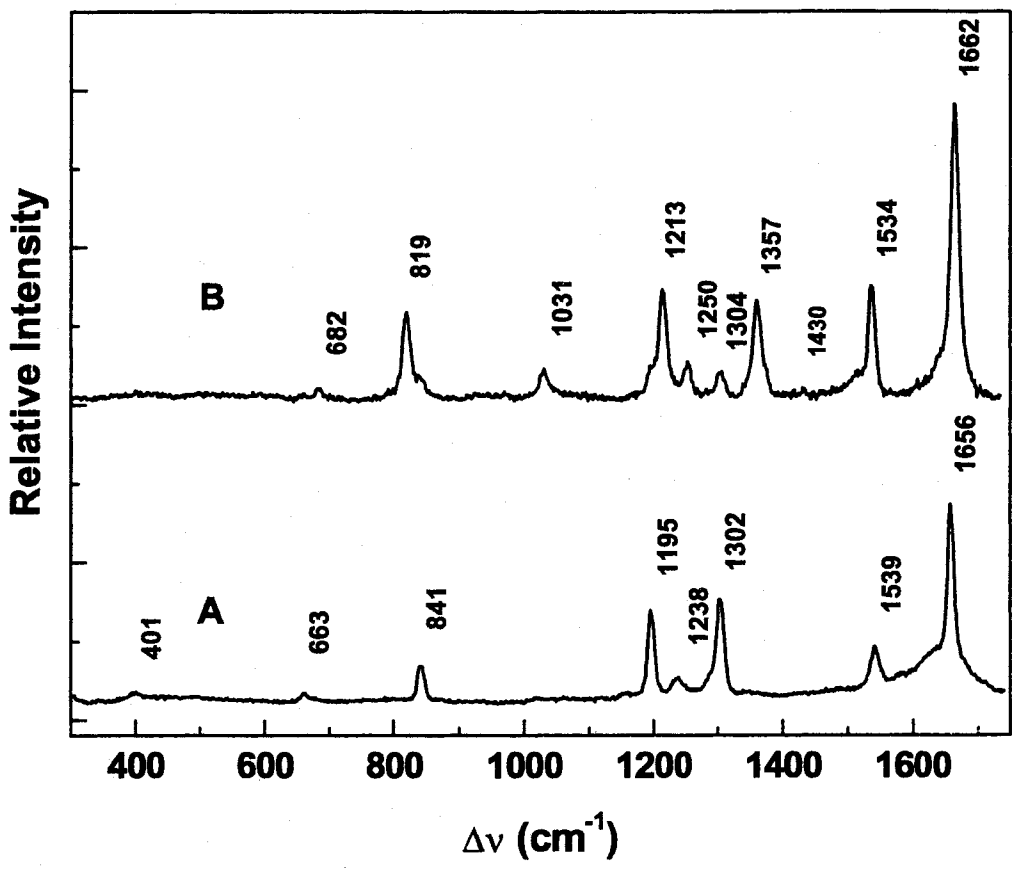

Figure V-3: Raman spectra of (A) MV^{2+}/MCM-41 and (B)$MV^{+\cdot}$ /MCM-41 suspensions in water using argon-ion laser excitation of 457.9 nm (power at the laser head: 150 mW).

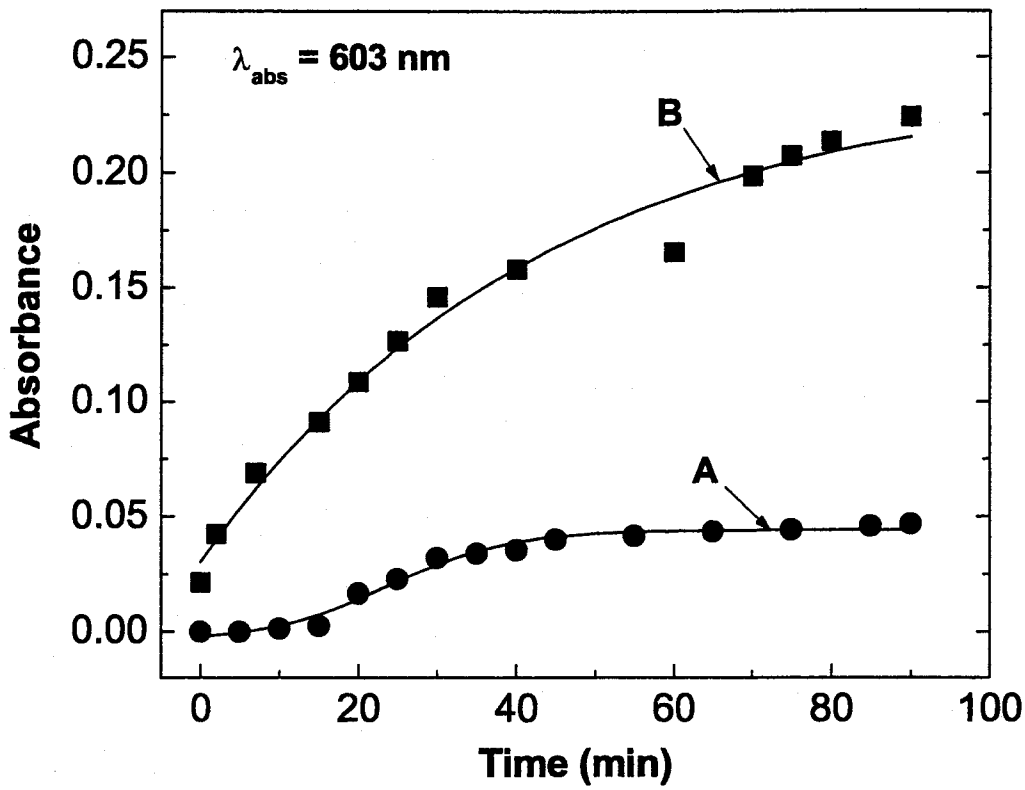

Figure V-4: Absorbance at 603 nm as a function of time for two reaction suspensions. (A) External surface passivated and internal surface functionalized MCM-41 (2 mg/mL) plus 2 mM of MV^{2+} and 5 mM of S^{2-} (●). (B) External surface passivated and internal surface functionalized MCM-41 with encapsulated CdS nanoparticle (2 mg/mL) plus 2 mM of MV^{2+} (■).

Supporting information: Chapter V: Catalytic Reduction of Methyl Viologen by Sulfide Ion within MCM-41

Supporting Information.

All the reactions at different concentrations of S^{2-} became saturated after ca. 50 mins1. In general, the reduction of MV^{2+} with S^{2-} was slow in the case of the MCM-41 with external surface passivation and internal surface functionalization. The reaction kinetics at different concentrations of S^{2-} all showed smooth Sigmoidal shape, with significant induction period. Only at a concentration above 2.0 mM can formation of $MV^{+\bullet}$ be detected.

The absorption spectra of the species ($MV^{+\bullet}$) produced from the reduction of MV^{2+} by CdS nanoparticles are shown in SI-Figure 2, where one can see that both the structure of the two absorption bands (395 and 603 nm) and the ratio of the absorption coefficients of the two bands are the same as those depicted in Figure 1. This implies that the surface hanging sulfide ion of CdS nanoparticle function as the same reducing agent as the free S^{2-} ions.

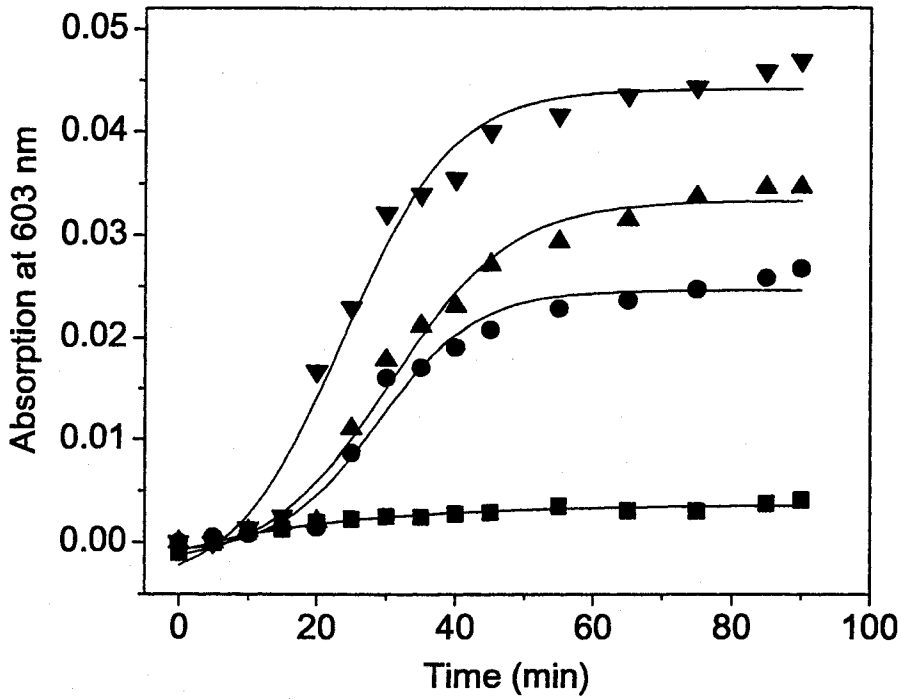

Figure V-S1. Growth of absorption at 603 nm as a function of time for the reaction suspension of the external surface passivated and internal surface functionalized MCM-41 (2 mg/mL) and 2 mM of MV^{2+} with different concentrations of added S^{2-} ions: 1.0 (■), 2.5 (●), 3.5 (▲), 5.0 mM (▼).

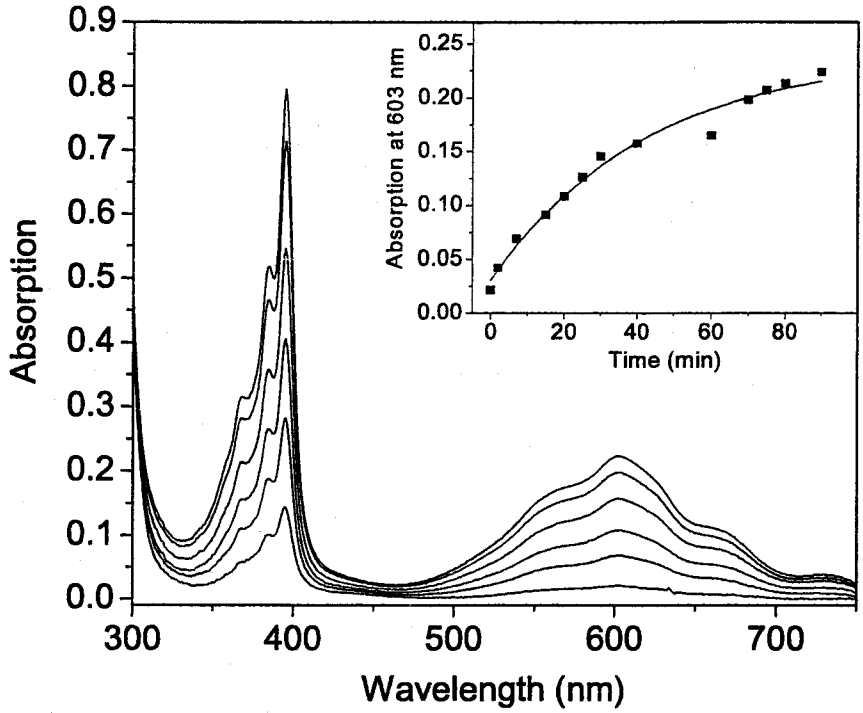

Figure V-S2. Absorption spectra of the reaction suspension of the external surface passivated and internal surface functionalized MCM-41 with CdS nanoparticle encapsulated (2 mg/mL) containing 2 mM of MV^{2+} at different time intervals; from bottom to top: 3, 10, 23, 43, 73, 93 min. The inset shows the growth of the absorption at 603 nm as a function of time.

Summary

Cadmium sulfide (CdS) nanoparticles are successfully synthesized in narrow size distribution and well dispersion by using ordered mesoporous materials (MCM-41) as host. MCM-41 not only functionalizes as host but also prevents the semiconductor nanoparticles within from aggregation when re-dispersed into different solvents. The physical and chemical properties of CdS nanoparticles dispersed in different solvents have been extensively investigated. In solid state, the nanocomposites showed unique temperature dependence of the emission; the emission intensity changes linearly with temperature, leading to a promising application in luminescence thermometry. The breathtaking results obtained in this study should bring to the nanoscience community new insights into the optoelectronic properties of semiconductor nanoparticles, and help pave the way to development of new devices of nanoparticles.

In Chapter I, I report successful synthesis of CdS nanoparticles within both modified mesoporous aluminosilicate MCM-41 and siliceous SBA-15. XRD, UV-vis absorption, fluorescence measurement at low temperature and Raman measurement were used to characterize the photophysical and chemical properties. The effects of temperature, excitation laser intensity and particle size on the acquired spectrum were also studied. Both MCM-41 and SBA-15 were functionalized by a silylation reagent, (3-mercaptopropyl) trimethoxysilane, for rigidifying the inner wall of mesoporous materials and facilitating proper guest-host interaction. Apparent blue shifts of the

absorption band edge of CdS were observed as a result of the quantum confinement effect. For Raman spectra, the relative intensity of the fundamental band and the overtone band of the nanoparticles were found to differ from that of the bulk material. This difference is discussed in terms of electronic anharmonicity. The blue shifts in Raman spectra between the CdS/MCM-41 and bulk CdS sample were observed and explained in terms of CdS lattice compression and/or sulfide vacancies. Further, it was suggested that the stoichiometry for the nanoparticle is more appropriately expressed in the form of CdS_{1-x}.

The solvent dependence of optical properties of CdS nanoparticles remains poorly understood, mainly due to the technical difficulty in re-dispersing the nanoparticles in different solvents. CdS nanoparticles synthesized within MCM-41 have proven a stable system capable for being re-dispersed in various solvents without aggregation or precipitation. Chapter II presents the steady state spectroscopy investigation of CdS nanoparticles within MCM-41. The surface of CdS nanoparticles were modified with either ion doping or adsorption. Such a combined nanoparticle system is quite re-suspendable in both protic and aprotic solvents. Solvent polarity and surface modification affect the luminescence of CdS nanoparticles. The mechanism of the solvent dependence of luminescence is discussed with regard to environment polarity. The interesting and rare property found for CdS nanoparticles within MCM-41 is the emission polarization. The origin of anisotropy fluorescence of CdS nanoparticles within mesoporous materials is explained with regard to solvent relaxation. Constant positive anisotropy would allow for the possibility of using such nanoparticles for biological labeling.

To understand the fundamental processes and dynamics of the photogenerated charge carriers within the particle, the investigation of the solvent effects on the emission quenching of CdS nanoparticles was carried out. This is reported in detail in Chapter III. The time-resolved fluorescence measurement provided rich information on the surface structure and solvent effects on luminescence quenching of CdS nanoparticles. Such information helps us understand the relation between the surface structure of nanoparticles and their optoelectronic properties (e.g., absorption and luminescence). It also provides important guideline to fabricate nanoparticles with optimized surface properties for application in certain types of optoelectronic devices, such as sensors. The quenching behavior of CdS was investigated mainly in systems using methyl viologen or copper ions as the quencher. The quenching kinetics was explained in terms of solvent effects, surface charge carriers and host influence of mesoporous materials.

The development of fluorescence nanothermometry has specific significance in industrial or biomedical diagnostic and treatment processes, in which it is imperative to detect real-time, spatial-resolved and precise temperature. There are several advantages to using fluorescence nanothermometry as opposed to the traditional ones, including high sensitivity, accuracy, and spatial resolution. In Chapter IV, a potential fluorescence nanothermometric material, cadmium sulphide nanoparticles embedded in MCM-41 is introduced. It is found that the emission intensity of CdS/MCM-41 changed linearly with temperature in a wide temperature range from 77 K to 298 K. The excellent linearity of emission intensity on

temperature promise nanocomposite to be used in fluorescence thermometry in industrial and biological fields or for thermal imaging.

Mesoporous materials have been regarded as "natural reactors" due to the strong electric fields existing in the channels and the electronic confinement of the guest molecules. In many cases, the preactivation of the reactant molecules under such strong electric fields results in efficient catalytic reactions. In Chapter V, an unusual reduction reaction of methyl viologen is reported. It is astonishing to observe the spontaneous formation of methyl viologen radicals within mesoporous. MCM-41, which functions as a unique micro-reactor with a catalytic function and the sulphide ions function as the reductant. The mechanism of reaction was investigated by spectroscopic analysis of the methyl viologen radical, exploiting UV-vis and Raman measurements. The reaction is reasonably attributed to the space confinement effect and the enhanced localized electric field within the channels of MCM-41. The source of the sulfide ions can be either an added sulfide salt or coordinatively unsaturated surface sulfide ions of an occluded sulfide nanoparticle. The reduction reaction of methyl viologen within MCM-41 is not only a complementary means in combination with electron microscope to determine the presence and location of sulfide nanoparticles synthesized within such mesoporous materials, but also provides an opportunity to explore the dynamic mechanism of methyl viologen radicals.

References for General Introduction

(1) Brus, L. E.; Efros, A.; Itoh, T. *J. Lumin.* **1996**, *76*, 1.

(2) Alivisatos, A. P. *Science* **1996**, *271*, 933.

(3) Colvin, V. L.; Schlamp, M. C.; Alivisatos, A. P. *Nature* **1994**, *370*, 354.

(4) Klein, V. L.; Lim, A. K. L.; Alivisatos, A. P.; McEuen, P. L. *Nature* **1997**, *389*, 699.

(5) Ridley, B. A.; Nivi, B.; Jacobson, J. *Science* **1999**, *286*, 746.

(6) Henglein, A. *Chem. Rev.* **1989**, *89*, 1861.

(7) Kamat, P. V. *Chem. Rev.* **1993**, *93*, 267.

(8) Bruchez Jr, M.; Moronne, M.; Gin, P.; Weiss, S.; Alivisatos, A. P. *Science* **1998**, *281*, 2013.

(9) Empedocles, S.; Bawendi, M. *Acc. Chem. Res.* **1999**, *32*, 389.

(10) Huynh, W. U.; Dittmer, J. J.; Alivisatos, A. P. *Science* **2002**, *295*, 2425.

(11) Nirmal, M.; Dabbousi, B. O.; Bawendi, M. G.; Macklin, J. J.; Trautman, J. K.; Harris, T. D.; Brus, L. E. *Nature* **1996**, *383*, 802.

(12) Nirmal, M.; Brus, L. E. *Acc. Chem. Res.* **1998**, *32*, 407.

(13) Redl, F. X.; Cho, K. S.; Murray, C. B.; O'Brien, S. *Nature* **2003**, *423*, 968.

(14) Shim, M.; Guyot-Sionnest, P. *Nature* **2000**, *407*, 981.

(15) Chestnoy, N.; Harris, T. D.; Hull, R.; Brus, L. E. *J. Phys. Chem.* **1986**, *90*, 3393.

(16) Brus, L. *J. Phys. Chem.* **1986**, *90*, 2555.

(17) Brus, L. E. *J. Phys. Chem.* **1983**, *79*, 5566.

(18) Steigerwald, M. L.; Brus, L. E. *Acc. Chem. Res.* **1990**, *23*, 183.

(19) Lakowicz, J. R. *Principle of Fluorescence Spectroscop 2nd* Kluwer Academic/Plenum, *New York*, **1999**

(20) Zhang, J. Z. *Acc. Chem. Res.* **1997**, *30*, 423.

(21) Zhang, J. Z. *J. Phys. Chem. B* **2000**, *104*, 7239.

(22) Rossetti, R.; Brus, L. E. *J.Phys.Chem.* **1986**, *90*, 558.

(23) Fischer, C.-H.; Henglein, A. *J. Phys. Chem.* **1989**, *93*, 5578.

(24) Colvin, V. L.; Goldstein, A. N.; Alivisatos, A. P. *J. Am. Chem. Soc.* **1992**, *114*, 5221.

(25) Henglein, A. *Ber. Bunsen-Ges. Phys. Chem.* **1982**, *86*, 301.

(26) Henglein, A.; Gutierrez, M. *Ber. Bunsen-Ges. Phys. Chem.* **1983**, *87*, 852.

(27) Wang, Y.; Herron, N. *Phys. Rev. B* **1990**, *42*, 7253.

(28) Alfassi, Z.; Bahnemann, D.; Henglein, A. *J. Phys. Chem.* **1982**, *86*, 4656.

(29) Kamat, P. V.; Dimitrijevic, N. M.; Fessenden, R. W. *J. Phys. Chem.* **1987**, *91*, 396.

(30) Kamat, P. V.; Dimitrijevic, N. M. *J. Phys. Chem.* **1989**, *93*, 4259.

(31) Sooklal, K.; Hanus, L., H.; Ploehn, H., J.; Murphy, C., J. *Adv. Mate.* **1998**, *10*, 1083.

(32) Mahtab, R.; Rogers, J. P.; Murphy, C. J. *J. Am. Chem. Soc.* **1995**, *117*, 9099.

(33) Mahtab, R.; Rogers, J. P.; Singleton, C. P.; Murphy, C. J. *J. Am. Chem. Soc.* **1996**, *118*, 7028.

(34) Lakowicz, J. R.; Gryczynski, I.; Gryczynski, Z.; Murphy, C. J. *J. Phys. Chem. B* **1999**, *103*, 7613.

References for Chapter I

1. Brus, L. E.; Efros, Al.; Itoh, T. (Eds.), "Spectroscopy of Isolated and Assembled Semiconductor Nanocrystals", *J. Lumin.* **1996**, *76*, 1 (special issue).

2. Alivisatos, A. P. *Science* **1996**, *271*, 933.

3. Colvin, V. L.; Schlamp, M. C.; Alivisatos, A. P. *Nature* **1994**, *370*, 354.

4. Klein, D. L.; Roth, R.; Lim, A. K. L.; Alivisatos, A. P.; McEuen, P. L. *Nature* **1997**, *389*, 699.

5. Ridley, B. A.; Nivi, B.; Jacobson, J. M. *Science* **1999**, *286*, 746.

6. Chen, L.; Klar, P.; Heimbrodt, W.; Brieler, F.; Fröba, M. *Appl. Phys. Lett.* **2000**, *76*, 3531.

7. Chen, L.; Klar, P.; Heimbrodt, W.; Brieler, F.; Fröba, M.; Nidda, H.; Loidl, A. *Physica E* **2001**, *10*, 368.

8. Wellmann, H.; Rathoussky, J.; Wark, M.; Zukal, A.; Schulz-Ekloff, G. *Micro. Meso. Mater.* **2001**, *44-45*, 419.

9. Hirai, T.; Okubo, H.; Komasawa, I. *J Phys. Chem. B* **1999**, *103*, 4228.

10. Zhang, Z.; Dai, S.; Fan, X.; Blom, D., Pennycook, S. J.; Wei, Y. *J Phys. Chem. B* **2001**, *105*, 6755.

11. Kresge, C. T.; Leonowicz, M. E.; Roth, W. J.; Vartuli, J. C.; Beck, J. S. *Nature* **1992**, *359*, 710.

12. Beck, J. S.; Vartuli, J. C.; Roth, W. J.; Leonowicz, M. E.; Kresge, C. T.; Schmitt, K. D.; Chu, C. T.-W.; Olsen, D. H.; Sheppard, E. W.; McCullen, B.; Higgins, J. B.; Schlenker, J. L. *J. Am. Chem. Soc.* **1992**, *114*, 10834.

13. Zhao, D.; Feng, J.; Huo, Q.; Melosh, N.; Fredrickson, G. H.; Chmelka, B. F.; Stucky, G. D. *Science* **1998**, *279*, 548.

14. Zhao, D.; Huo, Q.; Feng, J.; Chmelka, B. F.; Stucky, G. D. *J. Am. Chem. Soc.* **1998**, *120*, 6024.

15. Xu, W.; Akins, D. L. *J. Phys. Chem. B.*, **2001**, in press.

16. Xu, W.; Guo, H.; Akins, D. L. *J. Phys. Chem. B.*, **2001**, *105*, 1543.

17. Xu, W.; Guo, H.; Akins, D. L. *J. Phys. Chem. B.*, **2001**, *105*, 7686.

18. Spanier, J. E.; Robinson, R. D.; Zhang, F.; Chan, S.-W.; Herman, I. P. *Phys. Review B* **2001**, *64* 245407.

19. McBride, I. R.; Hass, K. C.; Poindexter, B. D.; Weber, W. H. *J Appl. Phys.* **1994**, *76*, 2435

20. Murphy, C. J.; Coffer, J. L. *Appl. Spectr.* **2002**, *56(1)*, 21A.

21. Kamalov, V. F.; Little, R.; Logunov, S. L.; M. A. El-Sayed. *J Phys. Chem.* **1996**, *100*, 6381.

22. Perna, G.; Capozzi, V.; Pagliara, S.; Ambrico, M. *Appl. Surf. Sci.* **2000**, *154*, 238.

23. Matsuura, D.; Kanemitsu, Y.; Kushida, T.; White, C.W.; Budai, J. D.; Meldrum, A. *Jpn. J. Appl. Phys.* **2000**, *40*, 2092.

References for Chapter II

(1) Henglein, A. *Chem. Rev.* **1989**, *89*, 1861.

(2) Kamat, P. V. *Chem. Rev.* **1993**, *93*, 267.

(3) Zhang, J. Z. *J. Phys. Chem. B* **2000**, *104*, 7239.

(4) Zhang, J. Z. *Acc. Chem. Res.* **1997**, *30*, 423.

(5) Bruchez Jr, M.; Moronne, M.; Gin, P.; Weiss, S.; Alivisatos, A. P. *Science* **1998**, *281*, 2013.

(6) Empedocles, S.; Bawendi, M. *Acc. Chem. Res.* **1999**, *32*, 389.

(7) Huynh, W. U.; Dittmer, J. J.; Alivisatos, A. P. *Science* **2002**, *295*, 2425.

(8) Nirmal, M.; Dabbousi, B. O.; Bawendi, M. G.; Macklin, J. J.; Trautman, J. K.; Harris, T. D.; Brus, L. E. *Nature* **1996**, *383*, 802.

(9) Nirmal, M.; Brus, L. E. *Acc. Chem. Res.* **1998**, *32*, 407.

(10) Redl, F. X.; Cho, K. S.; Murray, C. B.; O'Brien, S. *Nature* **2003**, *423*, 968.

(11) Shim, M.; Guyot-Sionnest, P. *Nature* **2000**, *407*, 981.

(12) Chestnoy, N.; Harris, T. D.; Hull, R.; Brus, L. E. *J. Phys. Chem.* **1986**, *90*, 3393.

(13) Xu, W.; Liao, Y.; Akins, D. L. *J. Phys. Chem. B* **2002**, *106*, 11127.

(14) Chae, W.-S.; Ko, J.-H.; Hwang, I.-W.; Kim, Y.-R. *Chem. Phys. Lett.* **2002**, *365*, 49.

(15) Zhang, Z.; Dai, S.; Fan, X.; Blom, D. A.; Pennycook, S. J.; Wei, Y. *J. Phys. Chem. B* **2001**, *105*, 6755.

(16) Wellmann, H.; Rathousky, J.; Wark, M.; Zukal, A.; Schulz-Ekloff, G. *Micropo. Mesopor. Mater.* **2001**, *44-45*, 419.

(17) Martin-Palma, R. J.; Hernandez-Velez, M.; Diaz, I.; Villavicencio-Garcia, H.; Garcia-Poza, M. M.; Martinez-Duart, J. M.; Perez-Pariente, J. *Mater. Sci. & Eng., C: Biomimetic and Supramolecular Systems* **2001**, *C15*, 163.

(18) Hirai, T.; Okubo, H.; Komasawa, I. *J. Phys. Chem. B* **1999**, *103*, 4228.

(19) Pradhan, N.; Efrima, S. *J. Am. Chem. Soc.* **2003**, *125*, 2050.

(20) Fischer, C.-H.; Henglein, A. *J. Phys. Chem.* **1989**, *93*, 5578.

(21) Ramsden, J. J.; Webber, S. E.; Graetzel, M. *J. Phys. Chem.* **1985**, *89*, 2740.

(22) Dannhauser, T.; O扒eil, M.; Johansson, K.; Whitten, D.; McLendon, G. *J. Phys. Chem.* **1986**, *90*, 6074.

(23) Landes, C. F.; Braun, M.; El-Sayed, M. A. *J. Phys. Chem. B* **2001**, *105*, 10554.

(24) Kumar, A.; Mital, A. S. *J. Colloid Interface Sci.* **2001**, *240*, 459.

(25) Lakowicz, J. R.; Gryczynski, I.; Piszczek, G.; Murphy, C. J. *J. Phys. Chem. B* **2002**, *106*, 5365.

(26) Lakowicz, J. R.; Gryczynski, I.; Gryczynski, Z.; Nowaczyk, K.; Murphy, C. J. *Anal. Biochem.* **2000**, *280*, 128.

(27) Lakowicz, J. R.; Gryczynski, I.; Gryczynski, Z.; Murphy, C. J. *J. Phys. Chem. B* **1999**, *103*, 7613.

(28) Sooklal, K.; Hanus, L., H.; Ploehn, H., J.; Murphy, C., J. *Adv. Mater. (Weinheim, Germany)* **1998**, *10*, 1083.

(29) Lai, C.-Y.; Trewyn, B. G.; Jeftinija, D. M.; Jeftinija, K.; Xu, S.; Jeftinija, S.; Lin, V. S. Y. *J. Am. Chem. Soc.* **2003**, *125*, 4451.

(30) Mahtab, R.; Rogers, J. P.; Murphy, C. J. *J. Am. Chem. Soc.* **1995**, *117*, 9099.

(31) Mahtab, R.; Rogers, J. P.; Singleton, C. P.; Murphy, C. J. *J. Am. Chem. Soc.* **1996**, *118*, 7028.

(32) Brus, L. *J. Phys. Chem.* **1986**, *90*, 2555.

(33) Lakowicz, J. R. *Principles of Fluorescence Spectroscopy, 2nd.* Kluwer Academic/Plenum, *New York* **1999**.

(34) Liao, Y.-T.; Zang, L.; Akins, D. *Catal. Comm.* **2005**, *6*, 141.

(35) O'Neil, M.; Marohn, J.; McLendon, G. *J. Phys. Chem.* **1990**, *94*, 4356.

(36) Bawendi, M. G.; Carroll, P. J.; Wilson, W. L.; Brus, L. E. *Journal of Chem. Phys.* **1992**, *96*, 946.

(37) Eychmuller, A.; Hasserlbarth, A.; Katsikas, L.; Weller, H. *Ber. Bunsenges. Phys. Chem* **1991**, *95*, 79.

(38) Chamarro, M.; Gourdon, C.; Lavallard, P.; Lublinskaya, O.; Ekimov, A. I. *Physical Review B: Condensed Matter* **1996**, *53*, 1336.

(39) Empedocles, S. A.; Neuhauser, R.; Bawendi, M. G. *Nature* **1999**, *399*, 126.

(40) Empedocles, S. A.; Bawendi, M. G. *Science* **1997**, *278*, 2114.

(41) Hu, J.; Li, L.-S.; Yang, W.; Manna, L.; Wang, L.-W.; Alivisatos, P. *Science* **2001**, *292*, 2060.

(42) Yang, J.; Zeng, J.-H.; Yu, S.-H.; Yang, L.; Zhou, G.-E.; Qian, Y.-T. *Chem. Mater.* **2000**, *12*, 3259.

(43) Ye, C.; Meng, G.; Wang, Y.; Jiang, Z.; Zhang, L. *J. Phys. Chem. B* **2002**, *106*, 10338.

(44) Manna, L.; Scher, E. C.; Li, L.-S.; Alivisatos, P. A. *J. Am. Chem. Soc.* **2002**, *124*, 7136.

(45) Murray, C. B.; Noms, D. J.; Bawendi, M. G. *J. Am. Chem. Soc.* **1993**, *115*, 8706.

(46) Liao, Y.-T.; Zang, L.; Akins, D. *the second paper of this series, submitted simultaneously with this manuscript.*

References for Chapter III

(1) Empedocles, S.; Bawendi, M. *Acc. Chem. Res.* **1999**, *32*, 389.

(2) Zhang, J. Z. *Acc. Chem. Res.* **1997**, *30*, 423.

(3) Nirmal, M.; Brus, L. E. *Acc. Chem. Res.* **1998**, *32*, 407.

(4) Kamat, P. V. *Chem. Rev.* **1993**, *93*, 267.

(5) Henglein, A. *Chem. Rev.* **1989**, *89*, 1861.

(6) Weller, H. *Curr. Opin. Colloid & Interface Sci.* **1998**, *3*, 194.

(7) Rogach, A. L.; Talapin, D. V.; Weller, H. *Colloids and Colloid Assemblies* **2004**, 52.

(8) Zhang, J. Z. *J. Phys. Chem. B* **2000**, *104*, 7239.

(9) Chandler, R. R.; Coffer, J. L.; Atherton, S. J.; Snowden, P. T. *J. Phys. Chem.* **1992**, *96*, 2713.

(10) Logunov, S.; Green, T.; Marguet, S.; El-Sayed, M. A. *J. Phys. Chem. A* **1998**, *102*, 5652.

(11) Chandler, R. R.; Coffer, J. L. *J. Phys. Chem.* **1993**, *97*, 9767.

(12) Kuczynski, J.; Thomas, J. K. *J. Phys. Chem.* **1983**, *87*, 5498.

(13) Bavykin, D. V.; Savinov, E. N.; Parmon, V. N. *Langmuir* **1999**, *15*, 4722.

(14) Landes, C. F.; Braun, M.; El-Sayed, M. A. *J. Phys. Chem. B* **2001**, *105*, 10554.

(15) Haesselbarth, A.; Eychmueller, A.; Weller, H. *Chem. Phys. Lett.* **1993**, *203*, 271.

(16) Wilcoxon, J. P.; Parsapour, F.; Kelley, D. F. *Proc. Electrochem. Soc.* **1997**, *97*, 16.

(17) Ramsden, J. J.; Webber, S. E.; Graetzel, M. *J. Phys. Chem.* **1985**, *89*, 2740.

(18) Fischer, C.-H.; Henglein, A. *J. Phys. Chem.* **1989**, *93*, 5578.

(19) Biancardo, M.; Schwab, P. F. H.; Argazzi, R. B., C. A. *Inorg. Chem.* **2003**, *42*, 3966.

(20) Cowdery-Corvan, J. R.; Whitten, D. G.; McLendon, G. L. C. P., 176, 377. *Chem. Phys.* **1993**, *176*, 377.

(21) Hashimoto, K.; Hiramoto, M.; Sakata, T. M., H.; Takemura, H.; Fujihira, M. *J. Phys. Chem.* **1987**, *91*, 6198.

(22) Yuan, Y.; Fendler, J. H.; Cabasso, I. *Chem. Mater.* **1992**, *4*, 312.

(23) Zang, L.; Rodgers, M. A. J. *J. Phys. Chem.* **2000**, *104*, 468.

(24) Liao, Y.-T.; Zang, L.; Akins, D. *the first paper of this series, submitted simultaneously with this manuscript.*

(25) Liao, Y.-T.; Zang, L.; Akins, D. L. *Catal. Comm.* **2005**, *6*, 141.

(26) Franzen, S.; Lao, K.; Boxer, S. G. *Chem. Phys. Lett.* **1992**, *197*, 380.

(27) Seki, K.; Traytak, S. D.; Tachiya, M. *J. Chem. Phys.* **2003**, *118*, 669.

(28) Ohta, N.; Koizumi, M.; Umeuchi, S.; Nishimura, Y.; Yanazaki, I. *J. Phys. Chem.* **1996**, *100*, 16466.

(29) Hilczer, M.; Traytak, S.; Tachiya, M. *J. Chem. Phys.* **2001**, *115*, 11249.

(30) Garcia, H.; Roth Heinz, D. *Chem. Rev.*, *102*, 3947.

(31) Marquez, F.; Garcia, H.; Palomares, E.; Fernandez, L.; Corma, A. *J. Am. Chem. Soc.* **2000**, *122*, 6520.

(32) Zicovich-Wilson, C. M.; Corma, A.; Viruela, P. *J. Phys. Chem.* **1994**, *98*, 10863.

(33) Mirodatos, C.; Barthomeuf, D. *J. Catal.* **1985**, *93*, 246.

(34) Yoon, K. B. *Chem. Rev.* **1993**, *93*, 321.

(35) Yoon, K. B.; Hubig, S. M.; Kochi, J. K. *J. Phys. Chem.* **1994**, *98*, 3865.

(36) Yoon, K. B.; Kochi, J. K. *J. Am. Chem. Soc* **1988**, *110*, 6586.

(37) Simoncic, P.; Armbruster, T.; Pattison, P. *J. Phys. Chem. B* **2004**, *108*, 17352.

(38) Hennessy, B.; Megelski, S.; Marcolli, C.; Shklover, V.; Barlocher, C.; Calzaferri, G. *J. Phys. Chem. B.* **1999**, *103*, 3340.

(39) Stramel, R. D.; Nakamura, T.; Thomas, K. J. *J. Chem. Soc., Faraday Trans. 1: Phys. Chem. Condensed Phases* **1988**, *84*, 1287.

(40) Lakowicz, J. R.; Gryczynski, I.; Piszczek, G.; Murphy, C. J. *J. Phys. Chem. B* **2002**, *106*, 5365.

(41) Lakowicz, J. R.; Gryczynski, I.; Gryczynski, Z.; Nowaczyk, K.; Murphy, C. J. *Analy. Biochem.* **2000**, *280*, 128.

(42) Lakowicz, J. R.; Gryczynski, I.; Gryczynski, Z.; Murphy, C. J. *J. Phys. Chem. B* **1999**, *103*, 7613.

(43) Kumar, A.; Mital, A. S. *J. Colloid Interface Sci.* **2001**, *240*, 459.

(44) Matsumoto, H.; Uchida, H.; Matsunaga, T.; Tanaka, K.; Sakata, T.; Mori, H.; Yoneyama, H. *J. Phys. Chem.* **1994**, *98*, 11549.

(45) Chestnoy, N.; Harris, T. D.; Hull, R.; Brus, L. E. *J. Phys. Chem.* **1986**, *90*, 3393.

(46) O'Neil, M.; Marohn, J.; McLendon, G. *J. Phys. Chem.* **1990**, *94*, 4356.

(47) Lakowicz, J. R., *Principle of Flurorescence Spectroscopy,* 2nd. ed.; Kluwer Academic/Plenum, *New York,* **1999**.

References for Chapter IV

(1) Gallery, J.; Gouterman, M.; Callis, J.; Khalil, G.; McLachlan, B.; Bell, J. *Rev. Sci. Instrum.* **1994**, *65*, 712.

(2) Allison, S. W.; Gillies, G. T. *Rev. Sci. Instrum.* **1997**, *68*, 2615.

(3) Wang, S.; Westcott, S.; Chen, W. *J. Phys. Chem. B* **2002**, *106*, 11203.

(4) Maruszewski, K.; Andrzejewski, D.; Strek, W. *J. Lumin.* **1997**, *72-74*, 226.

(5) Kauppinen, J. P.; Loberg, K. T.; Manninen, A. J.; Pekola, J. P. *Rev. Sci. Instrum.* **1998**, *69*, 4166.

6) Wang, Y.; Herron, N. *J. Phys. Chem.* **1988**, *92*, 4988.

(7) Joly, A. G.; Chen, W.; Roark, J.; Zhang, J. Z. *J. Nnanosci. Nanotech.* **2001**, *1*, 295.

(8) Walker, G. W.; Sundar, V. C.; Rudzinski, C. M.; Wun, A. W.; Bawendi, M. G.; Nocera, D. G. *Appl. Phys. Lett* .**2003**, *83*, 3555.

(9) Sebald, K.; Michler, P.; Passow, T.; Hommel, D.; Bacher, G.; Forchel, A. *Appl. Phys. Lett* . **2002**, *81*, 2920.

(10) Soloviev, V. N.; Eichhoefer, A.; Fenske, D.; Banin, U. *J. Am. Chem. Soc.* **2001**, *123*, 2354.

(11) Zhao, J.; Dou, K.; Chen, Y.; Jin, C.; Sun, L.; Huang, S.; Yu, J.; Xiang, W.; Ding, Z. *J. Lumin.***1996**, *66&67*, 332.

(12) Bol, A. A.; Van Beek, R.; Ferwerda, J.; Meijerink, A. *J. Phys. Chem. Solids* **2003**, *64*, 247.

(13) Tanaka, M.; Masumoto, Y. *Chem. Phys. Lett.***2000**, *324*, 249.

(14) Xu, W.; Liao, Y.; Akins, D. L. *J. Phys. Chem. B* **2002**, *106*, 11127.

(15) Liao, Y.-T.; Zang, L.; Akins, D. *Catal. Commu.*, ***2005, 6,*** 141.

(16) Zhang, Z.; Dai, S.; Fan, X.; Blom, D. A.; Pennycook, S. J.; Wei, Y. *J. Phys. Chem. B* **2001**, *105*, 6755.

(17) Zhang, W.-H.; Shi, J.-L.; Chen, H.-R.; Hua, Z.-L.; Yan, D.-S. *Chem. Mater.* **2001**, *13*, 648.

(18) Liao, Y.-T.; Zang, L.; Akins, D. *to be published somewhere else.*

References for Chapter V

(1) Beck, J. S.; Vartuli, J. C.; Roth, W. J.; Leonowicz, M. E.; Kresge, C. T.; Schmitt, K. D.; Chu, C. T. W.; Olson, D. H.; Sheppard, E. W.; McCullen, S. B.; Higgins, J. B.; Schlenker, J. L. *J. Am. Chem. Sot.* **1992**, *114*, 10834.

(2) Moller, K.; Bein, T. *Chem. Mater.* **1998**, *10*, 2950.

(3) Corma, A. *Chem. Rev. (Washington, D. C.)* **1997**, *97*, 2373.

(4) Garcia, H.; Roth, H. D. *Chem. Rev.* **2002**, *102*, 3947.

(5) Marquez, F.; Garcia, H.; Palomares, E.; Fernandez, L.; Corma, A. *J. Am. Chem. Soc.* **2000**, *122*, 6520.

(6) Zicovich-Wilson, C. M.; Corma, A.; Viruela, P. *J. Phys. Chem.* **1994**, *98*, 10863.

(7) Mirodatos, C.; Barthomeuf, D. *J. Catal.* **1985**, *93*, 246.

(8) Dean, J. A.; (Ed.) *Lange's Handbook of Chemistry, 13th ed.*; McGraw-Hill, 1985.

(9) Yoon, K. B.; Hubig, S. M.; Kochi, J. K. *J. Phys. Chem.* **1994**, *98*, 3865.

(10) Yoon, K. B.; Kochi, J. K. *J. Am. Chem. Soc* **1988**, *110*, 6586.

(11) Xu, W.; Liao, Y.; Akins, D. L. *J. Phys. Chem. B* **2002**, *106*, 11127.

(12) Zhang, W.-H.; Shi, J.-L.; Chen, H.-R.; Hua, Z.-L.; Yan, D.-S. *Chem. Mater.* **2001**, *13*, 648.

(13) Zhang, W.-H.; Shi, J.-L.; Wang, L.-Z.; Yan, D.-S. *Chem. Mater.* **2000**, *12*, 1408.

(14) Abe, T.; Tachibana, Y.; Uematsu, T.; Iwamoto, M. *J. Chem. SOC., Chem. Commun.* **1995**, 1617.

(15) Winkler, H.; Birkner, A.; Hagen, V.; Wolf, I.; Schmechel, R.; Von Seggern, H.; Fischer, R. A. *Adv. Mater. (Weinheim, Germany)* **1999**, *11*, 1444.

(16) Zhang, Z.; Dai, S.; Fan, X.; Blom, D. A.; Pennycook, S. J.; Wei, Y. *J. Phys. Chem. B* **2001**, *105*, 6755.

(17) Borja, M.; Dutta, P. K. *Nature (London, United Kingdom)* **1993**, *362*, 43.

(18) Castagnola, N. B.; Dutta, P. K. *J. Phys. Chem. B* **2001**, *105*, 1537.

(19) Watanabe, T.; Honda, K. *J. Phys. Chem.* **1982**, *86*, 2617.

(20) Melendres, C. A.; Lee, P. C.; Meisel, D. *J. Electrochem. Soc.* **1983**, *130*, 1523.

(21) Forster, M.; Girling, R. B.; Hester, R. E. *J. Raman Spectrosc.* **1982**, *12*, 36.

(22) Forster, M.; Hester, R. E. *Chem. Phys. Lett.* **1982**, *85*, 287.

(23) Hester, R. E.; Suzuki, S. *J.Phys. Chem.***1982**, *86*, 4626.

(24) Feilchenfeld, H.; Chumanov, G.; Cotton, T. M. *J. Phys. Chem.***1996**, *100*, 4937.